

AN EXPERIMENTAL STUDY OF TURBULENCE IN AN URBAN ENVIRONMENT

by

John F. Clarke, Jason K.S. Ching, and James M. Godowitch

Meteorology and Assessment Division  
Environmental Sciences Research Laboratory  
U.S. Environmental Protection Agency  
Research Triangle Park, North Carolina 27711

ENVIRONMENTAL SCIENCES RESEARCH LABORATORY  
OFFICE OF RESEARCH AND DEVELOPMENT  
U.S. ENVIRONMENTAL PROTECTION AGENCY  
RESEARCH TRIANGLE PARK, NORTH CAROLINA 27711

## DISCLAIMER

This report has been reviewed by the Environmental Sciences Research Laboratory, U.S. Environmental Protection Agency, and approved for publication. Mention of trade names or commercial products does not constitute endorsement or recommendation for use.

## AFFILIATION

Dr. Clarke, Dr. Ching, and Mr. Godowitch are meteorologists in the Meteorology and Assessment Division, Environmental Sciences Research Laboratory, U.S. Environmental Protection Agency, Research Triangle Park, North Carolina. They are on assignment from the National Oceanic and Atmospheric Administration, U.S. Department of Commerce.

## ABSTRACT

The structure of turbulence in the urban surface boundary layer is discussed. Wind and temperature fluctuations were measured with fast-response sensors at a height of 31 m in four areas of varied land use in the St. Louis environs (a rural and three urban sites). The second moments of the fluctuations were computed for one-hour time series and analyzed within the framework of Monin-Obukhov similarity theory (i.e., normalized by appropriate velocity and temperature scales). The results are discussed relative to observed land-use features and calculated surface roughness lengths for each of the sites.

Average surface roughness lengths ranged from 0.7 to 1.7 m for the urban sites, varying by several meters as a function of wind direction at individual sites. The normalized velocity and temperature variances for the rural site were consistent with similarity theory. For the urban sites, plots of the normalized velocity variances showed an orderly departure from similarity theory for both neutral and unstable stratifications; they were smaller than the corresponding normalized variance for the rural site.

The urban anomalies are discussed relative to the terms in the turbulent kinetic energy budget equation. For neutral stratification, the normalized velocity variances are up to 15% lower at the urban sites compared to the rural site. They appear to be inversely proportional to surface roughness length. The nondimensionalized dissipation rate of turbulent energy was less than unity at an urban site with tall rough-

ness elements, and spectral peak wavelengths were generally larger at the urban sites. These anomalies to similarity theory are suggested to be due to the wake region of the roughness elements extending to near the height of the measurements. For unstable stratification, the normalized velocity variances and the nondimensionalized energy dissipation rate for the urban sites are about 50% lower than for the rural site. This anomaly is suggested to be due to increased importance of vertical transport processes within the urban area.

Ancillary analyses suggest that the spectral peak wavelength, not the mixed layer height, is the proper scaling length for free convection similarity. During the afternoon transition period the two scales may differ significantly.

## TABLE OF CONTENTS

ABSTRACT.....	iii
LIST OF TABLES.....	vii
LIST OF FIGURES.....	viii
LIST OF SYMBOLS.....	xi
ACKNOWLEDGEMENTS.....	xv
1.0 INTRODUCTION.....	1
1.1 Problem Area.....	1
1.2 Research Objectives.....	3
1.3 Similarity Theory.....	4
1.4 Urban Turbulence Measurements.....	8
1.5 Scope and Conduct of study.....	10
2.0 EXPERIMENTAL PROGRAM.....	12
2.1 Regional Air Pollution Study.....	12
2.2 St. Louis Environs.....	12
2.3 Turbulence Program.....	14
2.3.1 Description of Sites And Measurements.....	14
2.3.2 Instrumentation.....	25
a. Gill Anemometer.....	25
b. Temperature System.....	26
c. Moisture and Net Radiation.....	26
2.3.3 Data Processing.....	27
3.0 RESULTS.....	28
3.1 Surface Roughness Length.....	28
3.1.1 Land Use Evaluation of $z_0$ .....	30
3.1.2 $z_0$ from Similarity Profile Assumption.....	35
3.1.3 Application.....	42
3.2 Reynold Stresses and Temperature Variances.....	43
3.2.1 Velocity Variances.....	43
a. Neutral Stratification.....	43
b. Dependence on $z'/L$ .....	47
c. Dependence on $z_i/L$ .....	64
d. Ratio of Variances.....	73
e. Intensity of Turbulence.....	75
3.2.2 Temperature Variance.....	84
3.2.3 Covariances.....	86
a. Momentum Flux.....	87
b. Heat Flux.....	87

3.3	Spectral Characteristics.....	93
3.3.1	Introduction.....	93
3.3.2	Background.....	95
3.3.3	Dimensionless Dissipation Rate.....	96
3.3.4	Vertical Velocity Spectra.....	101
3.3.5	Horizontal Velocity Components.....	107
3.3.6	Temperature Spectra.....	115
4.0	SYNTHESIS OF RESULTS.....	119
4.1	Introduction.....	119
4.2	Boundary Layer Phenomena.....	119
4.3	Similarity Theory.....	122
4.4	Conclusions.....	128
	REFERENCES.....	130
	APPENDICES.....	137
A.	Gill UVW Anemometer.....	137
A-1	Leveling.....	137
A-2	Calibration.....	139
A-3	Response Characteristics.....	141
B.	Data Processing.....	144
B-1	Initial Processing.....	144
B-2	Spectral Computations.....	146

## LIST OF TABLES

<u>Table</u>	<u>Page</u>
1.1. Similarity Prediction for the Relevant Second Moments and Form of the Asymptotic Limits.....	7
2.1. Starting and Ending Dates of Instrument Operation and Total Hours of Data Obtained for Each Site and Experi- mental Period.....	16
3.1. Site Land-Use Characteristics and Estimated Displacement Lengths and Roughness Lengths Based on the Empirical Results of Kutzbach (1961) and Counihan (1971), and Average Calculated Roughness Lengths.....	34
3.2. Averages and Standard Deviations of the Normalized Velocity Standard Deviations for Neutral Stratifica- tion, Number of Observations, and Average Roughness Lengths for the Summer and Fall Data Sets.....	45
3.3 The Ratio $\sigma_w/u^*$ as a Function of $z'/L$ and Correla- tion Coefficients $R^*$ , for Summer and Fall Data Sets.....	58
3.4 Same as for Table 3.3 but for $\sigma_v/u^*$ .....	64
3.5 The Ratio $\sigma_u/u^*$ as a Function of $L_m(u)/L$ and Correlation Coefficients $R^*$ , for the Summer Data Set.....	73
3.6. Averages and Standard Deviations of Intensity of Turbulence Components for Neutral and Slightly Unstable Conditions, Number of Observations, and Average Roughness Lengths for Summer and Fall Data Sets.....	81
3.7. Average Hourly Values of $-\overline{u'w'}$ and $-\overline{v'w'}$ X100 for the Summer Data Set.....	88
A-1. Effect of Instrument Response on Second Moments.....	143
B-1. Number of Spectra for Each Site, Spectral Component, and Stability Class Used in Analyses.....	149

## LIST OF FIGURES

<u>Figure</u>	<u>Page</u>
2.1. Map of St. Louis Metropolitan area showing the 25-station RAMS network and major population centers .....	13
2.2. Topographic map of the city of St. Louis.....	15
2.3. Aerial photograph of site 105 looking southwest.....	17
2.4. Photograph of tower at site 105.....	19
2.5. Photograph from tower at site 107 looking north.....	20
2.6. Aerial photograph of site 109 looking northwest.....	22
2.7. Photograph from tower at site 111 looking east.....	23
2.8. Photograph from tower at site 111 looking southwest.....	24
3.1. The ratios $z_0/h$ and $d/h$ as a function of $A_r/A$ from the empirical data of Kutzbach (1961) and Counihan (1971) .....	33
3.2. Schematic of land-use features and average heights for site 107.....	33
3.3. Surface roughness length vs. wind direction for neutral, unstable, and stable conditions for site 107.....	37
3.4. Surface roughness length vs. wind direction.....	38
3.5. Surface roughness length averaged over 20 degree wind direction sectors for the summer data .....	39
3.6. Same as for Figure 3.5 for fall data set.....	41
3.7. Site averaged values of $\sigma/u^*$ vs. the corresponding average $Z_0$ and linear regression fits.....	46
3.8. Plots for $\sigma_w/u^*$ vs. $Z_0$ for neutral stratification.....	48.
3.9. Individual data plots for $\sigma_w/u^*$ vs. $U$ for neutral stratification for the four sites.....	49
3.10. $\sigma_w/u^*$ vs. $z'/L$ for summer data set.....	50
3.11 $\sigma_w$ vs. $u^*$ for $z'/L < 1.0$ .....	52



<u>Figure</u>	<u>Page</u>
3.12. $\sigma_w$ vs. $u^*$ for $z'/L < -1$ .....	54
3.13. $\sigma_w$ vs. $C(u^{*3}+0.4u_f^3)^{1/3}$ for $z'/L$ between 0 and -1.....	56
3.14. Same as for Figure 3.13 but for $z'/L < -1$ .....	57
3.15. $\sigma_w$ vs. $u^*$ for stable stratification.....	59
3.16. Plots of $\sigma_v/u^*$ vs. $z'/L$ for site 105.....	61
3.17. $\sigma_v/u^*$ averaged over intervals of $z'/L$ of 0.25 vs. $z'/L$ for sites 105 and 109.....	62
3.18. $\sigma_v$ vs. $u_f$ for $z'/L < -1$ .....	63
3.19. Average mixing heights near the urban center and average surface heat flux for sites 105 and 107 for 26 July through 13 August.....	66
3.20. The ratio $\sigma_v/u^*$ vs. $z_i/L$ for sites 105, 107, and 109 for the period 0900 to 1200 h and 1300 to 1600 h.....	68
3.21 $\sigma_u$ vs. $(g\overline{w'T'L_m(u)}/T)^{1/3}$ for $z'/L < -1$ .....	70
3.22. $\sigma_u$ vs. right-hand side of Eq. 3.12 for $z'/L$ between 0 and -1.....	71
3.23. Same as for Figure 3.22 but for $z'/L < -1$ .....	72
3.24. Plots of $\sigma_v/\sigma_u$ vs. $z'/L$ for the summer data set.....	74
3.25. Plots of $\sigma_w/\sigma_u$ vs. $z'/L$ for the summer data set.....	76
3.26. Diurnal variation of vertical and lateral intensities of turbulence for the summer data set.....	77
3.27. Vertical and lateral intensities of turbulence vs. $z'/L$ for the summer data set.....	79
3.28. Plots of site averaged values of $\sigma_w/U$ (a) and $\sigma_v/U$ (b) vs. $z'/Z_0$ for neutral and slightly unstable stratifications.....	82
3.29. Individual plots of $\sigma_w/U$ vs. $Z_0$ for neutral stratification.....	83
3.30. The ratio $\sigma_T/T^*$ for the summer data set.....	85

<u>Figure</u>	<u>Page</u>
3.31. Plots of $u^*$ vs. $U$ for site 107 and estimated linear fit to plots for all four sites.....	89
3.32. Plots of $U/u^*$ vs. $z'/L$ .....	90
3.33. Diurnal variation of the average heat flux for sites 105, 107, and 109 and net radiation for site 105.....	91
3.34. Ratio $-\overline{u'T'}/\overline{w'T'}$ vs. $z'/L$ .....	94
3.35. Turbulent energy dissipation rate $\epsilon$ vs. $z'/L$ .....	97
3.36. The ratio $\epsilon/g\overline{w'T'}/T$ vs. $z'/L$ .....	99
3.37. Estimated fit to plots of the nondimensionalized energy dissipation rate vs. $z'/L$ for a) site 105 and the Kansas data and b) for sites 105, 107, and 109.....	100
3.38. Vertical velocity spectra for sites and stability classes indicated.....	102
3.39. Plots of $z'/L_m(w)$ vs. $z'/L$ for summer data set.....	105
3.40. Estimated fit to plots of the diurnal variation of $L_m(w)$ for sites 105, 107, and 109.....	106
3.41. $L_m(w)$ vs. wind direction for site 107 for neutral stratification.....	108
3.42. Lateral velocity spectra for sites and stability classes indicated.....	109
3.43. Same as for Figure 3.42 for the longitudinal velocity component.....	110
3.44. Estimated fit to plots of diurnal variation of $L_m(v)$ for sites 105, 107, and 109.....	113
3.45. Same as for Figure 3.44 for the $L_m(u)$ .....	114
3.46. Comparison of $z_i$ , $L_m$ , $\overline{w'T'}$ , and $\sigma_v$ for the urban sites and $\sigma_v$ for the rural site for the heating period of the day.....	116
3.47. Temperature spectra for sites and stability classes indicated.....	118
4.1. Normalized velocity profile in vicinity of roughness elements.....	126

<u>Figure</u>	<u>Page</u>
A-1. Photograph of Gill anemometer showing attached plumb bob leveling device.....	138
A-2. Time constants for temperature system and Gill anemometer for four wind angles to the propeller.....	142
B-1. Simplified flow diagram of data processing.....	145

## ABBREVIATIONS AND SYMBOLS

### Abbreviation

A	--constant
A	--area
$A_i$	--constant
$A_r$	--area of roughness elements
b	--constant
B	--constant
BR	--Bowen ratio
C	--regression slope
$C_1, C_2$	--constants
$C_p$	--specific heat at constant pressure
d	--displacement length
$D, D'$	--regression constants
$E, E'$	--regression constants
f	--normalized frequency
$f_m$	--normalized frequency associated with peak in the $nS(n)$ spectrum
$F_n$	--net radiation
$F(n)$	--power spectrum function
g	--acceleration due to gravity
$g/T$	--buoyancy parameter
h	--height of roughness elements
k	--von Karman constant
$\ell$	--mixing length
L	--Monin-Obukhov length

$LE$	--latent heat flux
$L_m$	--spectral length scale (peak wave length)
$L_i$	--integral length scale
$L_\epsilon$	--dissipation length scale
$n$	--cyclic frequency
$n_m$	--frequency associated with peak in $nS(n)$ spectrum
$N^*$	--dissipation rate for temperature variance
$N$	--number of sampling points
$p'$	--fluctuating pressure
$q^2$	--turbulent kinetic energy
$R$	--sample rate
$R'$	--residual term in energy equation
$R^*$	--correlation coefficient
$R(t)$	--auto-correlation coefficient
$s$	--silhouette area of roughness elements
$S$	--specific area of roughness elements
$S(n)$	--absolute spectrum function
$t$	--time
$T$	--temperature
$T'$	--fluctuating temperature
$T^*$	--scaling temperature
$u', v', w'$	--fluctuating velocity components
$u^*$	--friction velocity
$u_f$	--convection velocity scale
$U$	--mean wind speed
$w^*$	--free convection velocity scale

$w^{*'} $	--modified free convection velocity scale
$z$	--height above the surface
$z'$	--height minus displacement length ( $z-d$ )
$z_i$	--planetary boundary layer height
$z_0$	--roughness length
$Z_0$	--effective roughness length

#### Symbol

$\alpha$	--spectral constant
$\beta$	--spectral constant
$\epsilon$	--dissipation rate of turbulent energy
$\kappa$	--wave number
$v$	--count
$\rho$	--density of air
$\sigma$	--standard deviation
$\tau$	--time constant
$\tau_0$	--surface shear stress
$\phi_\epsilon$	--dimension dissipation rate of turbulence
$\phi_N$	--dimensionless dissipation rate for temperature variance
$\phi_m$	--dimensionless wind shear
$\psi$	--adiabatic correction to logarithmic wind profile

## ACKNOWLEDGEMENTS

The authors would like to express their appreciation to Dr. F. S. Binkowski for his frequent and very helpful advice and Dr. S. P. S. Arya for his critical review of the manuscript.

Our graditude also extends to J. W. Ashley, A. Busse and D. H. Coventry for their assistance in the computer aspects of the research, and to C. Rodriques and B. Poole for help in preparation of the manuscript.

## 1.0 INTRODUCTION

### 1.1 PROBLEM AREA

The study of turbulence or eddy motion as a transport process for momentum, heat, and water vapor is basic to understanding and predicting of the structure of the atmospheric boundary layer. Under stationary, homogeneous flow conditions the spectra and cross-spectra of the turbulent components of the wind, temperature, and moisture provide a complete description of the turbulence structure at the height of measurement, and are usually analyzed in terms of three features:

- a) the shape of the spectrum or cospectrum as a measure of the distribution of the variance or covariance as a function of wavelength or frequency;
- b) the integral scale, which is usually assumed proportional to the location of the peak in the spectrum; and
- c) the total variance or covariance.

These features, particularly the latter two, are directly relevant to diffusion of pollutants in the atmosphere.

Obtaining turbulent fluctuation data and subsequent computing of spectra and cospectra are difficult and costly. The study of turbulence, therefore, is often a process of defining physical concepts that are based largely on the interpretation of empirical data, and organizing these results into a theoretical or empirical framework such that the turbulent structure can be deduced from the relevant driving parameters. This process is usually accomplished within the framework of similarity theory, where turbulence is assumed dynamically similar over any surface when properly scaled.



For flow in the surface boundary layer above low and homogeneous roughness features, Monin and Obukhov (1954) similarity theory provides a reasonable description and parameterization of mean flow and turbulent processes (see Ariel' and Nadezhina, 1976; Monin and Yaglom, 1965). By contrast, the turbulent structure of boundary layer flows over large and irregular roughness features is poorly understood. Monin-Obukhov similarity theory does not contain a length scale characteristic of the roughness elements, and is thus valid only away from the direct influence of the roughness features (Tennekes, 1973). Wind tunnel studies have provided valuable insight on the nature of ideal flows over rough surfaces (see Counihan, 1971; Raupach et al., 1980), and the effect of change of roughness on mean profiles and turbulent characteristics of the flow field. Numerical models of change-of-roughness flows (e.g., see Peterson, 1969) are helpful to understanding such flows. However, like wind tunnel studies, the models have been applied mostly for neutral conditions, and the necessary closure assumptions are inadequately tested with atmospheric data. Meteorological towers located in nonhomogeneous roughness fields provide a source of atmospheric data; with few exceptions these have been limited to wind and temperature profiles and lacked measurement of turbulence parameters. Relatively little turbulence data have been obtained in the surface boundary layer over the very complex roughness features of an urban area. Such data are important for modeling the mean flow and dispersion processes in these environs.

## 1.2 RESEARCH OBJECTIVES

The research reported here is concerned with the structure of turbulence in the surface boundary layer over a city. It is based on extensive observations of the turbulent wind and temperature above four varied land-use areas in the St. Louis, Missouri, environs. The purpose of the study is to suggest a framework for parameterizing urban turbulence statistics.

The research approach was to seek relations between turbulence parameters based on the interpretation of empirical data. The form of selected nondimensionalized urban turbulence statistics as a function of atmospheric stratification is tested against the form predicted by Monin and Obukhov (1954) similarity theory. In this respect, the empirical specification of similarity relationships resulting from the Kansas (e.g., see Wyngaard et al., 1971) and Minnesota (Izumi and Caughey, 1976) boundary layer experiments are used as a standard for comparing the urban results.

The Monin-Obukhov similarity relationships cannot be expected to hold for urban areas a priori due to the large and nonhomogeneous surface features. The similarity relationships may also be invalid in the turbulent wake region of the roughness elements; at the urban sites in the present study the wake region may extend to the height of measurement (31 m). Thus the specific objectives of this study are:

- 1) to determine how extensively the similarity relationships, as verified empirically for ideal rural sites, apply to urban data; and
- 2) to discuss significant and orderly differences between the

urban results and the similarity predictions in terms of site land-use, i.e., surface scaling, features.

### 1.3 SIMILARITY THEORY

Within the constant stress layer, Monin and Obukhov (1954) similarity theory is a useful tool for making predictions about certain statistics of atmospheric turbulence. According to similarity theory the mean velocity gradients and turbulence characteristics are completely determined by the height  $z$ , the surface momentum flux  $\tau_0/\rho$ , the kinematic heat flux  $H/\rho C_p$ , and the buoyancy parameter  $g/T$ . From these parameters velocity, temperature, and length scales can be defined as:

$$\begin{aligned} u^* &= \overline{-u'w'}^{1/2} \\ T^* &= \overline{-w'T'}/u^* \\ L &= -Tu^{*3}/gk\overline{w'T'}. \end{aligned} \tag{1.1}$$

It follows that any other parameter describing the structure of ideal flow in the surface boundary layer, nondimensionalized by the above scaling parameters, should be a universal function of the only other dimensionless quantity that can be formed, i.e.,  $z/L$ . Such parameters include the velocity and temperature gradients, the second moments of the fluctuations of the velocity components and temperature, spectra and cospectra, and other higher-order quantities. The meaning of  $L$  is that when  $z$  is small compared to the magnitude of  $L$ , mechanical turbulence predominates. For  $z > |L|$ , buoyancy effects become important. Thus  $z/L$  indicates the relative importance of mechanical and buoyancy effects similar to the Richardson number ( $Ri$ ) and can indeed be specified in terms of  $Ri$  (Monin and Yaglom, 1965; Binkowski, 1974; Businger et al., 1971).

The velocity gradient when nondimensionalized by  $kz/u^*$  is a universal function of  $z/L$ :

$$\frac{kzdu}{u^*dz} = \phi_m(z/L). \quad (1.2)$$

With the right-hand side of the above expression equal to unity, Eq. 1.2 is the familiar differential equation of the logarithmic wind profile that has been established and verified for neutral stratification by laboratory and field experiments. Thus as  $z/L$  tends to zero, i.e., neutral stratification,  $\phi_m(z/L) \rightarrow 1$ . In the asymptotic limits as  $z/L \rightarrow -\infty$  and  $z/L \rightarrow +\infty$ , similarity theory predicts  $\phi_m(z/L)$  to be proportional to  $(-z/L)^{-1/3}$  and a linear function, respectively (Monin and Obukhov 1954). Businger et al. (1971) presented semi-empirical relationships for  $\phi_m(z/L)$  that in the unstable limit, indicate  $\phi_m(z/L) \sim (-z/L)^{-1/4}$ . While this form is in conflict with the free convective similarity prediction, it is the current basis for estimating the wind profile for homogeneous, stationary conditions. Paulson (1970), Nickerson and Smiley (1975), and Benoit (1977) have integrated Eq. 1.2 (using the Businger et al. form) to obtain mathematical expressions for wind speed in the diabatic surface layer. The Nickerson-Smiley integration was used in this study.

Similarity theory also predicts that the second moments of the fluctuations of velocity and temperature, when appropriately normalized by  $u^*$  and  $T^*$ , are a function of  $z/L$ . Those of interest here are  $-\overline{u'w'} = u^{*2}$  and  $\overline{w'T'} = H/\rho C_p$ , which have constant values of unity when normalized; the horizontal heat flux  $\overline{u'T'}$ ; and the variance of the fluctuations, which are usually considered in terms of the standard deviations  $\sigma_u$ ,  $\sigma_v$ ,  $\sigma_w$ , and  $\sigma_T$ .

The form of the similarity predictions in the asymptotic limits of  $z/L \rightarrow -\infty$ , 0, and  $+\infty$  can be obtained through simple dimensional analysis of the relevant variables. Consider for example:

$$\sigma_w = f(u^*, g/T, \overline{w'T'}, z). \quad (1.3)$$

In the limit as  $\overline{w'T'} \rightarrow 0$  (neutral stratification) the buoyancy parameter must disappear and it can be easily shown that  $\sigma_w/u^*$  should be constant. Similarly, in the limit of free convection the dependence on  $u^*$  must vanish and from dimensional considerations alone it can be shown that  $\sigma_w/u^*$  should be proportional to  $(-z/L)^{1/3}$ . For extremely stable stratification the turbulent eddies are very small such that little exchange occurs between different levels. Thus  $\sigma_w$ , away from the immediate influence of the surface, is independent of  $z$  and from dimensional considerations is proportional to  $u^*$ . The similarity predictions for the relevant second moments are discussed in detail by Monin and Yaglom (1965) and are summarized in Table 1.1.

The empirical verification of the similarity predictions are as yet inconclusive, as well as determination of the functional form of the relations at intervening values of  $z/L$ . Excellent summaries of recent progress in empirical determination of the functional forms are provided by Ariel' and Nadezhina (1976) and Monin and Yaglom (1965). The form of the relationship is agreed upon in general: however, scatter of the data points among the many investigators is large. This scatter is partially due to nonstandard techniques for measuring the stress and heat flux, vertical variation of these parameters in the boundary layer, variations of sampling times, and possibly to the influence of mesoscale circulation features.

Table 1.1. Similarity Predictions for the Relevant Second Moments and Form of the Asymptotic Limits.

GENERAL MONIN - OBUKHOV SIMILARITY PREDICTION	FORM AS $z/L$ GOES TO .		
	$-\infty$	0	$+\infty$
$\overline{u'^2} = u_*^2 f_1(z/L)$	$A_1 u_*^2 (-z/L)^{2/3}$	$A_1' u_*^2$	$A_1'' u_*^2$
$\overline{v'^2} = u_*^2 f_2(z/L)$	$A_2 u_*^2 (-z/L)^{2/3}$	$A_2' u_*^2$	$A_2'' u_*^2$
$\overline{w'^2} = u_*^2 f_3(z/L)$	$A_3 u_*^2 (-z/L)^{2/3}$	$A_3' u_*^2$	$A_3'' u_*^2$
$\overline{T'^2} = T_*^2 f_4(z/L)$	$A_4 T_*^2 (-z/L)^{-2/3}$	$A_4' T_*^2$	$A_4'' u_*^2$
$\overline{u'w'} = -u_*^2 f_5(z/L)$	$-u_*^2$	$-u_*^2$	$-u_*^2$
$\overline{w'T'} = -u_* T_* f_6(z/L)$	$-u_* T_*$	$-u_* T_*$	$-u_* T_*$
$\overline{u'T'} = u_* T_* f_7(z/L)$	0	$A_7' u_* T_*$	$A_7'' u_* T_*$

Similarity theory can be extended to specify relationship between parameters (e.g.,  $\sigma_v/\sigma_u$ ,  $\sigma_w/\sigma_u$ ), correlation coefficients, turbulence intensities, third moments, spectral forms, etc. Thus, to determine any of the normalized parameters in the surface boundary layer, it is sufficient to specify  $u^*$  and  $\overline{w'T'}$ , and to know the functional form of the similarity relationship. These relationships are often the basis for evaluating the importance of the various terms in the set of equations of the turbulent covariances (see Wyngaard and Coté, 1971 and Wyngaard et al., 1971). These equations, when coupled with the equations for mean quantities and for the conservation of species, form a consistent set for the prediction of turbulence and the dispersal of pollutants in the atmospheric surface layer (see Donaldson, 1973).

#### 1.4 URBAN TURBULENCE MEASUREMENTS

Relatively few studies of turbulence within urban environments have been conducted, and these studies for the most part lack temporal and spatial resolution as well as a complete set of parameters for the evaluation of the similarity functions. Graham (1968) reported on the spatial variation of the  $u$  and  $v$  components of turbulent intensity in the urban and rural environs of Fort Wayne, Indiana. The data represented twenty sampling periods and were obtained during nocturnal hours and generally with northwest winds. The standard deviations of the velocity fluctuations were roughly the same for both urban and rural sites. However, wind speeds at the city stations were only about half those at the rural site, such that turbulence intensities were about twice as great for the city sites.



Bowne and Ball (1970) made a more extensive analysis of the same data set, concentrating on data from an urban and a rural tower equipped to measure the stress, mean wind, turbulent components of the wind, and Richardson number. Ratios  $\sigma_u/u^*$ ,  $\sigma_v/u^*$ , and  $\sigma_w/u^*$  at the rural site were comparable to those measured in other homogeneous terrain studies and were slightly lower than those for the urban site. Spectral analysis of the wind fluctuations indicated a shift of energy to higher frequencies at the urban site. Urban studies by Brook (1972) and Peschier (1972) showed turbulence intensity to be primarily dependent on roughness features, which varied as a function of wind direction. Jones et al. (1971), reporting on tethered balloon measurements to about 300 m above two urban sites in Liverpool, England, found the neutral wind velocity power law exponent to be about 0.21.

Yokoyama (1971) made an extensive study of turbulence parameters at 45, 180, and 313 m on a tower in a suburban area north of Tokyo; however, the tower was surrounded by open areas to a minimum distance of 1 km. His results indicate the similarity relationship for  $\sigma_w/u^*$  (where  $u^*$  was determined locally) for neutral stratification holds to 313 m, with the proportionality constant being about 1.16. Wamser and Müller (1977), reporting on vertical spectral scale lengths at a suburban tower near Hamburg, Germany, found that roughness lengths in the vicinity of the tower were a function of wind direction. Their results indicate a decrease of the vertical spectral length scale with increasing roughness, and a dependence of the spectral length scale on  $z/L$  similar to that for sites with small homogeneous roughness features. Jackson (1978) discussed turbulence parameters and wind and temperature



profiles from a 70 m tower at an urban site in Wellington, New Zealand; he found the power law velocity profile exponent to be about 0.5 for neutral stratification. Jackson's analyses of turbulence intensities, local friction velocity, and spectral scale lengths suggest a universal structure of turbulence over the exceptionally rough terrain.

Ramsdell (1975) reported on power spectral shapes, variances, and length scales from three-dimensional wind velocity measurements at an urban site, an open suburban area, and an airport in Seattle, Washington. Ramsdell concluded that the urban turbulence structure does not differ significantly from that observed over flat terrain. His analyses, however, were based on only 25 hours of data, and he lacked a direct measurement of stratification.

The papers noted above represent the bulk of turbulence measurements over urban areas in the past 10 years. Although hardly definitive, many of the results are qualitatively consistent with similarity theory to the extent that some urban turbulence statistics can be described as a function of  $z/L$  and the intensity of turbulence is a function of surface roughness. Similarity theory, however, does not predict a dependence of the vertical scale length on surface roughness.

### 1.5 SCOPE AND CONDUCT OF STUDY

The analyses in this study are based on high resolution measurements of the three components of the wind and temperature, at 31 m above four land-use areas in the St. Louis environs. Profile data were not obtained and thus the study is limited to turbulent quantities. In other respects the data are extensive, covering a total of nine weeks during two seasonal periods; about 3800 hours of data were obtained and

processed. With few exceptions (to be discussed later) all the data were used in the analyses, i.e., the data were not screened to eliminate nonstationary periods or nonhomogeneous flow situations.

A primary objective of the study is to relate the turbulent structure to land-use features. Site land-use characteristics are described and surface roughness lengths are determined for each of the sites at the outset. The relevant wind and temperature variances and covariances are presented for the four sites and analyzed within the framework of Monin-Obukhov similarity theory. The results are discussed with respect to the surface roughness lengths determined for the individual sites, and are compared to similar observations and analyses presented by other investigators as representative of turbulent flow above small and homogeneous roughness elements. The spectral characteristics of the turbulent fluctuations (spectral shapes, peak wavelengths, and energy dissipation rates) are determined and compared with similar analyses from the Kansas and Minnesota boundary layer studies. Emphasis is placed on the vertical velocity component. Finally, the results of the analyses are summarized and discussed with respect to the turbulent energy budget.

## 2.0 EXPERIMENTAL PROGRAM

### 2.1 REGIONAL AIR POLLUTION STUDY

The data for this study were obtained during intensive field programs within the framework of the Regional Air Pollution Study (RAPS). The RAPS program, conducted in St. Louis, Missouri, from 1973 through early 1977, had as its prime purpose the collection of a complete and accurate data base for use in development, modification, and evaluation of urban air quality simulation models (Schiermeier, 1978). The basic component of RAPS, the Regional Air Monitoring System (RAMS), consisted of a 25-station aerometric network (Figure 2.1). In addition to extensive air quality measurements, all stations were equipped to measure wind direction and wind speed. Temperature difference between 5 and 30 meters, atmospheric pressure, direct and diffuse solar radiation, and infrared sky radiation were measured at selected stations. Special intensive field studies lasting about six weeks were conducted within RAPS about twice yearly. During these periods, research support was provided to principal investigators on special projects related to the overall purpose of RAPS. One such project was the study of the turbulent structure of the urban surface boundary layer reported herein.

### 2.2 ST. LOUIS ENVIRONS

The city of St. Louis, Missouri, lies on the west bank of the Mississippi River about 16 km south of the conjunction of the Mississippi and Missouri Rivers (see Figure 2.1). The city proper has a population of about 622,000 in an area of 158 km<sup>2</sup>, and extends along the Mississippi River for 31 km and westward approximately 11 km. The

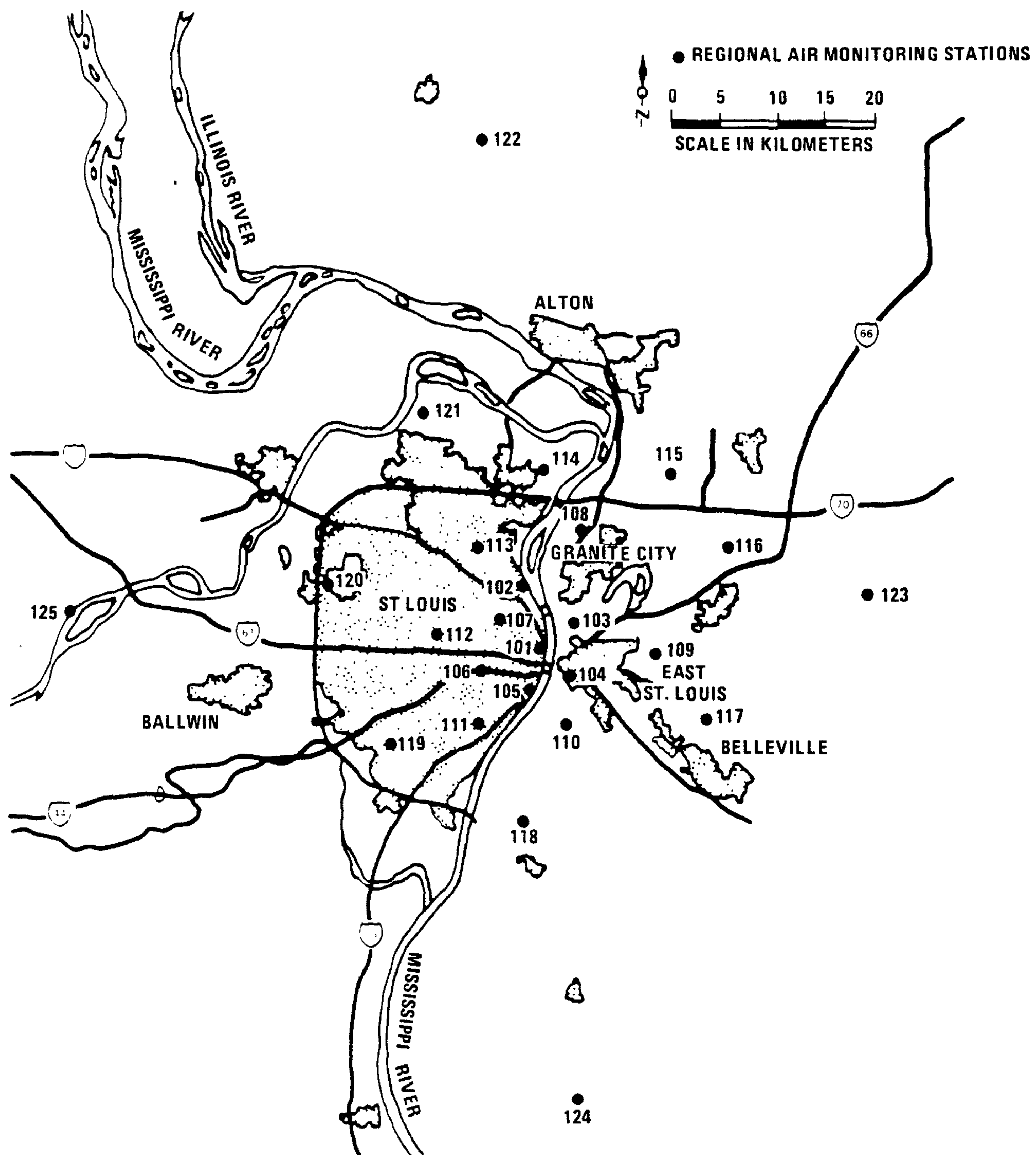


Figure 2.1. Map of St. Louis metropolitan area showing the 25-station RAMS network and major population centers (shaded).

metropolitan area, which includes communities on both sides of the Mississippi, has a population of 2.4 million in an area of 7,203 km<sup>2</sup>. The major population areas are shaded in Figure 2.1.

The elevation of the terrain in the St. Louis area varies from 122 m MSL (elevation of the river) to about 184 m. The west bank of the Mississippi rises abruptly to the city. A flat area, known as the American Bottoms, with an average elevation of about 128 m, extends to about 15 km east of the river. Topographic features for the city of St. Louis are shown in Figure 2.2.

### 2.3 TURBULENCE PROGRAM

During the RAPS 1976 summer intensive field program, special instrumentation was mounted atop 30-m RAMS towers at sites 105, 107, 109, and 111 (see Figure 2.1) to measure the three-component turbulent wind and temperature fluctuations. In addition, humidity fluctuations and net radiation were measured at sites 105 and 109. Starting and ending dates of instrument operation and total hours of data obtained are given in Table 2.1.

#### 2.3.1 Description of Sites and Measurements

Site 105 was located in a high density urban commercial area 3 km south of the urban center and 1 km west of the Mississippi River. Land in the vicinity of the station was used for trucking, warehousing, and commercial operations. Buildings, predominately two-story and of large aerial extent, contributed about 25% of the land-use features. About 60% of the area was paved; the remainder was primarily lawn with a few small trees along the streets. Figure 2.3 is an aerial view from the



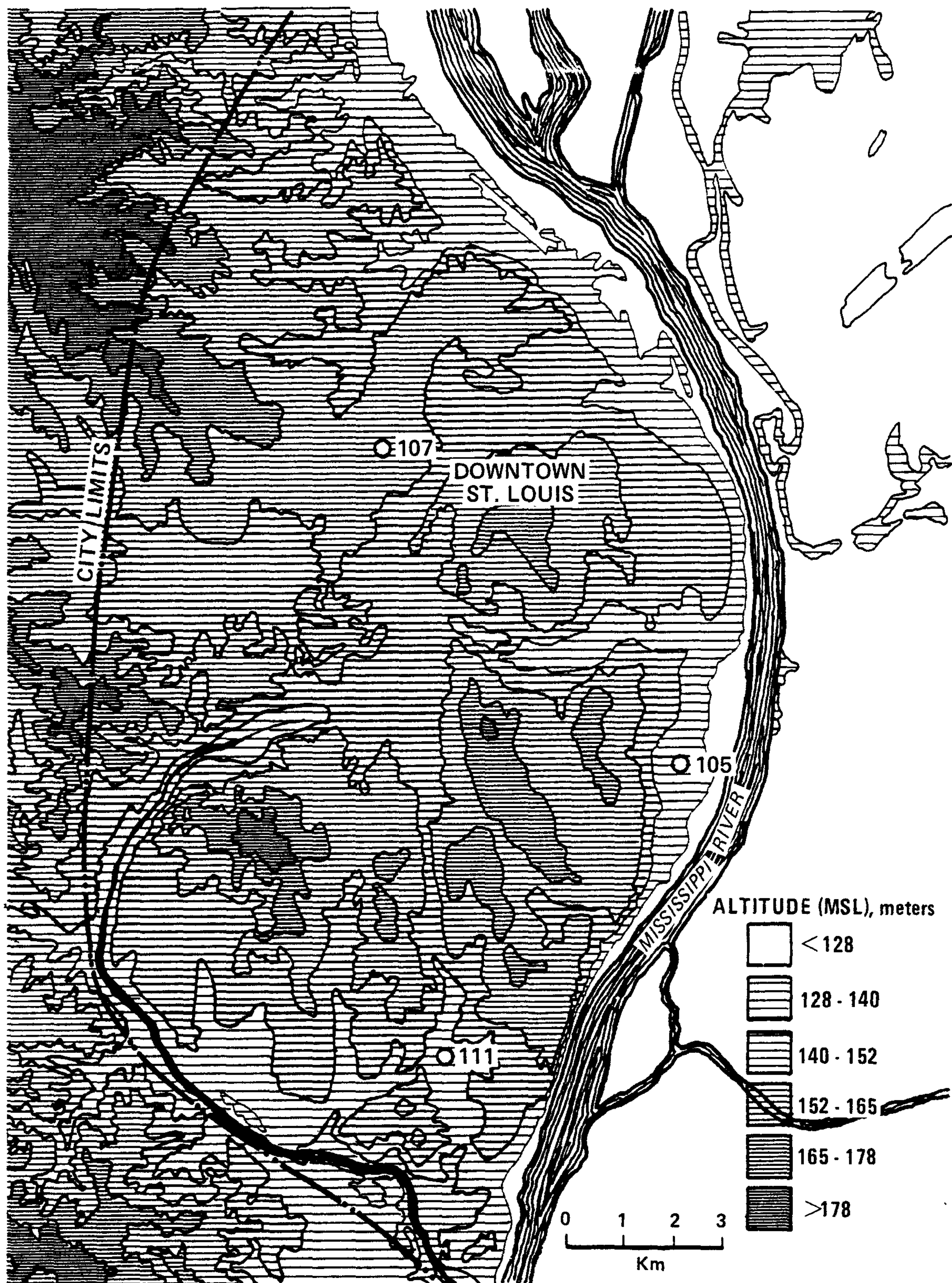


Figure 2.2. Topographic map of the city of St. Louis.

Table 2.1. Starting and Ending Dates of Instrument Operation and Total Hours of Data Obtained for Each Site and Experimental Period.

SUMMER			
SITE	INSTRUMENT	DATES	HOURS
105	Gill UVW	July 21 to Aug 31	855
	Temperature	July 28 to Aug 31	673
	Humidity	July 28 to Aug 7	63
	Net Radiation	July 18 to Aug 31	1030
107	Gill UVW	July 28 to Aug 31	603
	Temperature	July 26 to Aug 31	593
109	Gill UVW	July 20 to Aug 31	695
	Temperature	July 20 to Aug 30	691
	Humidity	Aug 9 to Aug 13	26
	Net Radiation	July 15 to Aug 28	1038
111	Gill UVW	July 21 to Aug 13	321
	Temperature	Aug 1 to Aug 13	208
FALL			
105	Gill UVW	Oct 26 to Nov 20	449
	Temperature	Oct 26 to Nov 20	447
107	Gill UVW	Oct 26 to Nov 20	419
	Temperature	Oct 26 to Nov 20	386
109	Gill UVW	Oct 26 to Nov 20	459
	Temperature	Oct 26 to Nov 20	453

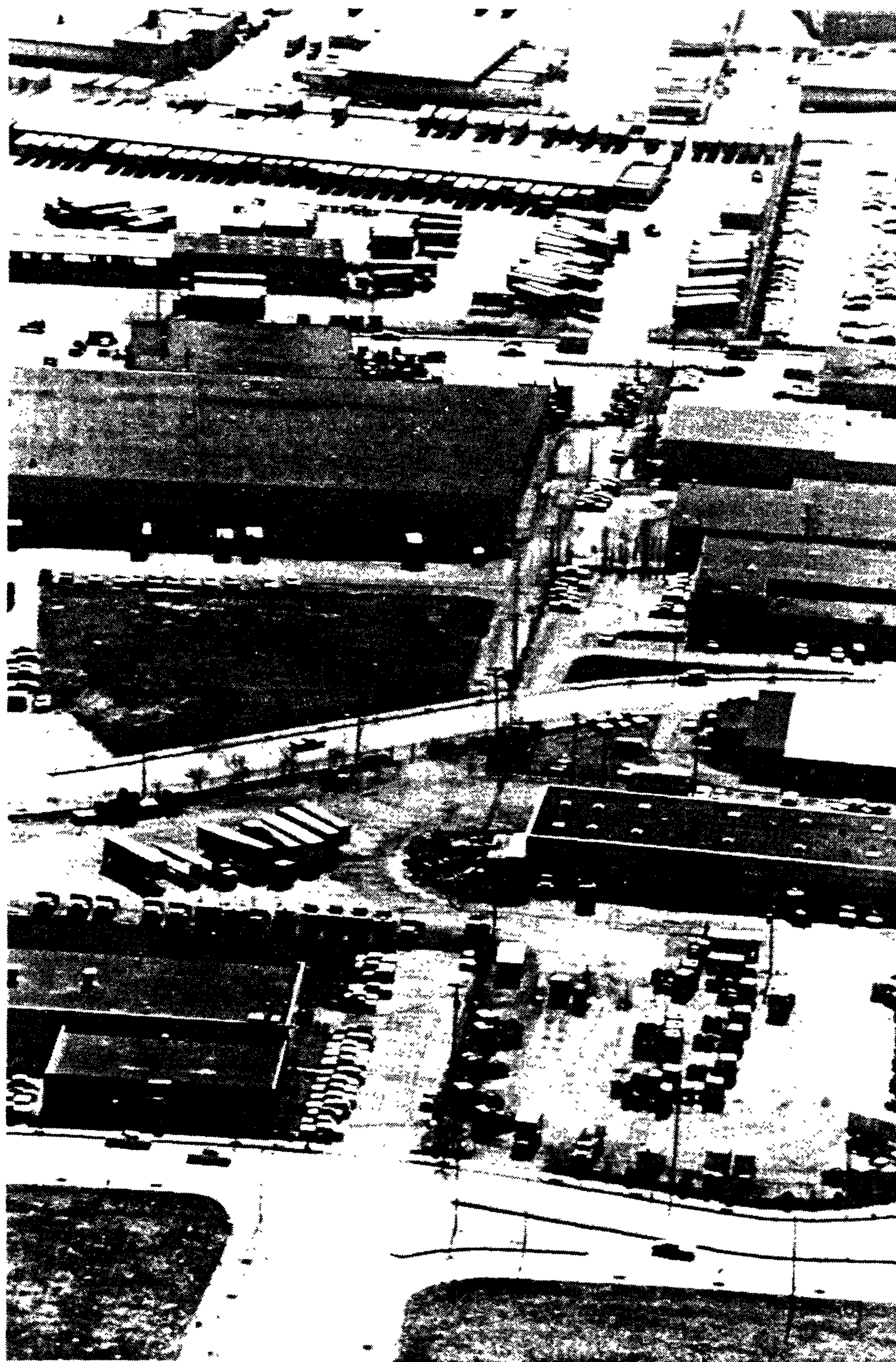


Figure 2.3. Aerial photograph of site 105 looking southwest.



northeast showing the surface features in the vicinity of the tower. The elevation of the site was about 131 m. The terrain is relatively flat to the northeast through south, but rises abruptly to the southwest through north. Topographic features for sites 105, 107, and 111 are shown in Figure 2.2. Special instrumentation at site 105 included a Gill UVW anemometer, a fast response temperature system of in-house design, and a Lyman-alpha humidimeter. All instruments were located at the top of the tower. Figure 2.4 is a photograph of the tower at site 105 with the Gill anemometer mounted at the top. The temperature sensor was located on the w-propeller arm, which was approximately 31 m above the surface. Values from these systems were recorded every 1/2 second in the RAMS data acquisition system. A Swissteco net radiometer was extended 2 m from the tower about 29 m above the surface. Output from this system was recorded on strip charts.

Site 107 was located in the northwest section of St. Louis about 6 km from the center of the city. Land use for several kilometers surrounding the site consisted mostly of older single family and duplex two-story dwellings. Population density is high and the area is considered urban in nature. However, in contrast to site 105, about 60% of the land area is covered by trees or grass. Twenty-five percent of the land is used for buildings; streets and other paved surfaces make up the remaining 15%. Figure 2.5 is a photograph taken from the tower looking north. The site was located on a small north-south ridge at an elevation of 158 m (Figure 2.2). Special instrumentation at the station consisted of a Gill anemometer and a fast-response temperature system exposed as described for site 105.

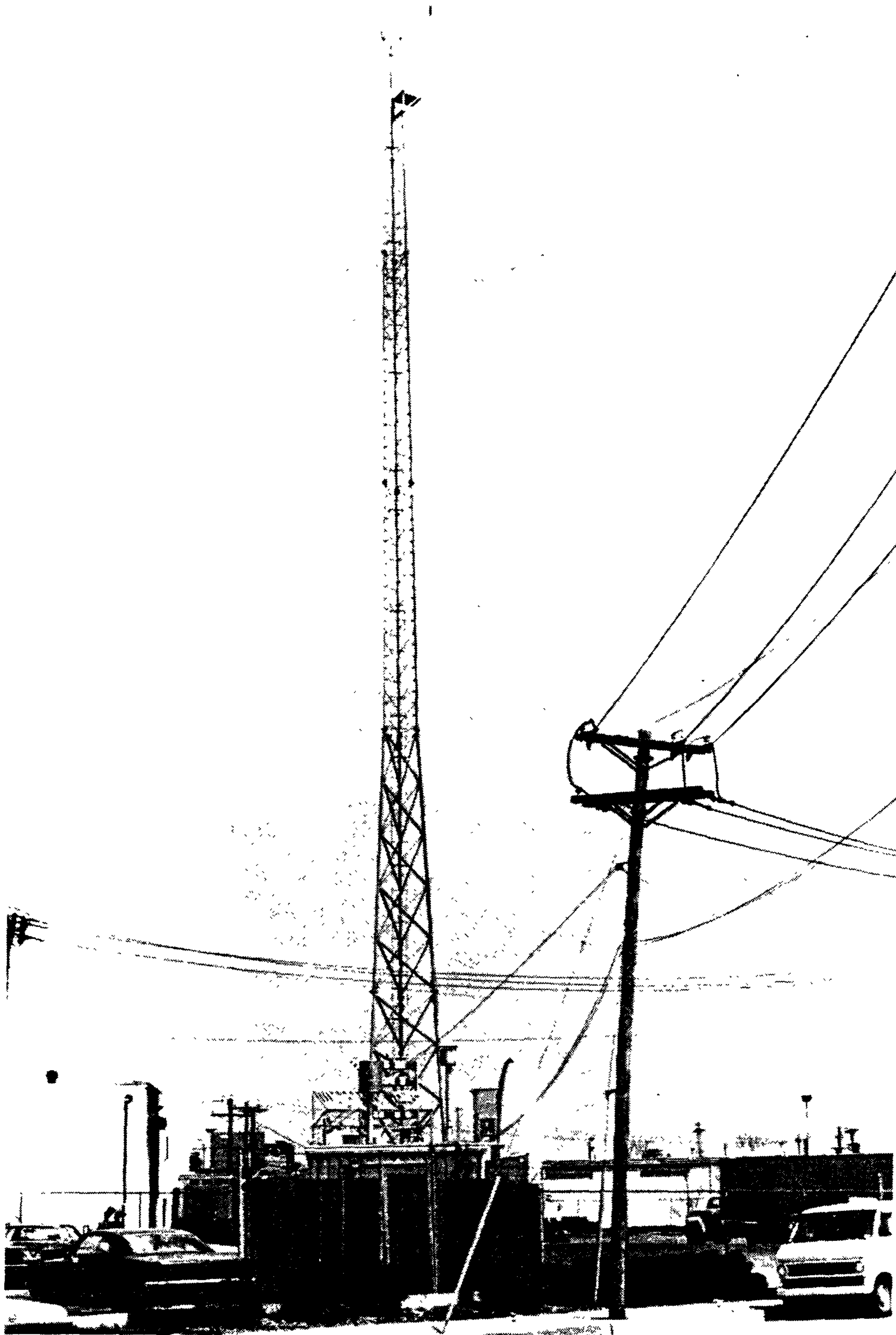


Figure 2.4. Photograph of tower at site 105.



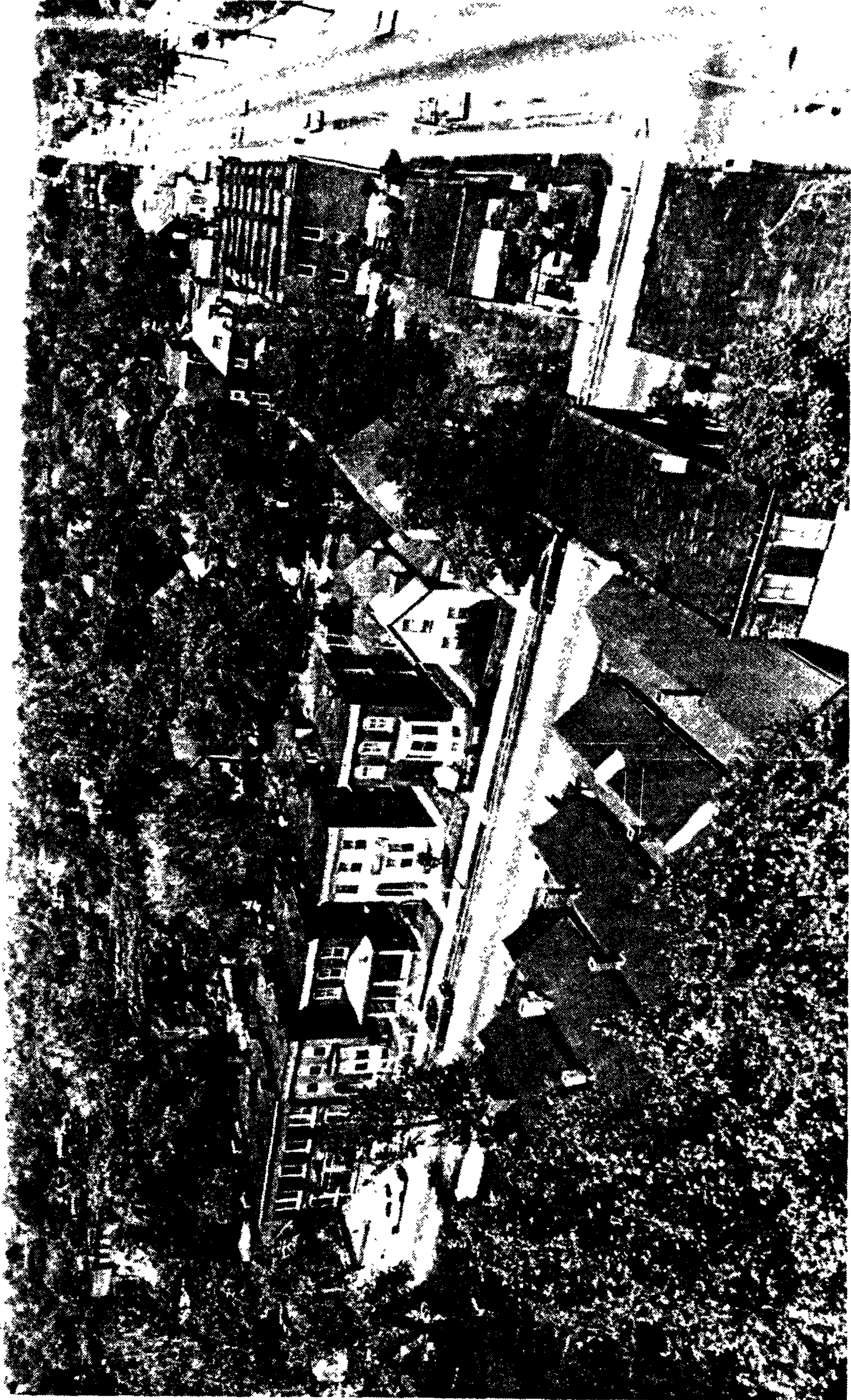


Figure 2.5. Photograph from tower at site 107 looking north.

Site 109 was located in a rural agricultural area about 10 km east of the city. Farm land generally surrounded the station; however, a group of farm buildings was located in the immediate northeast quadrant, and small trees and underbrush in the immediate southeast quadrant. Small fields separated by hedgerows and scattered homes characterized the land use at greater distances in the easterly quadrants. Figure 2.6 is an aerial view of the station looking northwest, showing these features and the relatively flat land of the American Bottoms (elevation 128 m MSL). A bluff rising 67 m lies approximately 5 km to the east. Special instrumentation and exposure were the same as for station 105. Only one Lyman-alpha humidimeter was available to the program. This instrument was moved from site 105 to site 109 on 9 August and removed 13 August.

Site 111 was located in an older residential community approximately 9 km southwest of the urban center. The area immediately surrounding the site was utilized primarily for high-density single family residences. A lumber yard was located about 65 m east of the station and a small sand and gravel plant 0.5 km to the north. Figure 2.7 is a view from the tower looking east over the lumber yard and some of the larger roughness features. Figure 2.8 is a view looking southwest over the residential community. Buildings at an average height of 7.5 m covered about 15% of the area and trees averaging about 13.5 m made up about 25% of the land use. The site was located in a small valley at an elevation of 134 m (Figure 2.2) with terrain rising 30 m within 3 km to the northwest through the northeast. Special instrumentation at the site consisted of a Gill UVW anemometer and a fast response temperature sensor.





Figure 2.6. Aerial photograph of site 109 looking northwest.





Figure 2.7. Photograph from tower at site 111 looking east.





Figure 2.8. Photograph from tower at site 111 looking southwest.

An abbreviated turbulence measurement program was conducted during the RAPS 1976 fall intensive field study. The three-component turbulent wind and temperature fluctuations were obtained at sites 105, 107, and 109, as described for the summer program, from 26 October to 20 November. Operational statistics for this data set are included in Table 2.1.

### 2.3.2 Instrumentation

#### a. Gill Anemometer--

The Gill UVW anemometer is a three-component wind instrument designed for direct measurements of three orthogonal components of the wind. It employs foamed polystyrene propellers molded in the form of a true generated helicoid. The propellers drive miniature d.c. tachometer generators which provide an analog voltage output directly proportional to the rotation of the propellers. Details of the instrument are given by Gill (1975). The instruments, using maximum-response, 23-cm propellers (catalog numbers 21281 and 21180/27105), had an output of about 2400 mv at 1800 rpm (approximately 9.15 m/sec). The signal, when processed through RAMS data acquisition system, had an output of about 115 mv/m/sec for the horizontal components and 145 mv/m/sec for the vertical component. The RAMS system could detect a change of 2.4 mv providing a resolution of 0.021 m/sec and 0.017 m/sec for the vertical and horizontal components, respectively. Each component of each instrument was calibrated in the EPA wind tunnel and in the field, and individual calibrations varied slightly from the above representative values. The Gill UVW anemometer has been used extensively in micro-meteorological studies by other investigators and thus considerable



information on its limitations and operation for optimum response is available (e.g., see Hicks, 1972; Horst, 1973; Fichtl and Kumar, 1974; Wesely and Hicks, 1975). The response characteristics, calibration, and operation of the instruments used in this study are discussed briefly in Appendix A.

b. Temperature System--

The fast response temperature systems used in the field study consisted of a bead thermistor in a Wheatstone bridge circuit. The thermistor, a Fenwall type G112, had resistances of approximately 23,000, 8,000, and 3,000 ohms at 0, 25, and 50°C, respectively. The voltage output of the bridge circuit was linear from 0 to 5 volts over two pre-selected ranges of 0 to 25°C and 15 to 40°C. (The latter range was used in the summer field study and the former in the fall study.) Thus the system had an output of 200 mv/°C and, when applied through the RAMS data acquisition system, a resolution of 0.012°C.

The time constant of the temperature system, determined from wind tunnel tests, was a function of wind speed as shown in Figure A-2. For speeds between 2 and 5 m/sec, the time constant averaged 0.63 sec, and thus was reasonably matched to the w sensor (see Appendix A). The bead was extremely small, and atmospheric tests indicated that it could be freely exposed without a radiation shield for measurement of temperature fluctuations. The bead thermistor was exposed on the w-arm of the Gill anemometer about 20 cm from the propeller.

c. Moisture and Net Radiation--

The Lyman-alpha humidimeter (see Buck, 1976) and Swissteco net

radiometer measurements were used in an ancillary capacity in this study. The manufacturers' recommendations for calibration and exposure were followed and both instruments were cleaned about every other day of operation. The calibration of the Lyman-alpha changed significantly during the course of the summer field study. The change in calibration, however, was determined to be nearly linear and appropriate adjustments were made to the data.

### 2.3.3 Data Processing

The data acquired during the field studies were computer processed and analysed. Data processing was carried out in three phases. The first phase involved processing the data to obtain the basic turbulence parameters (these procedures are outlined in Appendix B). The second phase was essentially one of printing, plotting, and performing statistical analyses to test theoretical forms and determine empirical relationships between the basic turbulence parameters. The programming and procedures were standard and will not be discussed further. In phase 3, the data were subjected to time series analyses; spectra and turbulent length scales were determined for each of the hourly data series. Computational techniques are outlined in Section 3.3 and Appendix B.

### 3.0 RESULTS

#### 3.1 SURFACE ROUGHNESS LENGTH

Integration of Eq. 1.2 for neutral stratification gives the familiar logarithmic wind profile equation. For flow above tall roughness elements, relative to the height of wind measurement, a zero plane displacement length  $d$ , is customarily introduced, giving the wind profile for neutral stratification by the empirical modification:

$$U = \frac{u^*}{k} \ln \frac{z'}{z_0} \quad (3.1)$$

where  $z' = z - d$ . Thus the wind profile and the stress depend on two physical parameters, the roughness length  $z_0$ , and the displacement length  $d$ , which need be specified for each of the sites at the outset.

The roughness length  $z_0$ , a physical parameter dependent only on the characteristics of the surface, enters (along with  $d$ ) as a boundary condition into the logarithmic velocity profile equation. The roughness length is usually determined from measurements of the wind profile through the neutral surface boundary layer as the height at which extrapolation of the mean profile towards the surface produces a zero velocity. The profile method, although sensitive to errors in the wind measurements, has been used extensively for obtaining  $z_0$ . Counihan's (1975) summary of the results indicate  $z_0$  to vary from 0.0001 cm for calm seas to as great as 7.5 m for urban areas. Oke's (1974) summary of  $z_0$  values for suburban-urban areas ranged from 0.4 m to 4.5 m. Several empirical techniques have been suggested for estimating  $z_0$  from the density and/or height of roughness elements, e.g., see Counihan (1971), Brutsaert (1975), Lettau (1969).

Displacement length is poorly defined and parameterized by comparison with  $z_0$ . This problem is undoubtedly due to the insignificance of  $d$  in Eq. 3.1 above surfaces of relatively small roughness, as was the case in most field programs designed to define the nature of the atmospheric boundary layer. Physically,  $d$  is the displacement of the height of the surface seen by the air flow and resulting turbulent exchange processes, which is due to the presence of the roughness elements. Empirically,  $d$  is the vertical distance that the profile must be shifted such that a straight line can be drawn through a logarithmic plot of the neutral velocity profile. Hanna (1969) suggested a displacement length between 6 and 9 m for the urban environment; it should therefore not be ignored in describing the structure of the surface boundary layer over a city. Attempts to assign a  $d$  value to urban areas using profile data have generally presented considerable problems (see Pasquill, 1970), although efforts to obtain  $d$  above dense vegetation have proven more successful. Brutsaert (1975), in summarizing this work, suggested an empirical form of  $d = 2h/3$ , where  $h$  is the average height of the vegetation.

The above concepts and empirical procedures for determining  $z_0$  and  $d$  may be appropriate for flows of extended fetch over low and uniform roughness elements (i.e., to a surface boundary layer in equilibrium flow). Their validity is questionable at low heights above tall roughness elements, to abrupt changes of roughness, and to roughness elements of varying height and density. All of these conditions exist in an urban area and the flow is likely to "see" different surface characteristics at a fixed location as a function of wind direction and speed and

the height of observation. Thus the adequacy of  $z_0$  values derived for an urban area must be judged in several respects; the consistency of the results with previous studies, the extent to which equilibrium flow conditions exist, and the extent to which the results can be described within a theoretical or empirical framework of the total flow characteristics.

Profile data were not obtained in the present study. Values of  $z_0$  and  $d$ , however, can be estimated based on a visual site survey as suggested by Lettau (1969), using the empirical formulas of both Lettau and Counihan (1971). Derivation of  $z_0$  can also be achieved through the logarithmic profile law (Eq. 3.1), using measured values of  $U$  and  $u^*$  and an estimate of  $d$ . Both techniques were applied in this study and both gave results within the range of  $z_0$  values reported in the literature for urban areas by Oke (1974).

### 3.1.1 Land Use Evaluation of $z_0$

In concept, both  $z_0$  and  $d$  are determined by surface structural features. The behavior of these parameters is obvious in two asymptotic limits of roughness density. As the ratio of the area covered by larger roughness elements  $A_r$  to the total area  $A$  approaches zero,  $z_0$  approaches a finite but small value appropriate to the underlying surface, and  $d$  goes to zero for all practical purposes. As  $A_r/A$  approaches 1.0 (larger roughness elements completely cover the surface)  $z_0$  approaches a small value appropriate to the top surface of the larger elements, and  $d$  tends to the height of the larger roughness elements. Functional relationships for  $z_0$  and  $d$  at intermediate values of surface structural parameters have long been sought by micrometeorologists and fluid dynamicists.

Kutzbach (1961), using bushel baskets on an ice-covered lake, found the ratio of  $z_0/h$  ( $h$  is the height of the roughness elements) proportional to the basket density, to the 1.1 power. Displacement length was determined to be proportional to the same quantity, to the 0.29 power. Lettau (1969) described Kutzbach's data by suggesting the relationship,  $z_0/h = 0.5s/S$ . In this expression,  $s$  is the silhouette area of the average obstacle in the vertical-crosswind plane, and  $S$  is the specific area of roughness elements (total site area divided by the number of roughness elements) measured in the horizontal plane. Businger (1974), also using Kutzbach's data, suggested the empirical form  $z_0/h = 0.5C_1h^2(1-C_2h^2/S)^3/S$ . The constants  $C_1$  and  $C_2$  relate to the geometry of the roughness elements, i.e., their width, height, and separation distance. When the roughness elements are uniformly spaced cubes,  $h^2/S = s/S = A_r/A$ .

Kutzbach's results are based on a maximum ratio  $A_r/A$  of 0.25. Counihan (1971) created roughness densities ranging from 0 to 100% in a wind tunnel. He found  $z_0/h$  increased with increasing  $A_r/A$  to a maximum value of 0.3 at  $A_r/A = 0.25$  and then decreased asymptotically to the roughness length for the underlying baseboard at  $A_r/A = 1.0$ . Counihan has shown that equilibrium flow conditions were not established in the limited fetch of his experiments with the result that  $z_0$  was probably overestimated. He determined the displacement length to be on the order of  $z_0$  up to  $A_r/A = 0.25$ . However,  $d/h$  continues to increase with increasing density, approaching unity at  $A_r/A = 1.0$ . Curves representing the results of both Kutzbach and Counihan for  $z_0/h$  and  $d/h$  as



function of  $A_r/A$  are presented in Figure 3.1. The values of  $d$  from the two experiments are obviously quite different at low roughness densities. It is not clear if this difference is entirely due to the different shapes of roughness elements used in the two cases or to differences in the techniques.

Actual roughness features in urban areas vary significantly from the simple forms for which the above techniques are valid. Figure 3.2 is a diagram of percent land-use type and height estimated for site 107. The miscellaneous category is a gross estimate of vehicles, small structures, and small vegetation. The distribution of roughness elements is very complex, being nonuniform in space, and even in time (roughness effects of trees and other vegetation will vary with season). However,  $Z_0$  and  $d$  values were estimated from the curves in Figure 3.1 based on the average height of the higher roughness features and their spatial coverage.

The percentage of each of four land-use categories (buildings, trees, paved area, and low grass area) in the immediate vicinity of each site was estimated from site visits and studies of photographs taken from a helicopter and from the top of the towers. The average heights of buildings and trees were also estimated. The results for the four sites are given in Table 3.1. They are mainly representative of average features within a 200 to 300 m radius of the sites. Surface features farther upwind may affect the wind structure; however, differentiation of surface features as a function of distance and wind direction was not practical, except for site 109.

Displacement and roughness lengths, estimated for each of the

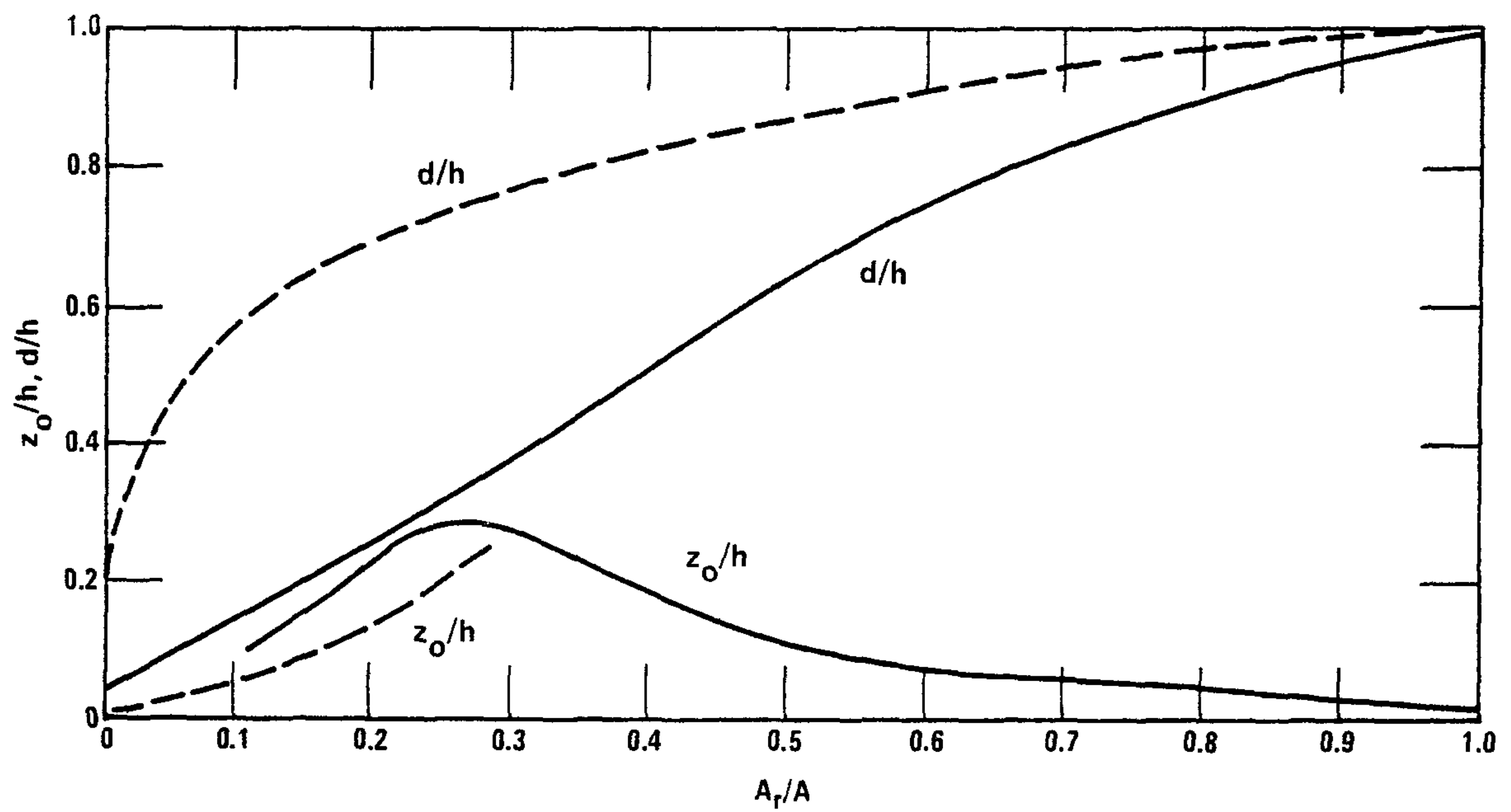


Figure 3.1. The ratios of  $z_0/h$  and  $d/h$  as a function of  $A_r/A$  from the empirical data of Kutzbach (1961) (dashed line) and Counihan (1971) (solid lines).

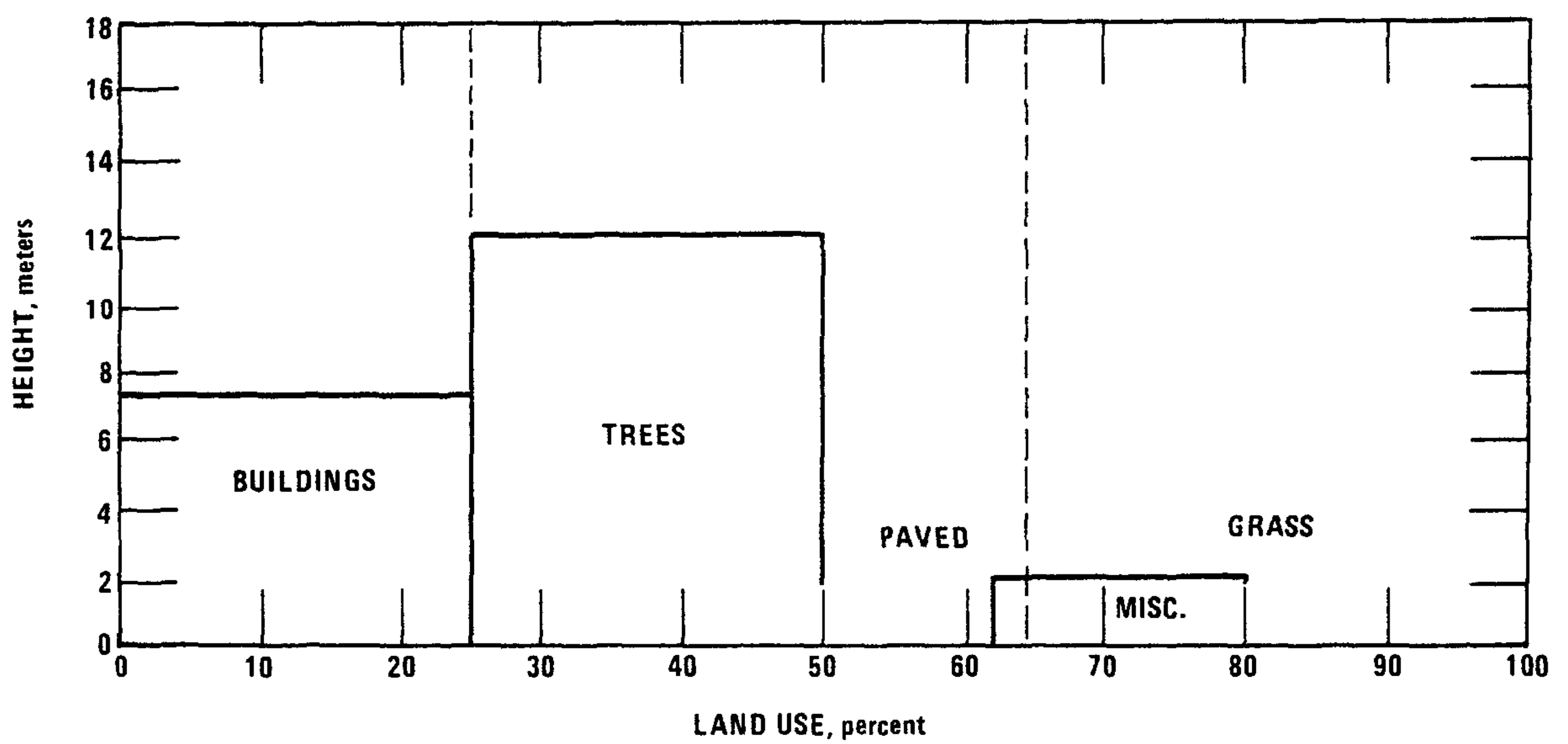


Figure 3.2. Schematic of land-use features and average heights for site 107.



Table 3.1. Site Land-Use Characteristics and Estimated Displacement Lengths (d) and Roughness Lengths ( $z_o$ ) Based on the Empirical Results of Kutzbach (1961) (K) and Counihan (1971) (C), and Average Calculated Values.

SITE	105		107		111		109	
LAND USE	Ar/A	h (m)	Ar/A	h (m)	Ar/A	h (m)	Ar/A	h (m)
BUILDINGS	.25	5.5	.25	7.5	.16	7.5	.05	4.5
TREES	.01	5.5	.25	12	.25	13.5	.05	3.0
PAVED	.59	0	.16	0	.14	0	.01	0
GRASS	.15	0	.34	0	.45	0	.89	0
d(K)	4.0		8.4		9.2		.84	
d(C)	1.65		6.3		5.8		.19	
Z <sub>o</sub> (K)	1.2		*		*		.04	
Z <sub>o</sub> (C)	1.65		1.17		1.89		.06	
CALCULATED VALUES								
d(1)	2		6		6		0	
Z <sub>o</sub> (2)	0.67		1.39		1.71		0.33	
Z <sub>o</sub> (3)	0.67		1.20		1.37		0.46	

\*METHOD OF CALCULATION NOT VALID FOR THIS CATEGORY OF Ar/A.

- (1) ESTIMATED FOR USE IN WIND PROFILE EQUATION (EQ. 3.1)
- (2) CALCULATED FROM PROFILE EQUATION.
- (3)  $Z_o = h/8.15$ .

sites from the empirical relations of both Kutzbach and Counihan, are given in Table 3.1. The values for  $z_0$  for the urban sites are consistent with previously reported values of  $z_0$  for urban-suburban areas (see Oke, 1974). The values for rural site 109 represent an average of individual estimates for four wind direction quadrants. Higher values of  $z_0$  and  $d$  were obtained for the northeast quadrant, which contained 4.5-m buildings, and for the southeast quadrant, which contained 3-m trees.

### 3.1.2 $z_0$ From Similarity Profile Assumption

Because of the height and spatial variation of roughness features, the total stress may result from a combination of form drag on the higher roughness elements (trees and buildings), and skin friction drag on the intervening surfaces. Arya (1975) suggested a region of merging of the two drag effects above the higher roughness elements. Within and above the region of merging, the flow characteristics depend on an "overall roughness parameter" (to be denoted by upper case  $Z_0$ ). This parameter, with sufficient height and fetch for equilibrium flow to be established and under neutral stability, satisfies the modified logarithmic profile law, Eq. 3.1. This equation in the form:

$$Z_0 = \frac{z'}{\exp(kU/u^*)} \quad (3.2)$$

was used to calculate  $Z_0$  for the four sites, using hourly average values of  $U$  and  $u^*$  derived from the tower UVW anemometers and an estimated value of  $d$ . Values of  $d$  used in the calculations are given in Table 3.1. They generally reflect Counihan's results, and like  $Z_0$ , may vary at a given site with wind direction. However, at the height of the

instrumentation of this study,  $Z_0$  is relatively insensitive to variations of  $d$ ; a change in  $d$  of three meters about any of the table values resulted in less than 15% variation in the calculated value of  $Z_0$ .

Surface roughness lengths from Eq. 3.2 using summer data for urban site 107 are shown in Figure 3.3 (circles) as a function of wind direction. The data points represent hourly values for  $u^* > 0.15$  m/sec and  $U > 2$  m/sec (to eliminate possible high noise to signal ratio in the measurement system), and neutral conditions (defined as  $0.05 > z'/L > -0.05$ ). The Nickerson-Smiley (1975) integration of Eq. 1.1, using the form of  $\phi_m(z/L)$  suggested by Businger et al. (1971), was used to extend the  $Z_0$  calculations over the diabatic range of the data. Results of these computations for  $z'/L < -0.1$  (squares) and  $z'/L > 0.1$  (triangles) are also given for site 107 in Figure 3.3. No obvious dependence of  $Z_0$  on stability is found. Surface roughness lengths over the total range of  $z'/L$  for the four sites are shown in Figure 3.4. An obvious wind direction dependence occurs at all sites, but  $Z_0$  also varies considerably for any given wind direction. This latter variation may represent noise in the technique.

The variation of derived roughness lengths averaged over 20 degree wind direction sectors is given in Figure 3.5 for the summer data set. The variation is large and suggests that a single roughness length cannot characterize an urban site (or the rural site). The derived roughness lengths, however, do reflect the general site features, (i.e., average  $Z_0$  values for each of the sites - given on the inset - appear to be a function of the height of buildings and trees). Brutsaert (1975) suggested that  $h/z_0 = 8.15$  to a first approximation. Average

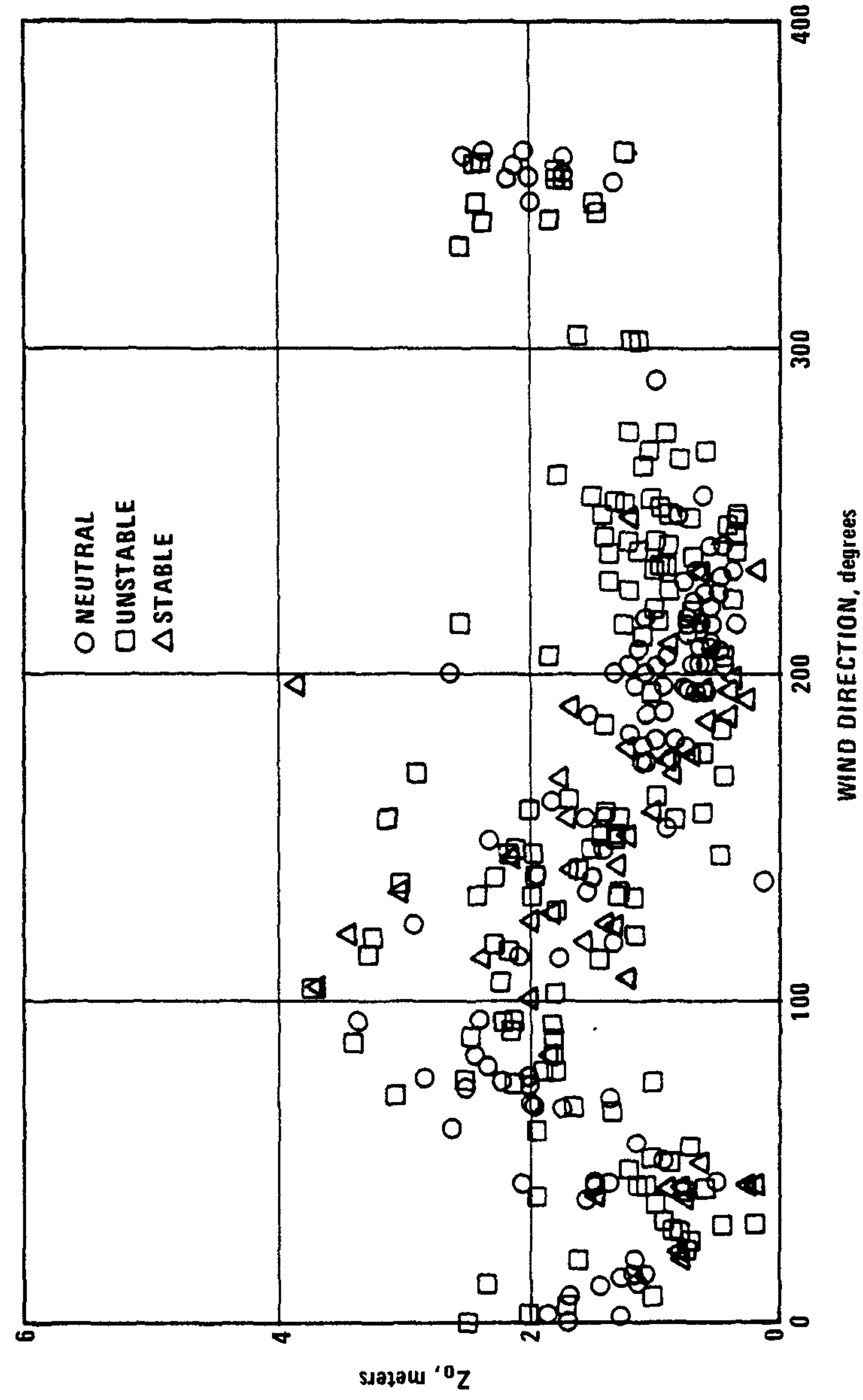


Figure 3.3. Surface roughness lengths vs. wind direction for neutral (○), unstable (□), and stable conditions (△) for site 107 (summer data).

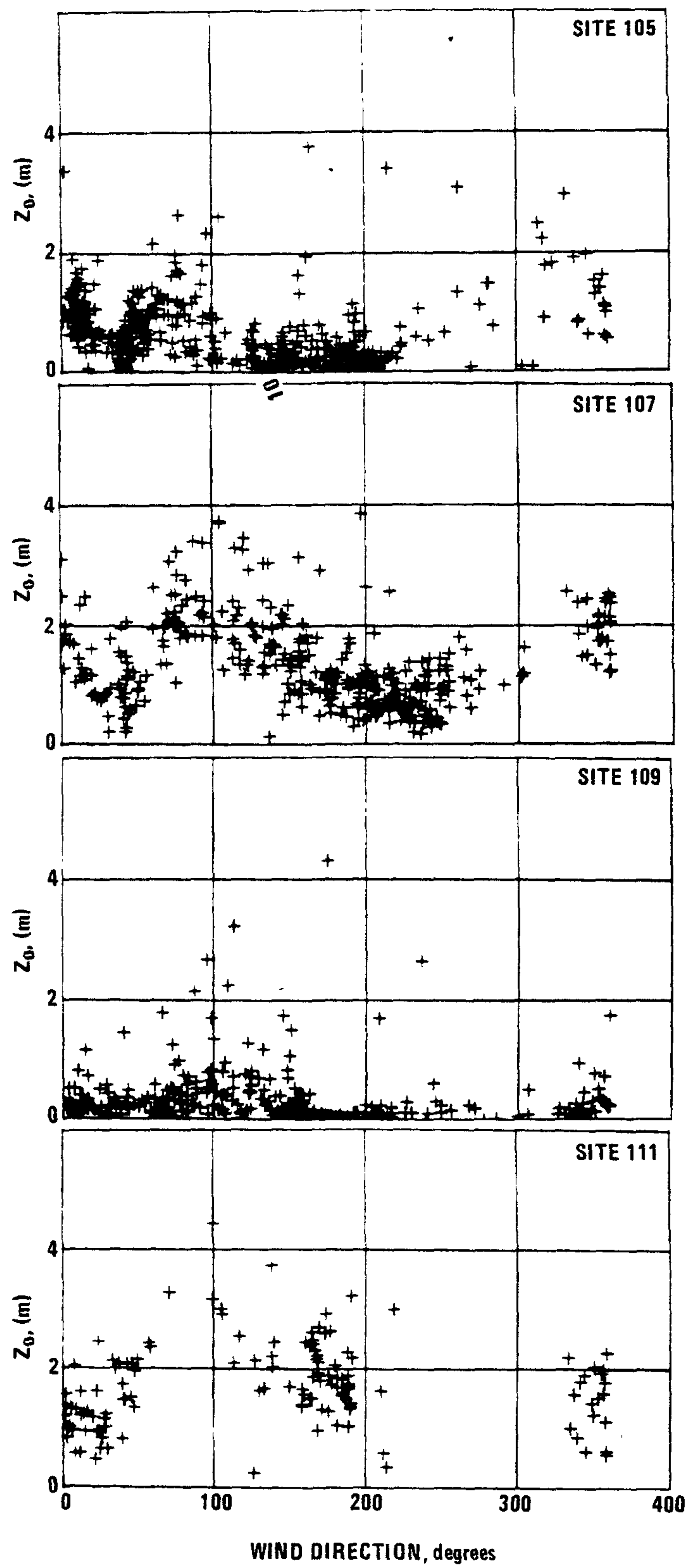


Figure 3.4. Surface roughness length vs. wind direction (summer data).



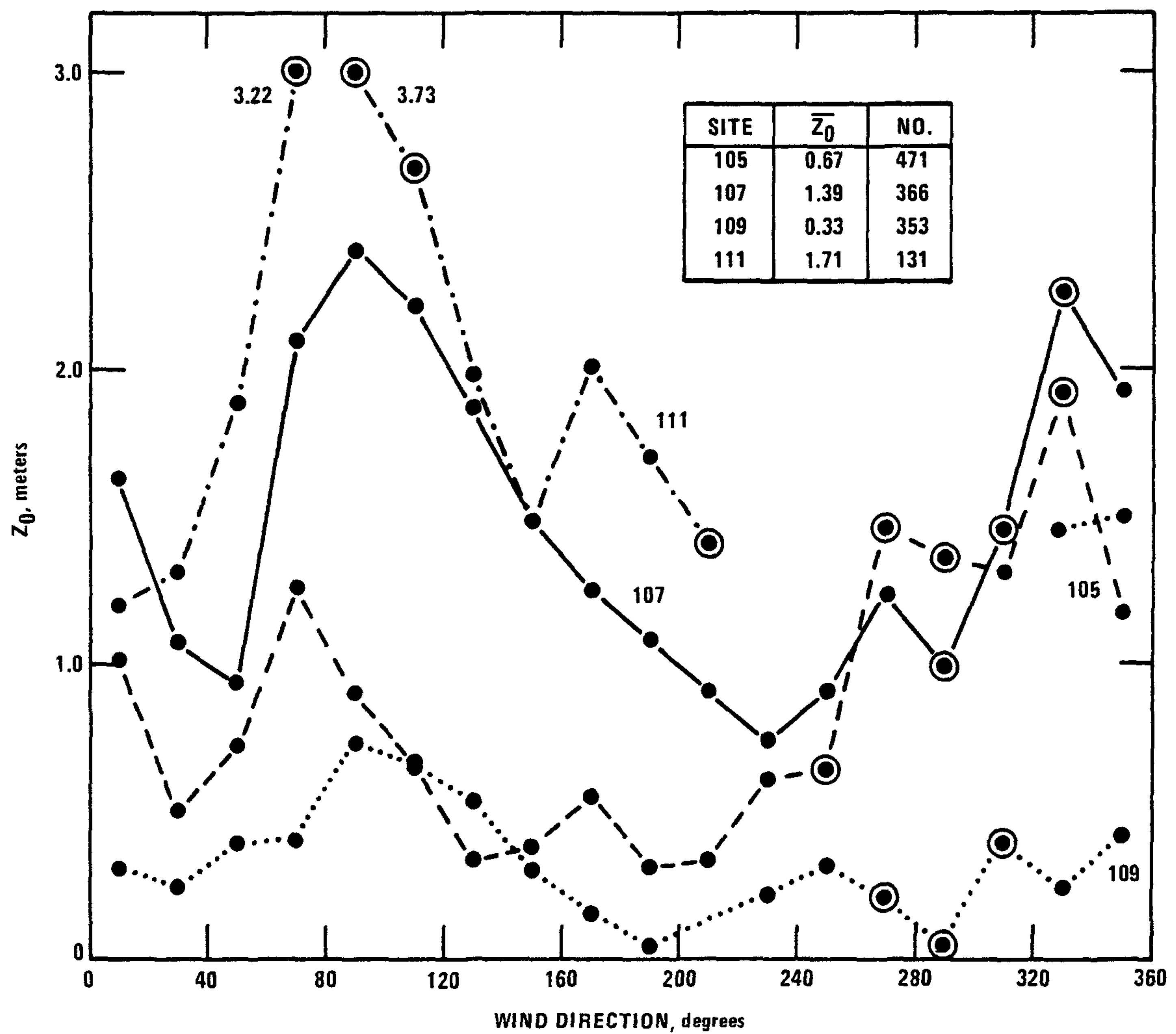


Figure 3.5. Surface roughness length averaged over 20 degree wind direction sectors for the summer data. The inset gives the site average  $\bar{Z}_0$  and number of data points for each site.

calculated  $Z_0$  values for the summer data set and those obtained by Brutsaert's relationship, both shown in Table 3.1, have a definite correspondence.

Roughness lengths similarly calculated for the fall data set (sites 105, 107, and 109) and averaged for 20 degree wind direction sectors are plotted in Figure 3.6. Average values for each site are given on the inset. A seasonal variation of  $Z_0$  is not unexpected at site 107, where deciduous trees comprise 25 percent of the roughness features, and at the rural site (109). Differences in the site average values between summer and fall also reflect changes in the prevailing seasonal wind direction.

The calculated values of  $Z_0$  are extremely sensitive to those parameters contained in the exponential term of Eq. 3.2;  $u^*$ ,  $k$ , and  $U$ . The value of  $u^*$  appropriate to the logarithmic wind profile equation (and also for normalizing the velocity standard deviations in the next section) is the spatially averaged surface value. The values used in this study are determined by the eddy correlation technique from measurements at 31 m above the surface, and thus are "local" values,  $u^*_L$ . They may differ from the average surface values, especially at low heights above tall roughness elements.

The similarity wind profile does not contain parameters representative of the surface roughness features and consequently is valid only at heights away from the direct wake influence of surface features. Tennekes (1973) suggested that the minimum height at which the logarithmic law becomes valid is on the order of  $z = 100Z_0$ , Plate and Quraishi (1965) indicated this height to be  $z > 2h$  ( $h$  is the height of the

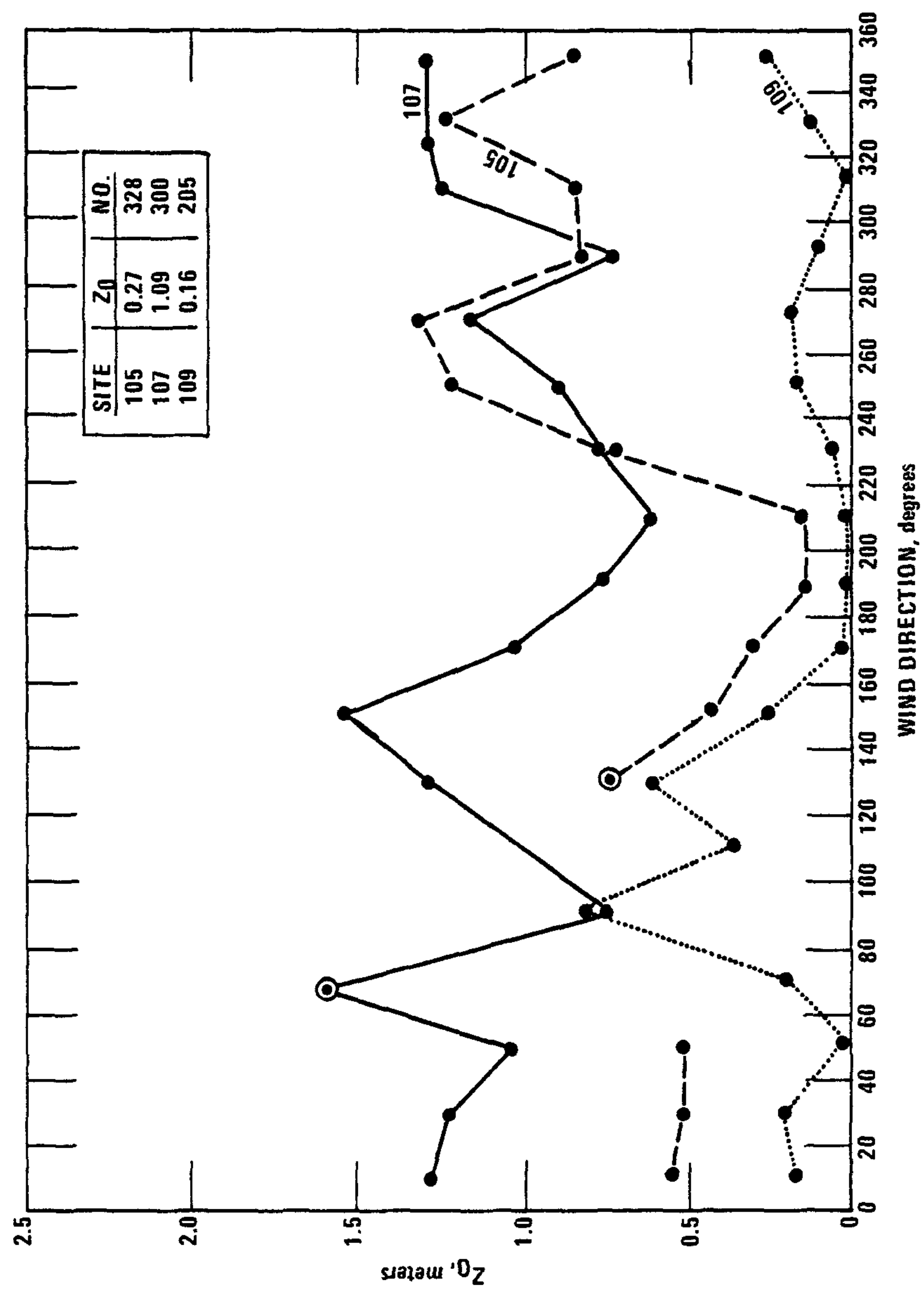


Figure 3.6. Same as for Figure 3.5 for fall data set.

roughness elements), and Garratt (1978a) suggested  $4.5h$ . The nature of the boundary layer in the wake region is uncertain. However, a departure of  $u^*$  or  $U$  by as little as 5% from the profile assumption can result in 25% variation in the value of  $Z_0$ . The calculations are equally sensitive to the value of  $k$ , which has been the subject of recent controversy. There is considerable experimental basis to retain the value at 0.40 (See Hicks, 1976; Garratt, 1977) as was done here.

In spite of these potentially large sources of error, the calculated roughness lengths are in good agreement with those expected from the land-use features and those reported in the literature for urban areas.

### 3.1.3 Application

Urban roughness lengths estimated from land-use features are in general agreement with those calculated through the logarithmic wind profile law. Roughness and displacement lengths may vary by a factor of at least three over an urban area and  $Z_0$  apparently may vary by that magnitude as a function of wind direction at a site selected to be representative of the surrounding land use. The results suggest that an average site roughness length may be obtained from knowledge of land-use features. Although the condition of equilibrium flow has not been demonstrated,  $Z_0$  values calculated from the tower turbulence measurements appear to be reasonable and are used in subsequent attempts to show order to the observed structure of turbulence over St. Louis. In some cases, the average site  $Z_0$  values are used in the analyses. Generally, however,  $Z_0$  values are averaged for the data set corresponding to the turbulence parameters being analyzed.

### 3.2 REYNOLD STRESSES AND TEMPERATURE VARIANCES

The second moments of the velocity and temperature fluctuations are presented in this section and are analyzed and discussed within the framework of Monin-Obukhov similarity theory. The variances  $\overline{u'^2}$ ,  $\overline{v'^2}$ ,  $\overline{w'^2}$ , and  $\overline{T'^2}$  and the longitudinal heat flux  $\overline{u'T'}$ , normalized by  $u^*$  and  $T^*$ , are assumed to be functions of  $z'/L$ . The stress  $\overline{u'w'}$  and heat flux  $\overline{w'T'}$  are unity when normalized, and the lateral component of stress  $\overline{v'w'}$  is theoretically zero in the horizontally homogeneous surface layer. Also discussed are turbulent characteristics specified as a consequence of the similarity relationships, such as the ratios  $\sigma_v/\sigma_u$  and  $\sigma_w/\sigma_u$ , and the turbulence intensities  $\sigma_u/U$ ,  $\sigma_v/U$ , and  $\sigma_w/U$ . These computed quantities are compared for the various sites/seasons and to corresponding relationships reported by other investigators for flow above small and homogeneous roughness elements.

#### 3.2.1 Velocity Variances

##### a. Neutral Stratification--

The similarity predictions for the normalized velocity standard deviations are given in Table 1.1. For neutral stratification (the heat flux approaches zero or at a height very near the surface) the buoyancy parameter has no effect and the velocity standard deviations are given by:

$$\sigma_u = A_1 u^*, \quad \sigma_v = A_2 u^*, \quad \sigma_w = A_3 u^* \quad (3.3)$$

where  $A_1$ ,  $A_2$ , and  $A_3$  are constants independent of height, wind speed, and surface roughness. The data summary of Ariel' and Nadezhina (1976) show this to be the case within limits that can be reasonably attributed



to experimental error. Their results for neutral stratification as given by Binkowski (1979) are:

$$\begin{aligned}\sigma_u/u^* &= 2.3(0.4) \\ \sigma_v/u^* &= 1.9(0.3) \\ \sigma_w/u^* &= 1.3(0.2).\end{aligned}\tag{3.4}$$

The numbers in parentheses are the standard deviation of the observations making up the mean value.

Averages and standard deviations (s.d.) of  $\sigma_u/u^*$ ,  $\sigma_v/u^*$ , and  $\sigma_w/u^*$  are given in Table 3.2 for neutral stratification (defined as  $0.05 > z'/L > -0.05$ ) for each of the sites for both summer (S) and fall (F) data sets. Also given are the number of observations, average surface roughness length for the specific data sets, and the overall weighted averages of the normalized velocity standard deviations. The weighted averages are in good agreement with the values referenced above. The individual means for each of the components were tested against the corresponding component for site 109S for independence of the samples using the Student t distribution. The null hypothesis was that the mean for site 109S was equal to the mean for the other sites at a level of significance of 0.05. The superscripts on Table 3.2 denote those data for which the null hypothesis was rejected. The urban sites generally have significantly smaller values of the ratios than site 109.

The average values of the normalized velocity components (from Table 3.2) for each of the sites/seasons are plotted against the corresponding average  $Z_0$  in Figure 3.7. An apparent inverse relationship exists; as  $Z_0$  increases from 0.2 to 1.6 m,  $\sigma_u/u^*$  and  $\sigma_v/u^*$  decrease about 12% and  $\sigma_w/u^*$  by about 16%. The slope of the regression lines for

Table 3.2. Averages and Standard Deviations (s.d.) of the Normalized Velocity Standard Deviations for Neutral Stratification, Number of Observations (No.), and Average Roughness Lengths for Summer (S) and Fall (F) Data Sets. See Text for Explanation of Superscript.

	NO.	$Z_o$	$\sigma_u/u_*$	s.d.	$\sigma_v/u_*$	s.d.	$\sigma_w/u_*$	s.d.
105S	97	.7	2.36 <sup>+</sup>	.43	1.81 <sup>+</sup>	.39	1.32	.18
107S	107	1.3	2.39 <sup>+</sup>	.26	1.78 <sup>+</sup>	.24	1.17 <sup>+</sup>	.08
109S	29	.2	2.57	.47	2.0	.41	1.33	.20
111S	36	1.6	2.19 <sup>+</sup>	.16	1.72 <sup>+</sup>	.21	1.28	.09
105F	125	.8	2.41 <sup>+</sup>	.22	1.78 <sup>+</sup>	.22	1.29	.15
107F	111	1.1	2.39 <sup>+</sup>	.18	1.74 <sup>+</sup>	.21	1.20 <sup>+</sup>	.09
109F	28	.4	2.54	.37	1.85	.44	1.45	.35
WEIGHTED AVERAGE			2.39		1.79		1.26	

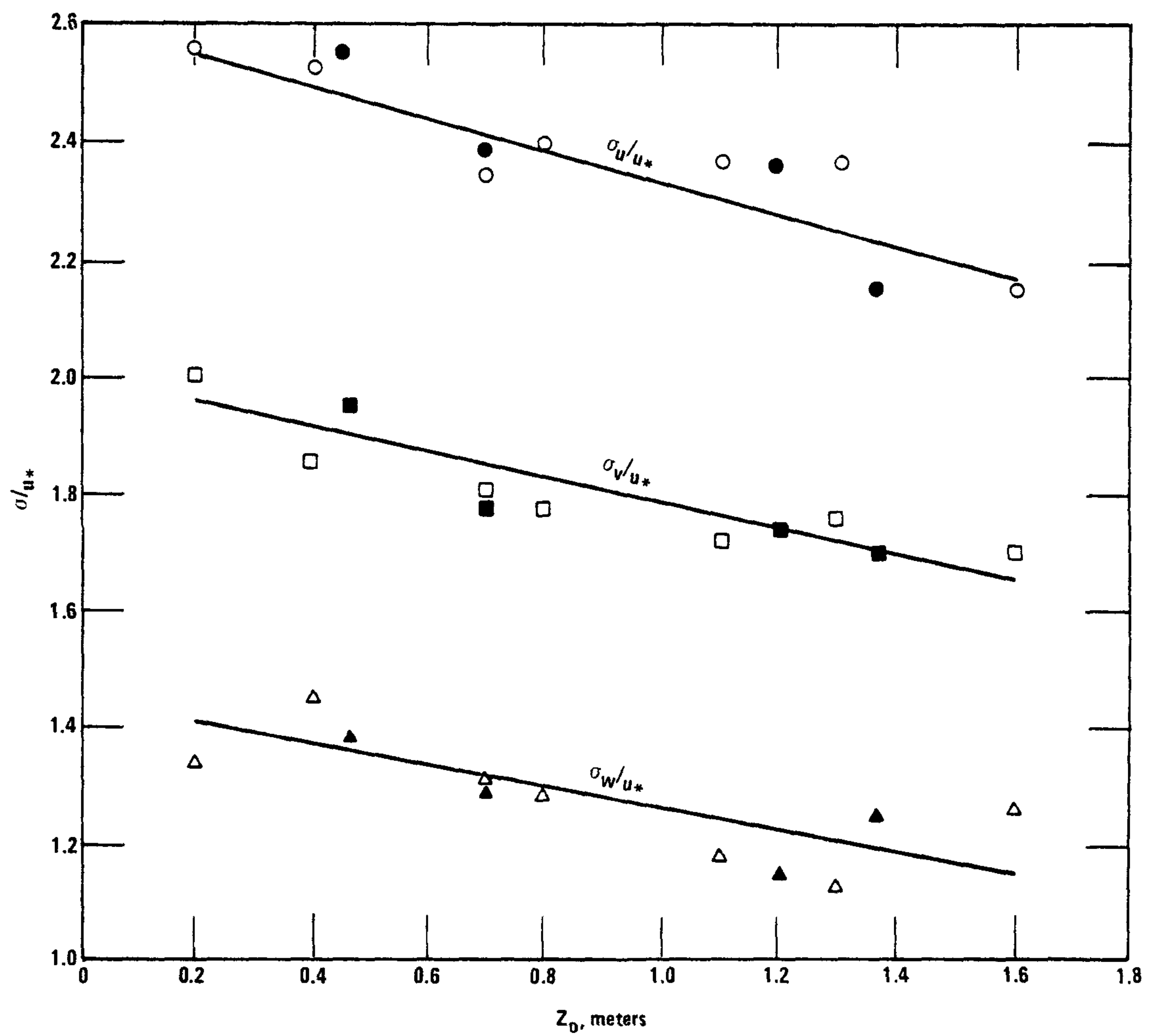


Figure 3.7. Site averaged values of  $\sigma/u^*$  vs. the corresponding average  $Z_0$  and linear regression fits. The solid symbols represent  $Z_0 = h/8.15$  for each of the sites.

$\sigma_u/u^*$  and  $\sigma_v/u^*$  are different from zero at a significance level of 0.05. The slope of the regression line for  $\sigma_w/u^*$  is different from zero at a significance level of 0.10 only if the data point for site 111 ( $Z_0 = 1.6$  m) is not included in the regression analysis. The solid symbols on Figure 3.7 represent  $Z_0 = h/8.15$  (Burtsaert, 1975); they further suggest that the ratios scale with the height of the roughness elements. There was also an apparent relationship between  $\sigma_w/u^*$  and  $Z_0$  for the individual hourly observations. This latter analysis, given in Figure 3.8 for neutral stratification, shows a decrease of  $\sigma_w/u^*$  with  $Z_0$  similar to that in Figure 3.7. Table 3.2 and Figures 3.7 and 3.8 suggest an apparent dependence of the normalized velocity standard deviations on surface roughness.

The similarity prediction that  $\sigma_w/u^*$  is independent of wind speed is tested in Figure 3.9 for the individual sites for neutral stratification. The slope of the least-squares fit to the data points (not shown) is different from zero at a significance level of 0.05 at sites 107 and 111. The slope, however, is positive for site 107 and negative for site 111, suggesting no physical dependence of  $\sigma_w/u^*$  on wind speed.

#### b. Dependence on $z'/L$ --

In the limit of free convection, Monin-Obukhov similarity theory predicts that the normalized velocity standard deviations are all proportional to  $(-z/L)^{1/3}$ . Recent experimental results confirm this prediction for  $\sigma_w/u^*$  (Merry and Panofsky, 1976; Panofsky et al., 1977; Wyngaard et al., 1971). The similarity prediction is also supported by the present data base, as shown in Figure 3.10 (where  $\sigma_w/u^*$  is presented as a function of  $z'/L$  for each of the four sites of the summer

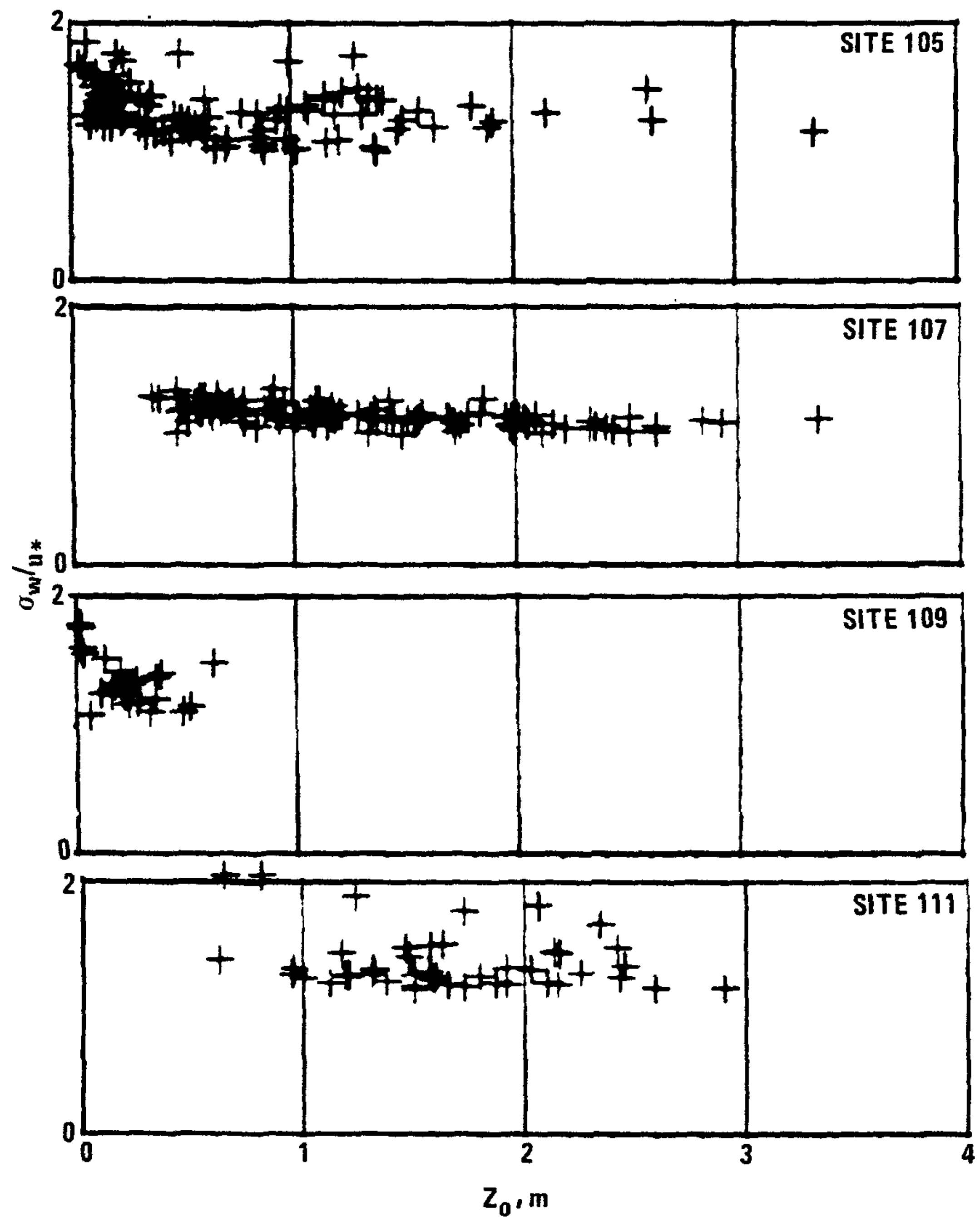


Figure 3.8 Plots for  $\sigma_w/u^*$  vs.  $Z_0$  for neutral stratification (summer data set).



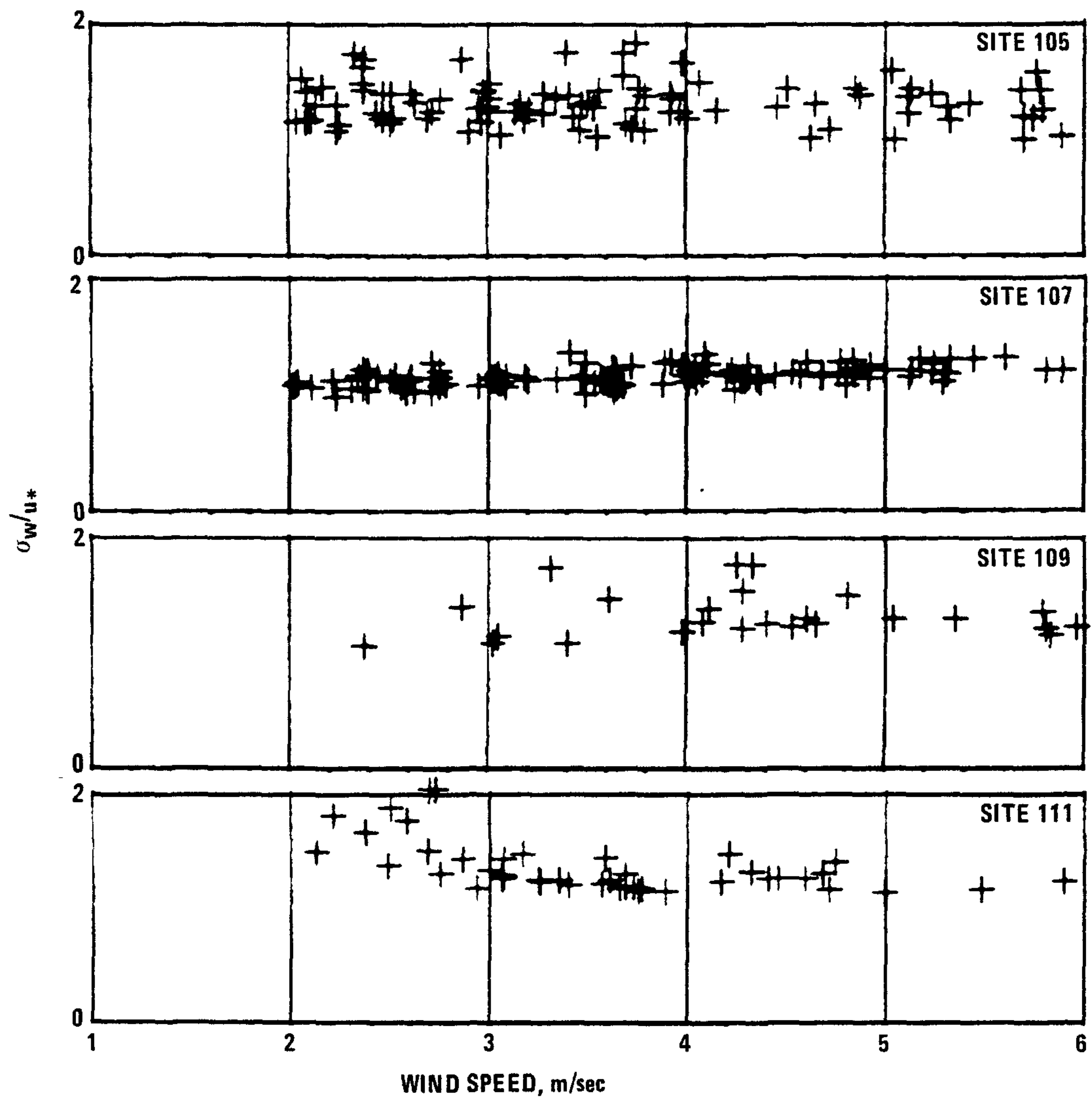


Figure 3.9 Individual data plots for  $\sigma_w/u^*$  vs.  $U$  for neutral stratification for the four sites (summer data set).

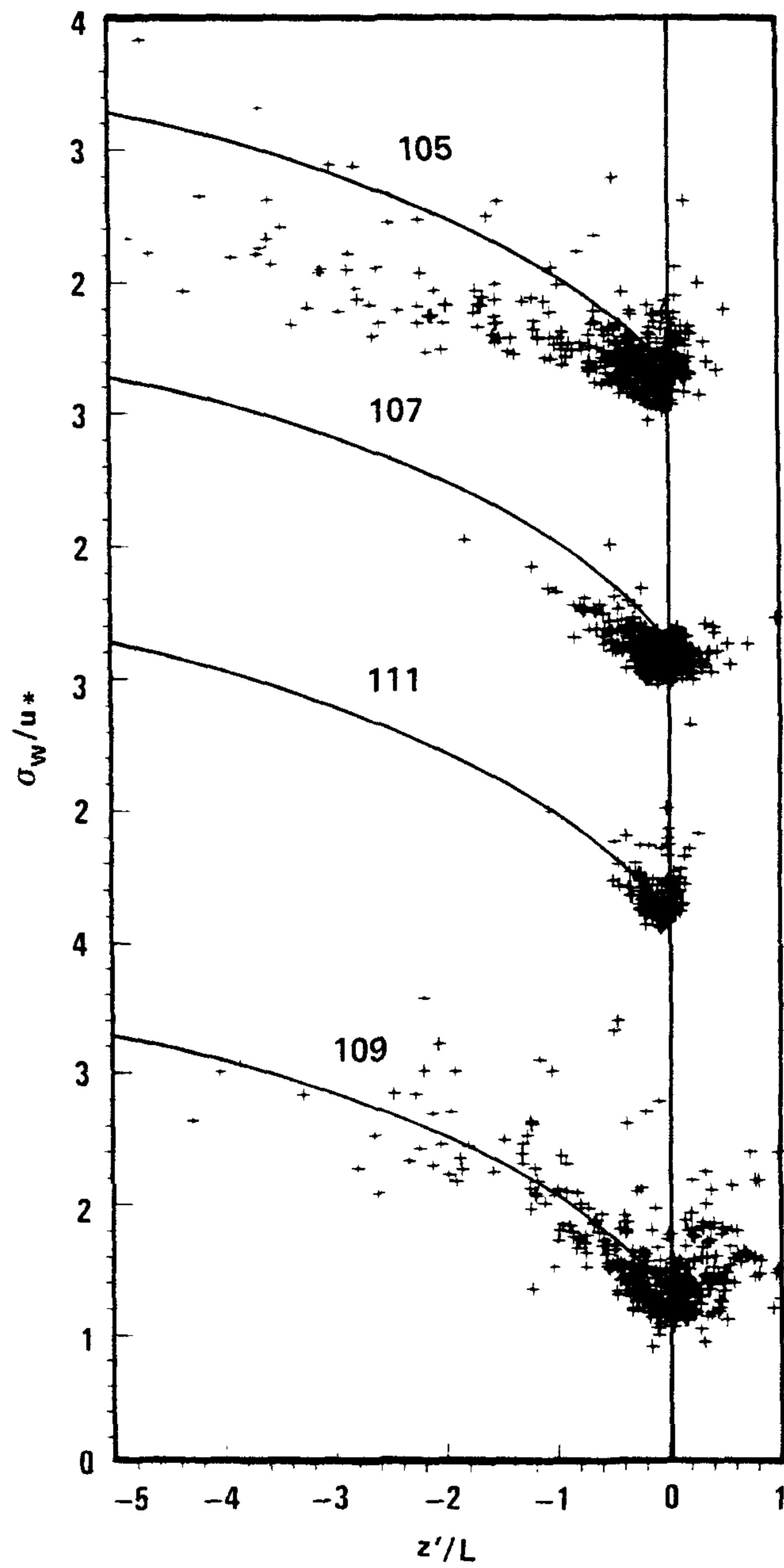


Figure 3.10  $\sigma_w/u^*$  vs.  $z'/L$  for summer data set. The solid line represents the Panofsky et al. (1977) empirical fit to tower and aircraft data ( $\sigma_w/u^* = 1.3 (1-3z/L)^{1/3}$ ).

data set). The solid line, given by  $\sigma_w/u^* = 1.3(1-3z'/L)^{1/3}$ , represents the Panofsky et al. (1977) empirical fit to tower and aircraft data. There is a difference in the plots for the rural site (109) and the urban sites. The data for site 109 are in reasonable agreement with the Panofsky et al. curve, whereas the data for the urban sites are lower in magnitude, especially in the region of forced convection (i.e., small negative values of  $z'/L$ ). The data plots for site 105 extend to large negative values of  $z'/L$ , and although the values are smaller than expected from the Panofsky et al. form, the slope approaches a  $1/3$  power law as suggested for free convection similarity (Deardorff and Willis, 1975).

The trend in  $\sigma_w/u^*$  for large negative  $z'/L$  cannot be considered a conclusive test for the free convection similarity relationship. A pseudo-correlation may be introduced because  $\sigma_w$  is normalized by  $u^*$  and  $z'/L$  contains  $u^{*3}$  in the denominator. A more critical test is the relationship between  $\sigma_w$  and the convective velocity scale  $u_f$  given by:

$$u_f = (g\overline{w'T'}z'/T)^{1/3}. \quad (3.5)$$

Obukhov (1946) and Priestley (1954) have suggested this velocity scale to be valid for strong upward heat flux and light winds.

Plots of  $\sigma_w$  versus  $u_f$  for the summer data set are given in Figure 3.11 for  $z'/L < -1$  (site 107 had only a few data points for  $z'/L < -1$ , thus only sites 105 and 109 are given). The solid lines on Figure 3.11 represents the estimated best fit to the data plots (the lines were forced to go through the origin). The dashed lines are similar estimates for the fall data set. These results suggest that  $\sigma_w \propto u_f$ ; however, the slope is slightly greater for site 109 and for

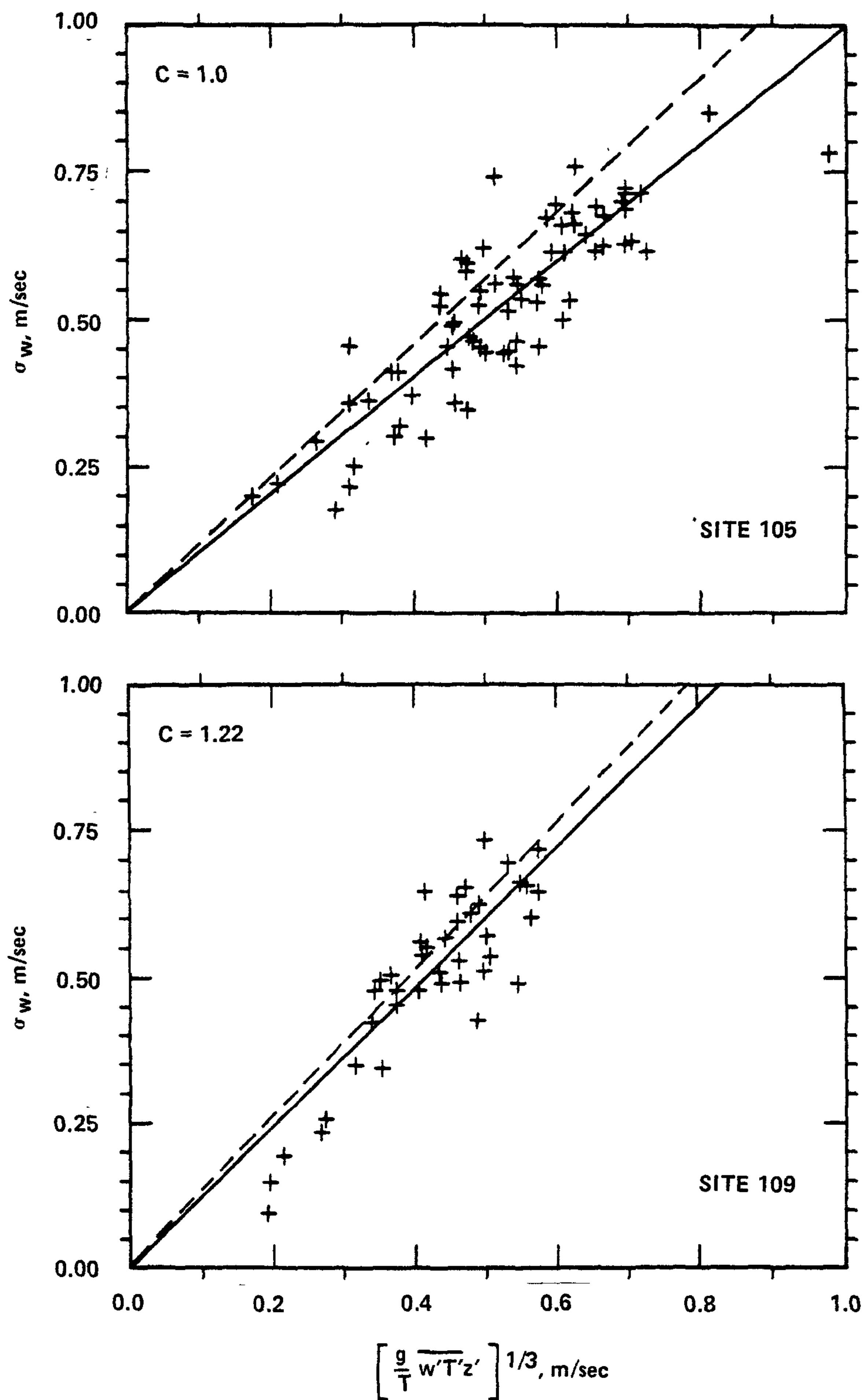


Figure 3.11  $\sigma_w$  vs.  $u_f$  for  $z'/L < -1.0$ .

the fall season. Plots of  $\sigma_w$  versus  $u^*$  for the summer data set are shown in Figure 3.12. These plots, along with the site and seasonal shift of the slopes on Figure 3.11, suggest that the friction velocity (as well as the heat flux) may be important for parameterizing the vertical velocity variance, even under conditions approaching free convection.

A functional dependence of  $\sigma_w$  on both  $u^*$  and  $u_f$  can be derived out of the turbulent kinetic energy budget equation which for the simplified conditions of homogeneity and stationarity is given by:

$$\epsilon = \frac{u^{*3}}{\lambda} + \frac{g \overline{w' T'}}{T} - \frac{1}{2} \frac{d \overline{w' q^2}}{dz} - \frac{1}{\rho} \frac{d \overline{p' w'}}{dz}. \quad (3.6)$$

The first term on the right-hand side represents the shear production, with  $\lambda$  being the mixing length; the second term represents the buoyancy production; the last two terms represent turbulent and pressure transports of energy due to flux divergence.  $\epsilon$  is the dissipation rate of turbulent energy per unit volume and can be expressed as (Tennekes and Lumley, 1972):

$$\epsilon = \sigma_w^3 / L_\epsilon(w) \quad (3.7)$$

where  $L_\epsilon$  is the dissipation length scale (see Appendix B). Neglecting the last two terms of Eq. 3.6 (Wyngaard and Coté, 1971, indicated the net effect of these two terms to be small) and assuming  $\lambda \propto kz'$ , Eqs. 3.6 and 3.7 yield:

$$\sigma_w = C(u^{*3} + 0.4u_f^3)^{1/3} \quad (3.8)$$

where  $C$  is on the order  $(L_\epsilon/\lambda)^{1/3}$ . Eq. 3.8 can be expressed as  $\sigma_w/u^* = C(1-z'/L)^{1/3}$ , a form similar to that suggested by Panofsky



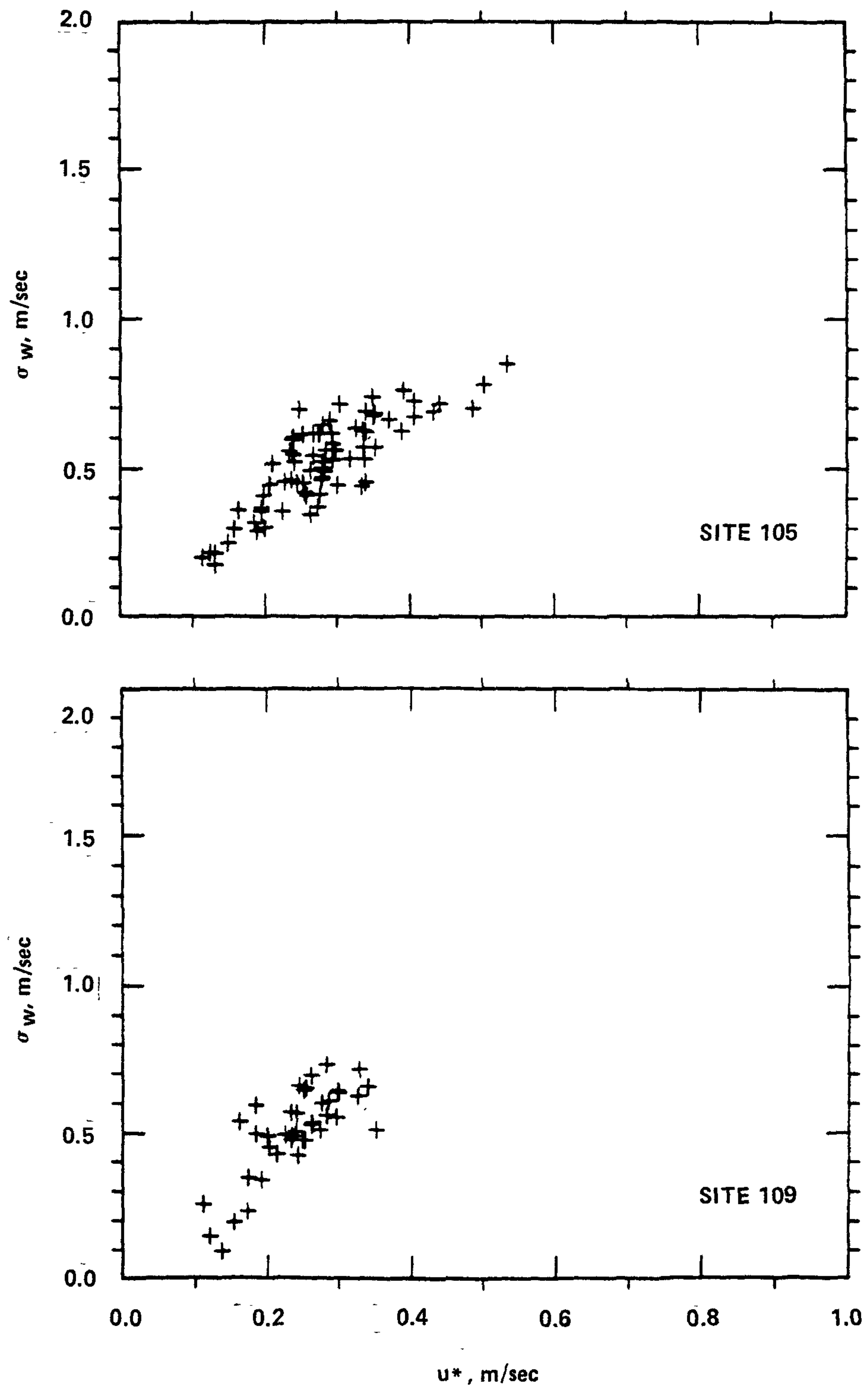


Figure 3.12.  $\sigma_w$  vs.  $u^*$  for  $z'/L < -1$ .

et al. (1977), but with less dependence on buoyancy-generated turbulence. Figure 3.13 shows plots of  $\sigma_w$  versus the right-hand side of Eq. 3.8 for  $z'/L$  between 0 and -1 for the summer data set. These data represent hours between 0700 and 2000 h with  $u^* > 0.15$  m/sec and  $U > 2.0$  m/sec. The solid lines represent the estimated linear fit to the data forced to go through the origin. A linear relationship is suggested for all three sites, with the constant  $C$  being about 1.28, 1.19, and 1.18 for sites 109, 105, and 107, respectively. The dashed lines represent the estimated fit to the fall data, and indicate the general consistency of the relationship for an independent data set. Plots of the same quantities are given in Figure 3.14 for  $z'/L < -1$ . The apparent differences in the slopes for the two figures may be due to neglect of the flux divergence terms in Eq. 3.6, or to the failure of Eq. 3.8 to adequately describe the relative importances of the shear and buoyancy production processes.

The relative importance of the two processes was sought through a least-squares fit to the data in the form  $\sigma_w^3 = Du^{*3} + Eu_f^3$ , over the range  $0 > z'/L > -5$ . These results are given in Table 3.3 in a form consistent with that suggested by Panofsky et al. (1977), i.e.,  $\sigma_w/u^* = D'(1 - E'z'/L)^{1/3}$ . In this equation,  $D' = D^{1/3}$  and  $E' = 2.5E/D$ . (The values of  $D'$  and  $E'$  given by Panofsky et al. are 1.3 and 3.0, respectively.) Note that the values of  $E'$  in Table 3.3 are consistently smaller for the urban sites. Correlation coefficients are large for all sites and for both seasons, suggesting that the neglected terms of Eq. 3.6 are unimportant or that a high correlation exists between the neglected terms and the buoyancy production term.

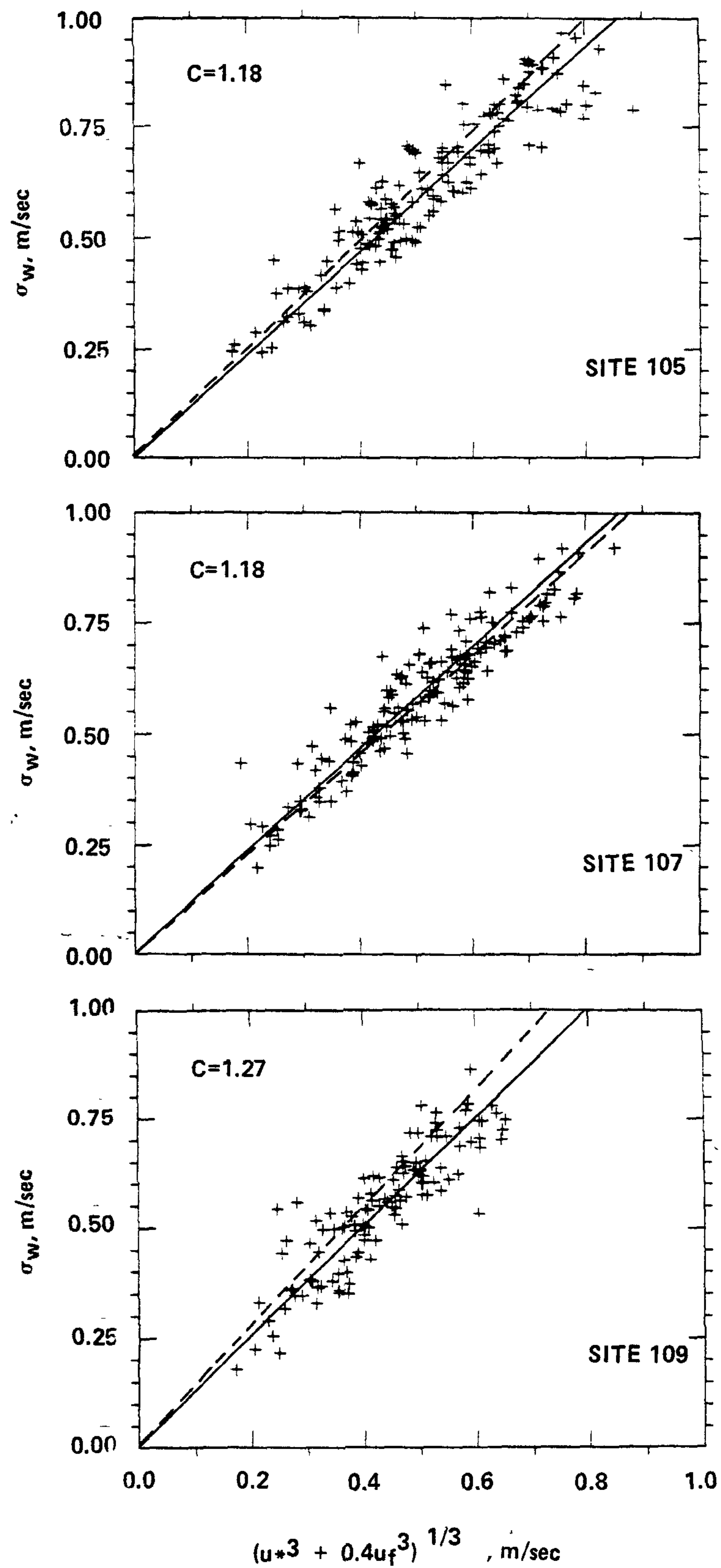


Figure 3.13.  $\sigma_w$  vs.  $C(u_*^3 + 0.4u_f^3)^{1/3}$  for  $z'/L$  between 0 and -1.

Ref. 17

1000

500

500

500

5

300

For the

10

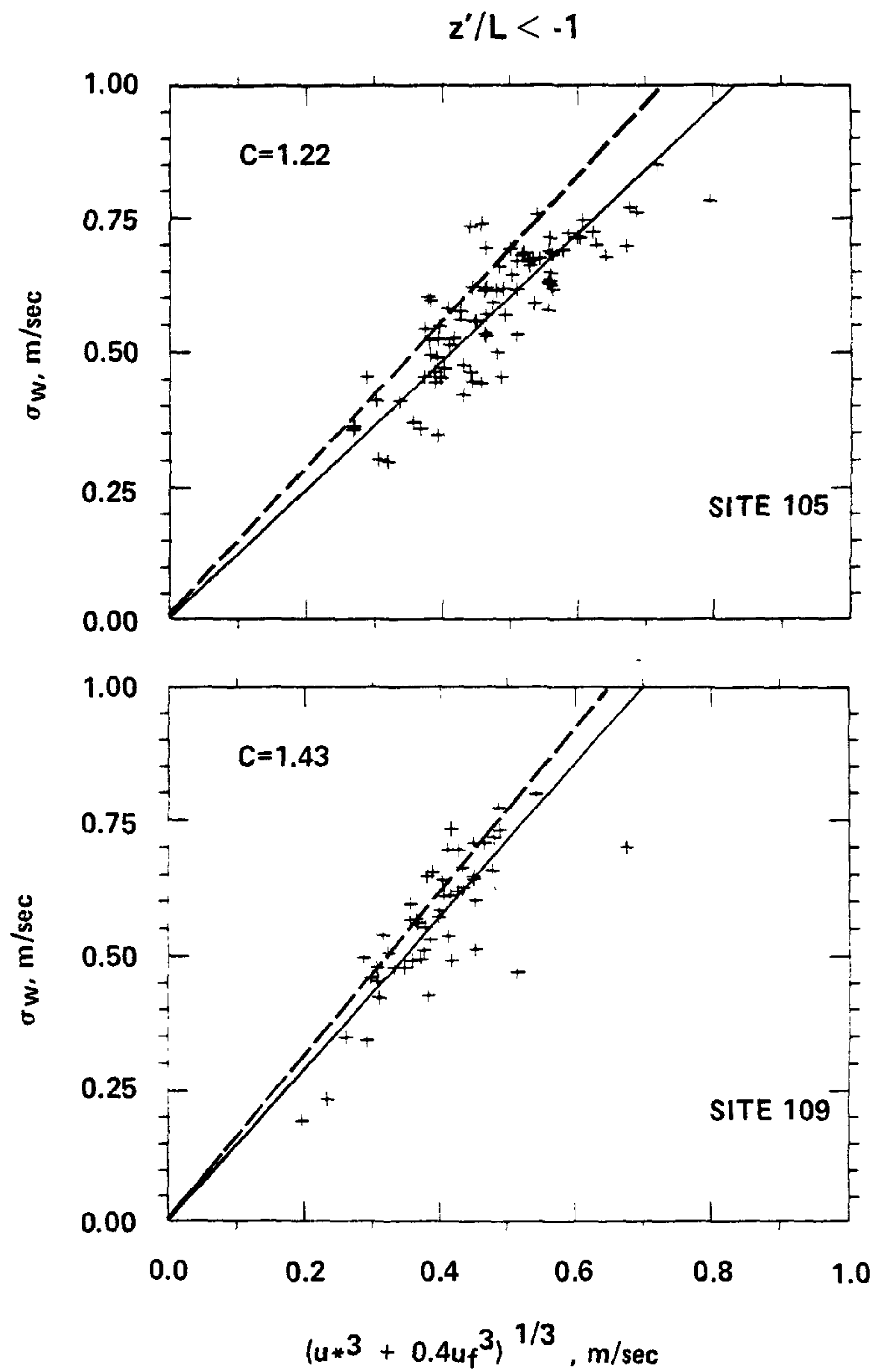


Figure 3.14. Same as for Figure 3.13 but for  $z'/L < -1$ .



Table 3.3. The Ratio  $\sigma_w/u^*$  as a Function of  $z'/L$  and Correlation Coefficients  $R^*$ , for Summer (S) and Fall (F) Data Sets. (The Expression for  $\sigma_w/u^*$  was Derived out of a Least-Squares Fit to  $\sigma_w^3 = Du^{*3} + Eu_f^3$  for  $0 > z'/L > -5$ .)

SITE	$\sigma_w/u^*$	$R^*$
105S	$1.16(1-1.2z'/L)^{1/3}$	0.96
107S	$1.10(1-1.9z'/L)^{1/3}$	0.96
109S	$1.07(1-3.8z'/L)^{1/3}$	0.96
111S	$1.20(1-2.5z'/L)^{1/3}$	0.95
105F	$1.10(1-1.1z'/L)^{1/3}$	0.95
107F	$1.11(1-1.1z'/L)^{1/3}$	0.98
109F	$1.25(1-2.1z'/L)^{1/3}$	0.95

In the limit as  $z'/L \rightarrow +\infty$  (stable stratification) similarity theory predicts each of the normalized velocity standard deviations to approach a constant value. The plots in Figure 3.10 suggest  $\sigma_w/u^*$  increases with increasingly positive  $z'/L$ . Results of Haugen et al. (1971) and the data summaries by Merry and Panofsky (1976) and Ariel' and Nadezhina (1976) also suggest that  $\sigma_w/u^*$  may increase with  $z'/L$  in the range of small positive  $z'/L$ . Merry and Panofsky (1976) suggested the increase may be due in part to errors in  $\sigma_w$  and  $u^*$ , when these quantities become very small under the buoyancy suppression of turbulence associated with stable stratification. The data plots in the present study were generally limited to  $u^* > 0.15$  m/sec and  $U > 2$  m/sec, values well above the noise level of the system, to minimize instrument response errors. An alternative presentation to Figure 3.10 is given in Figure 3.15, where  $\sigma_w$  is plotted against  $u^*$  for

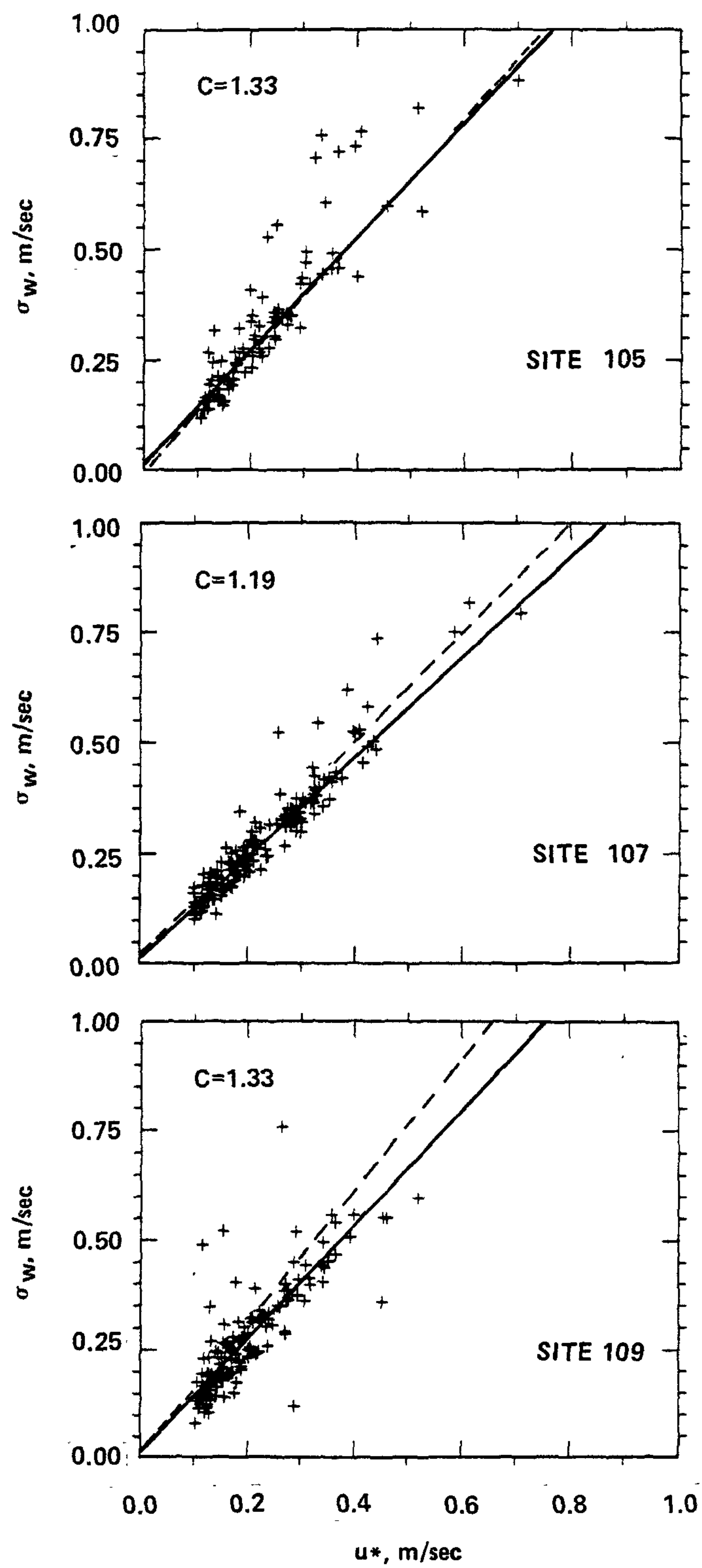


Figure 3.15.  $\sigma_w$  vs.  $u^*$  for stable stratification.

stable stratification ( $\overline{w'T'} < 0$ ). These plots suggest  $\sigma_w/u^*$  is constant for stable stratification as predicted by similarity theory. The estimated slopes through the data points are about 1.3 for sites 105 and 109 and 1.2 for site 107. These values are consistent with those obtained for neutral stratification. Estimated slopes for the fall data set (dashed lines on Figure 3.15) are consistent with those for the summer data set.

Experimental data for the horizontal components  $\sigma_u/u^*$  and  $\sigma_v/u^*$  are less supportive of the Monin-Obukhov similarity predictions than data for the vertical component. In the convective regime, the data scatter is large and little dependence of these quantities on  $z/L$  occurs (Ariel' and Nadezhina, 1976). However, Arya and Sundararajan (1976) show a definite increase of  $\sigma_v/u^*$  with increasing instability for the Kansas data. The ratio  $\sigma_v/u^*$  for site 105 (summer data) is plotted against  $z'/L$  in Figure 3.16. The scatter of the data points, which is similar to that for  $\sigma_u/u^*$  and also for the other sites, is significantly larger than for  $\sigma_w/u^*$  (Figure 3.10). However,  $\sigma_v/u^*$  increases with  $-z'/L$  approximately to the  $1/3$  power. This is more obvious in Figure 3.17, where  $\sigma_v/u^*$ , averaged over intervals of  $z'/L$  of 0.25, is plotted against  $z'/L$  for sites 105 and 109 for the summer data set. Note the site specific differences; the functional relationship in the limit approaching free convection is larger for site 109 than for site 105, as was the case for  $\sigma_w/u^*$ . Similar results were obtained for the fall data set. The free convection similarity prediction is alternately tested in Figure 3.18, where  $\sigma_v$  is plotted against  $u_f$  for  $z'/L < -1$ . The scatter is large; however,  $\sigma_v$  does increase with  $u_f$ . Results of

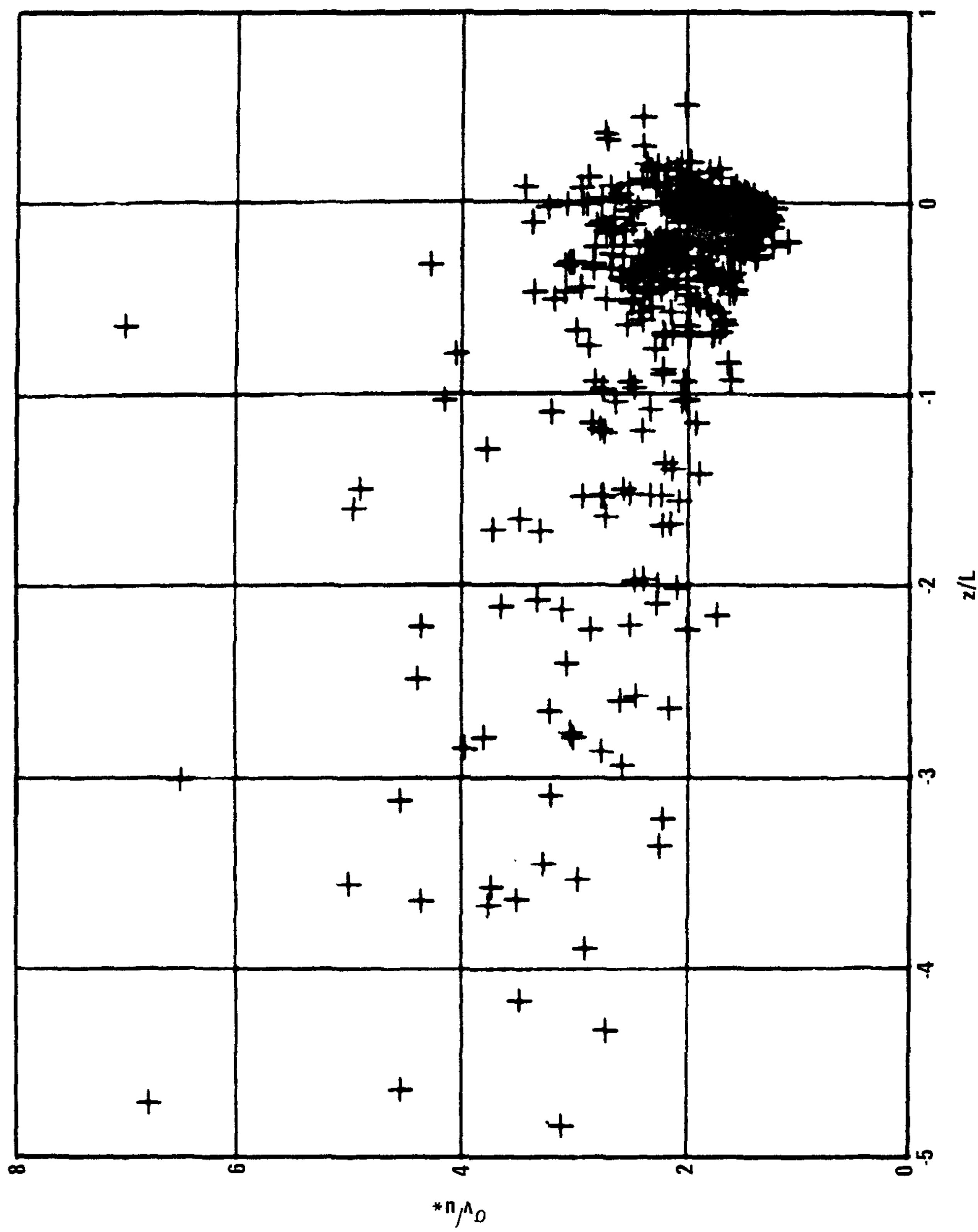


Figure 3.16. Plots of  $\sigma_v/u^*$  vs.  $z'/L$  for site 105 (summer data).

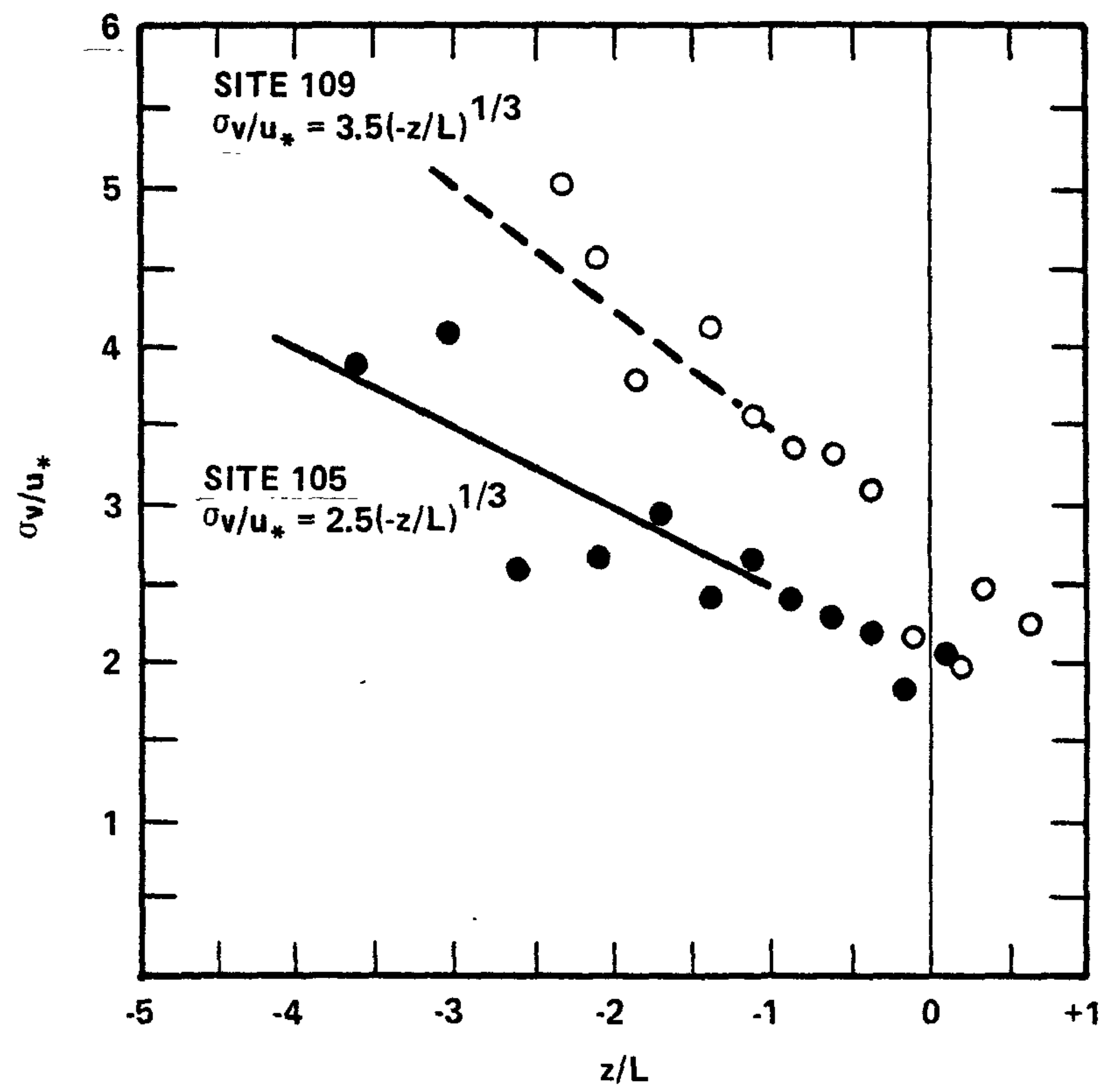


Figure 3.17.  $\sigma_v/u_*$  averaged over intervals of  $z'/L$  of 0.25 vs.  $z'/L$  for sites 105 and 109 (summer data).



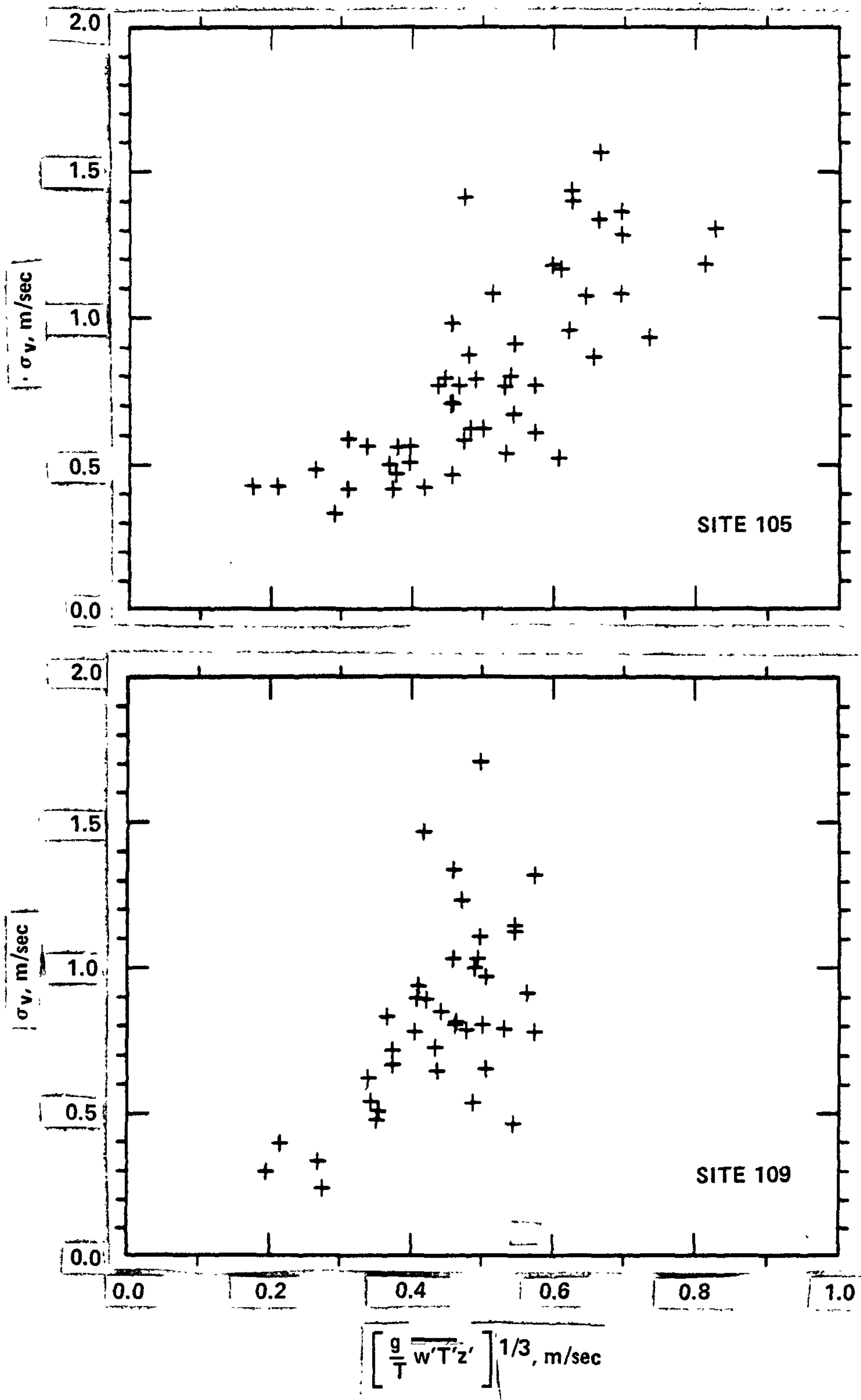


Figure 3.18.  $\sigma_v$  vs.  $u_f$  for  $z'/L < -1$ .

a least-squares fit of the form  $\sigma_v = Du^{*3} + Eu_f$  for  $0 > z'/L > -5$  are given for sites 105 and 109 in Table 3.4. As for  $\sigma_w/u^*$  the coefficients of the buoyancy term are smaller at the urban site for both seasons. Correlations coefficients are smaller than for  $\sigma_w/u^*$  (Table 3.3).

Table 3.4. Same as for Table 3.3 but for  $\sigma_v/u^*$ .

SITE	$\sigma_v/u^*$	R*
105S	$1.63(1-2.6z'/L)^{1/3}$	0.86
109S	$1.81(1-4.0z'/L)^{1/3}$	0.82
105F	$1.66(1-3.4z'/L)^{1/3}$	0.91
109F	$1.84(1-5.2z'/L)^{1/3}$	0.86

To the extent that the normalized velocity variances can be described as a function of  $z'/L$ , Monin-Obukhov similarity theory apparently holds for the data obtained in both urban and rural environs. However, the empirical form of the relationship differs; for any  $z'/L$  the normalized velocity variances are generally larger for the rural site compared to the urban site. The data scatter for the horizontal components was generally larger than for the vertical component. An alternative approach, i.e., free convection similarity theory is applied to the horizontal components below.

#### c. Dependence on $z_i/L$ --

The large scatter typically associated with plots of  $\sigma_v/u^*$  and  $\sigma_u/u^*$  as functions of  $z/L$  has generally led to the conclusion that Monin-Obukhov similarity does not hold for these parameters under convective conditions (Lumley and Panofsky, 1964). Kaimal et al. (1972)

show the peak wavelength of the  $w$  spectra to scale with  $z/L$ , but not the peak in the horizontal velocity components. From later experiments in northwestern Minnesota, Kaimal et al. (1976) concluded that the scaling height appropriate to the spectral peak of the horizontal velocity components in the convective boundary layer is the height of the mixed layer  $z_i$ . This scaling length also apparently applies in the surface layer. However, Kaimal (1978) noted that the interaction between terrain length scales and spectral length scales at low heights above tall roughness elements is an unknown factor.

For the limit approaching free convection, Deardorff (1970) suggested the horizontal velocity components to scale with the free convective velocity scale:

$$w^* = (\overline{gw'T'}z_i/T)^{1/3}. \quad (3.9)$$

Since  $\sigma_u \propto w^*$  and  $\sigma_v \propto w^*$ , even in the surface layer, the normalized velocity standard deviations are given by:

$$\sigma_v/u^* \propto \sigma_u/u^* \propto (z_i/L)^{1/3}. \quad (3.10)$$

Empirical support for this form is given by Panofsky et al. (1977).

Mixed layer height estimates were available from ancillary lidar measurements (Endlich et al., 1978) on 15 days during the summer experimental period for testing the convective boundary layer similarity relationship. The lidar data were obtained near the urban center and were generally available from sunrise through early evening. Hourly average values of mixing height estimated from the lidar returns are shown in Figure 3.19 for the 15 day period, along with smoothed average heat flux for sites 105 and 107. The spatial variation of the mixed layer over

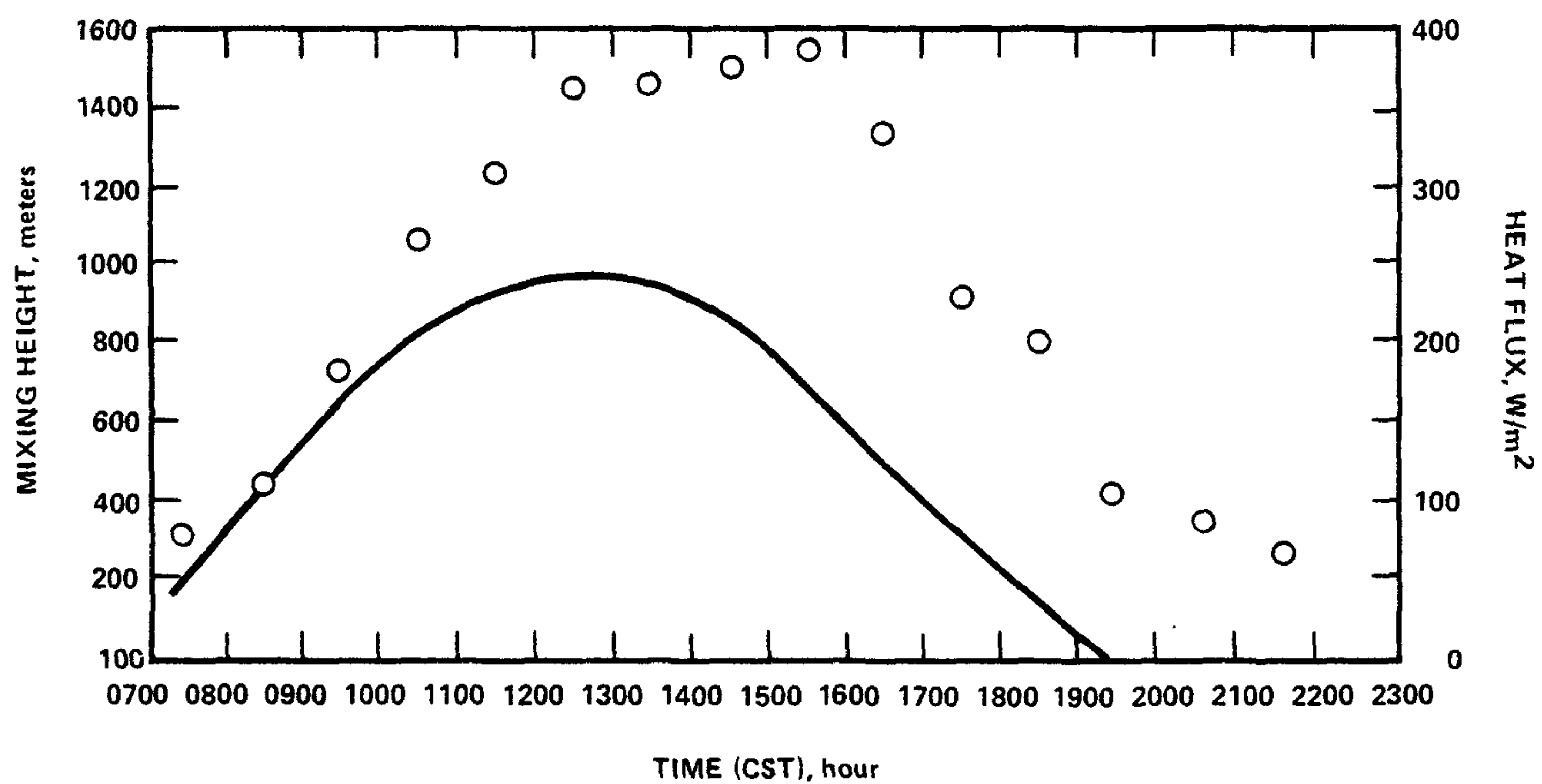


Figure 3.19. Average mixing heights near the urban center (open circles) and average surface heat flux for sites 105 and 107 (solid line) for 26 July through 13 August.

the St. Louis area is complex, especially during the morning transition period (Ching et al., 1978); however, the lidar estimated values were applied to both urban and rural sites.

Figure 3.19 shows two distinctly different periods in the evolution of the convective boundary layer that were reasonably consistent on all of the days. The first is the morning transition period when both heat flux and the height of the mixed layer increase rapidly. The second period begins about 1300 h and extends through the late afternoon and is characterized by a nearly constant mixed layer height and decreasing heat flux. The time scale of the changing boundary layer parameters for both periods is long compared to the convective time scale ( $z_i/w^*$ ), and thus the requirement of stationarity inherent in the similarity formulation should be met. However, it is of interest to test the consistency of the similarity relationship for the two periods; the data were stratified according to time periods: 0900 to 1200 h and 1300 to 1600 h.

Plots of  $\sigma_v/u^*$  versus  $z_i/L$  for sites 105, 107, and 109 are shown in Figure 3.20. The solid line represents the form postulated by Wyngaard and Coté (1974) ( $\sigma/u^* = (3.06 + 0.6(z_i/-L)^{2/3})^{1/2}$ ) and the dashed line for site 107 is the form suggested by Panofsky et al. (1977) ( $\sigma/u^* = (12 + 0.5z_i/-L)^{1/3}$ ). The free convection similarity form is generally supported by the present data set. However, for small values of  $-z_i/L$ , the plots for site 105 are inconsistent with those for site 109 (and the forms postulated by Wyngaard and Coté, and Panofsky et al.). There is no apparent stratification as a function of time period.

An alternative test of mixed layer scaling is derived out of Eq. 3.9, using the peak in the longitudinal velocity spectrum,  $L_m(u)$ , as a



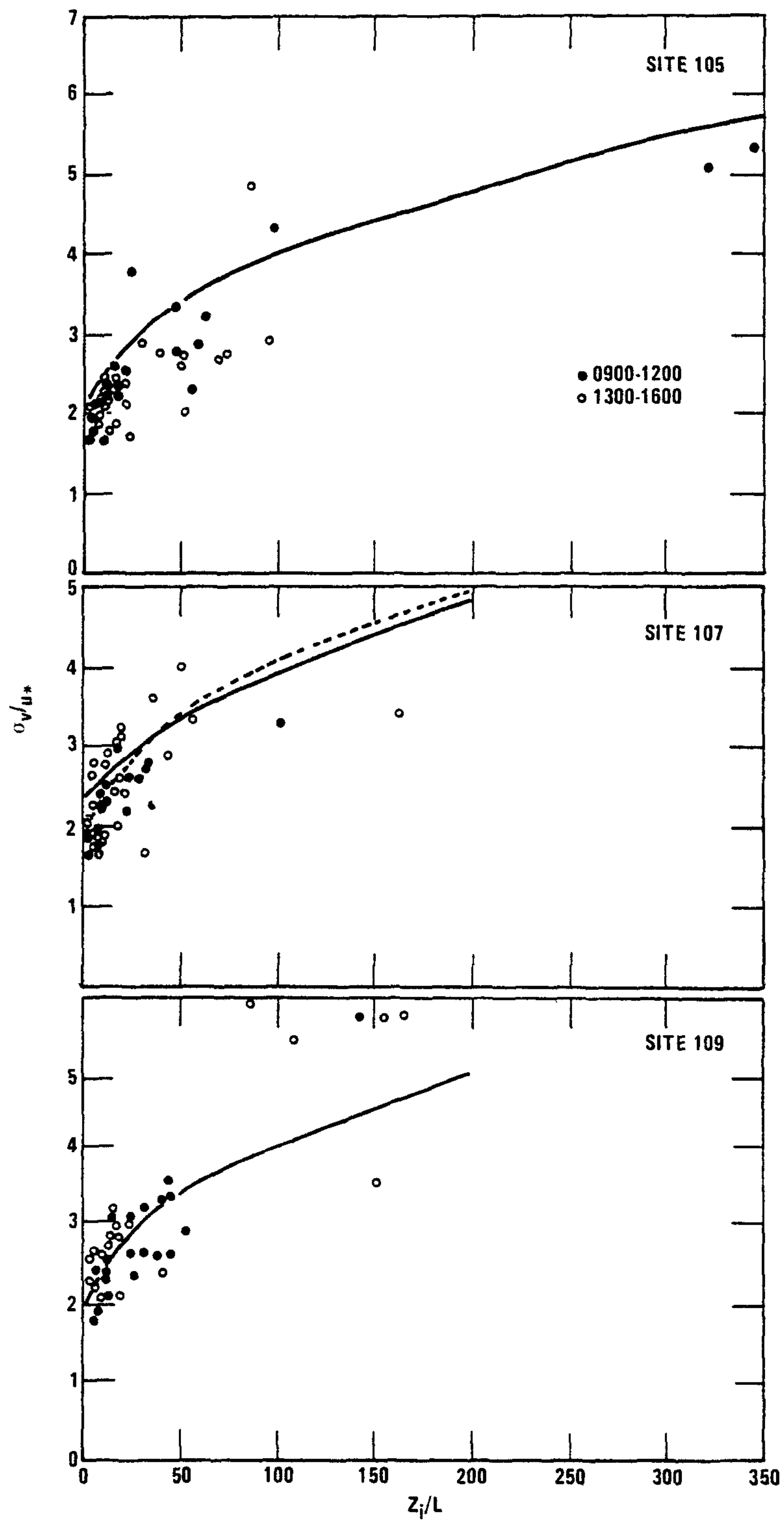


Figure 3.20. The ratio  $\sigma_v/u^*$  vs.  $z_i/L$  for sites 105, 107, and 109 (summer data) for the period 0900 to 1200 hrs. (solid dots) and 1300 to 1600 hrs. (open circles). The solid line represents the form postulated by Wyngaard and Coté (1974) and the dotted line that of Panofsky et al. (1976).

surrogate for  $z_i$  (Kaimal et al., 1976, has indicated the peak wavelength of the horizontal components to be proportional to  $z_i$ ):

$$w^{*'} = (\overline{g w' T'} L_m(u) / T)^{1/3}. \quad (3.11)$$

Plots of  $\sigma_u$  versus the right-hand side of the above expression for  $z'/L < -1$  (given in Figure 3.21) support the use of  $L_m(u)$  as a convective scaling length. The longitudinal velocity component is discussed here in preference to the lateral component because  $L_m(u)$  can be determined with greater confidence than  $L_m(v)$  (see Section 3.3).

The inclusion of a mechanical production term through Eq. 3.6, with the assumption that  $\epsilon \sim \sigma_u^3 / L_m(u)$  (Hanna, 1968), yields:

$$\sigma_u = C(u^{*3} L_m(u) / \ell + w^{*'}^3)^{1/3}. \quad (3.12)$$

Plots of  $\sigma_u$  versus the right-hand side of Eq. 3.12 ( $\ell$  was assumed proportional to  $kz'$ ) are given in Figure 3.22 for  $z'/L$  between 0 and -1 and in Figure 3.23 for  $z'/L < -1$ . Generally, Eq. 3.12 appears to be an appropriate predictor of  $\sigma_u$ ; however, total consistency does not exist for all sites and stratifications as indicated by the different values of  $C$ . A least-squares analysis of the form  $\sigma_u^3 = Du^{*3} + Ew^{*'}^3$  is given in Table 3.5 for the summer data set. The result for site 109 is similar to the empirical form suggested by Panofsky et al. (1977) ( $\sigma_u / u^* = 2.3(1 - 0.04z_i/L)^{1/3}$ ) when  $z_i$  is assumed given by  $L_m(u)/1.5$ . Correlations coefficients are slightly higher than obtained for  $\sigma_v / u^*$  using the convective velocity scale (Table 3.4) suggesting that  $w^{*'}$ , rather than  $u_f$ , may be the preferred scaling velocity. Consistent with previous results for  $\sigma_w / u^*$  and  $\sigma_v / u^*$ , the coefficient of the buoyancy term is smaller for the urban site (105).

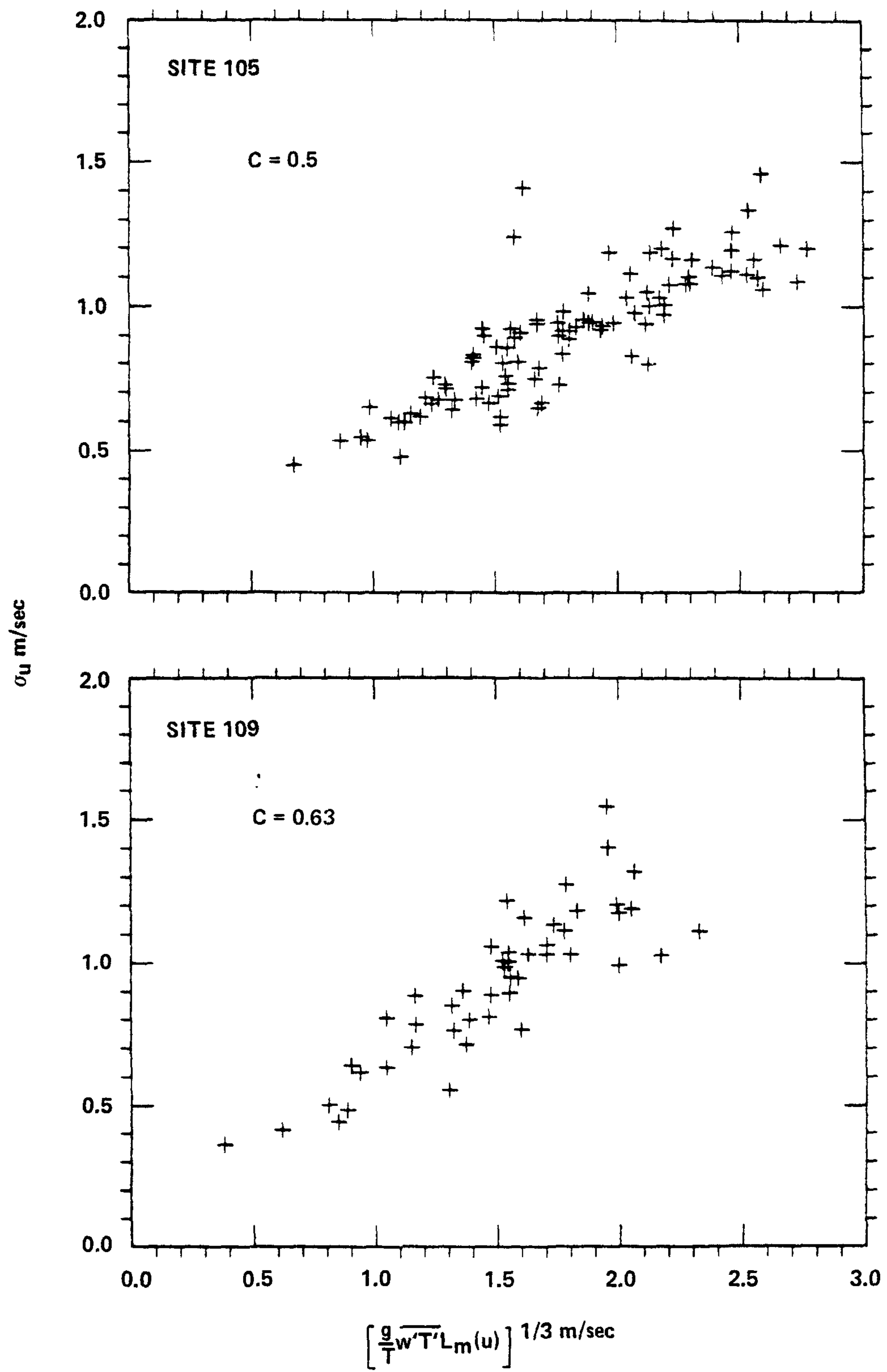


Figure 3.21  $\sigma_u$  vs.  $(g\overline{w'T'}L_m(u)/T)^{1/3}$  for  $z'/L < -1$ .

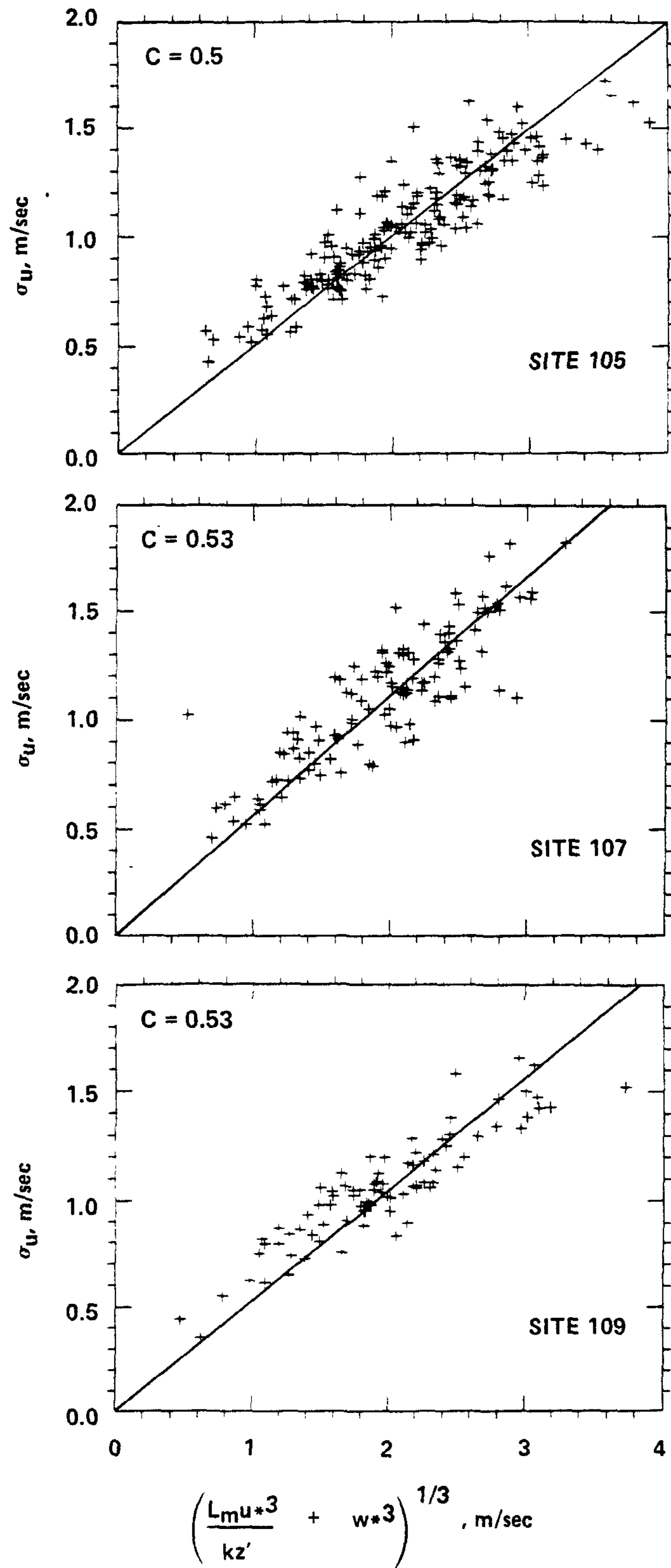


Figure 3.22  $\sigma_u$  vs. right hand of Eq. 3.12 for  $z'/L$  between 0 and  $-1$ .

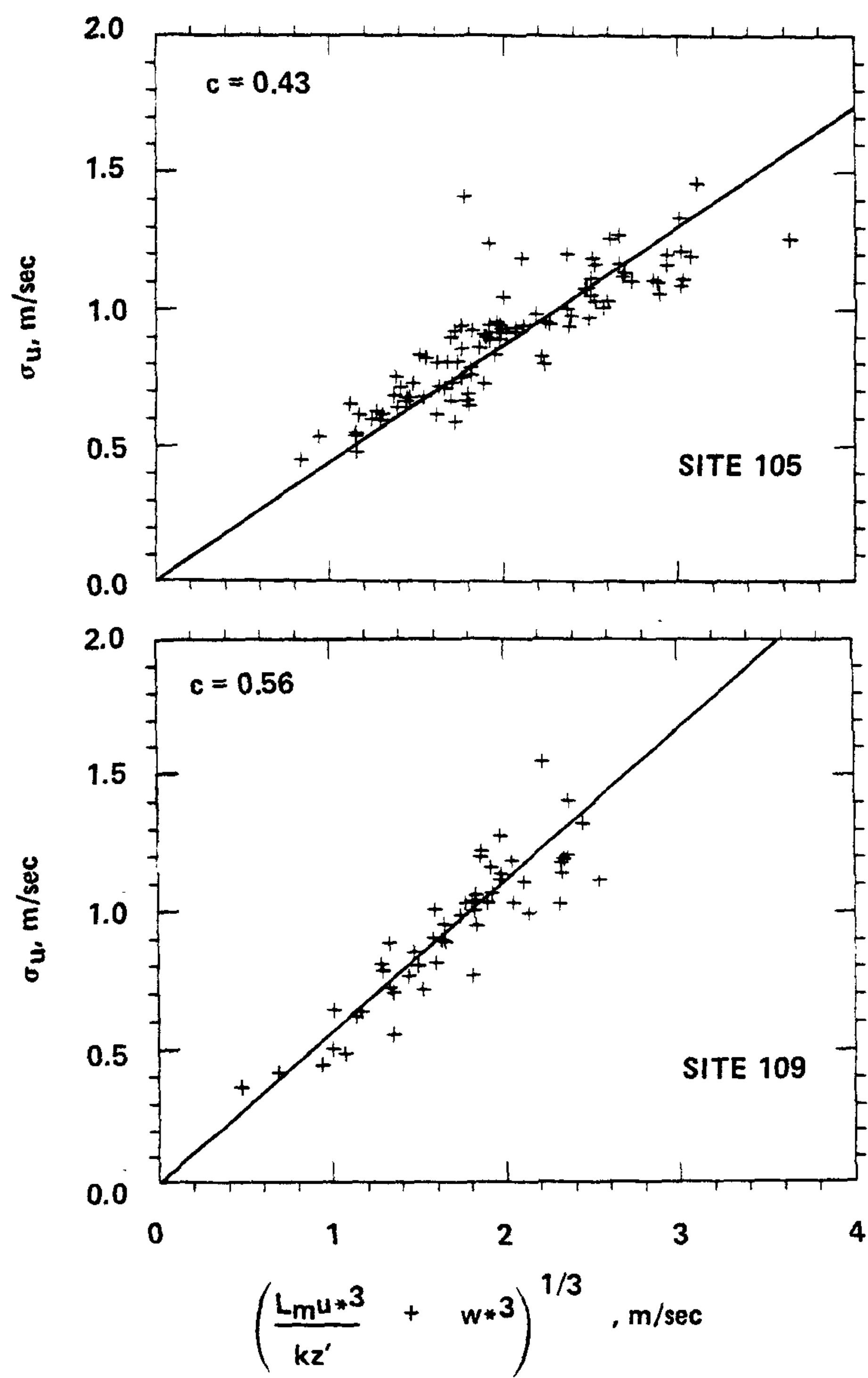


Figure 3.23 Same as for Figure 3.22 but for  $z'/L < -1$ .

Table 3.5. The ratio  $\sigma_u/u^*$  as a Function of  $L_m(u)/L$  and Correlation Coefficients  $R^*$ , for the Summer Data Set. (The Expression for  $\sigma_u/u^*$  was Derived out of a Least-Squares Fit to  $\sigma_u^3 = Du^{*3} + w^{*3}$  for  $0 > z'/L > -5$ .)

SITE	$\sigma_u/u^*$	$R^*$
105	$2.0(1-0.02L_m(u)/L)^{1/3}$	0.89
109	$2.2(1-0.04L_m(u)/L)^{1/3}$	0.91

d. Ratio of the Variances--

In the regime of buoyancy dominated turbulence,  $\sigma_u \sim \sigma_v$  and thus  $\sigma_v$  should behave as discussed above for  $\sigma_u$ . The ratio  $\sigma_v/\sigma_u$  versus  $z'/L$  is shown in Figure 3.24 for the summer data set. For  $z'/L < -1$ , the ratio behaves as expected from free convective similarity; i.e., both normalized standard deviations scale with mixed layer height such that the average ratio  $\sigma_v/\sigma_u$  is about unity.

The ratio  $\sigma_w/\sigma_u$  for the summer data set is given in Figure 3.25. The theoretical form of this ratio is derived out of both Monin-Obukhov and free convective similarity:

$$\sigma_w/\sigma_u = f(z'/L)/f(z_i/L) = C(z'/z_i)^{1/3} \quad (3.13)$$

Thus  $\sigma_w/\sigma_u$ , which characterizes the anisotropy of the turbulence, depends on both the height of measurement and the depth of the convective mixed layer (or alternately  $L_m(u)$ ). For neutral and stable stratifications, the dependence on mixed layer height and height vanishes, and the ratio approaches a constant value which for neutral stratification is about 0.53 (from Table 3.2). Busch (1973), for measurements at 5.66 m, found the ratio essentially constant for stable conditions at a value of 0.6, a sharp transition near  $z/L = 0$ , and



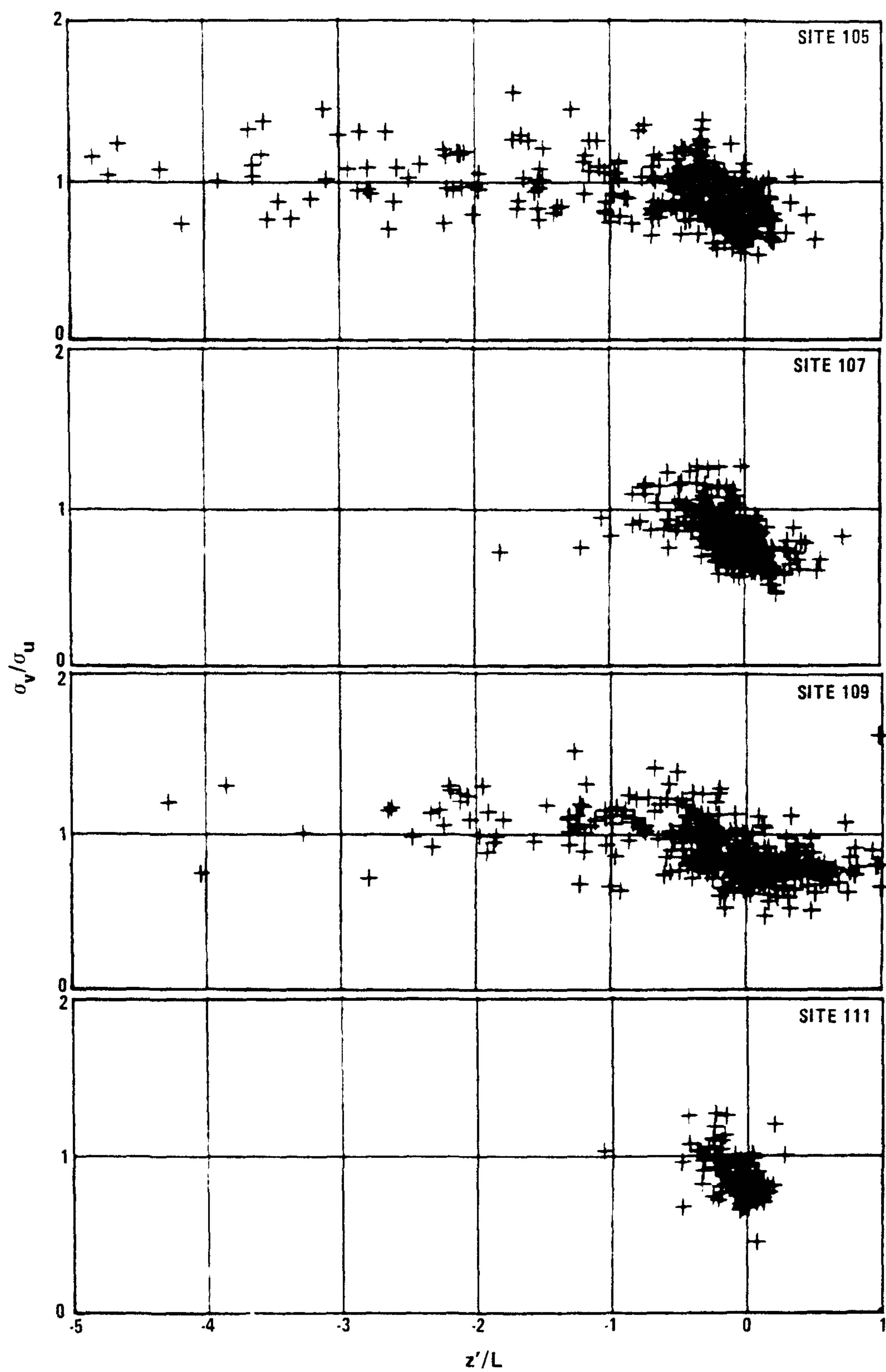


Figure 3.24 Plots of  $\sigma_v/\sigma_u$  vs.  $z'/L$  for summer data set.

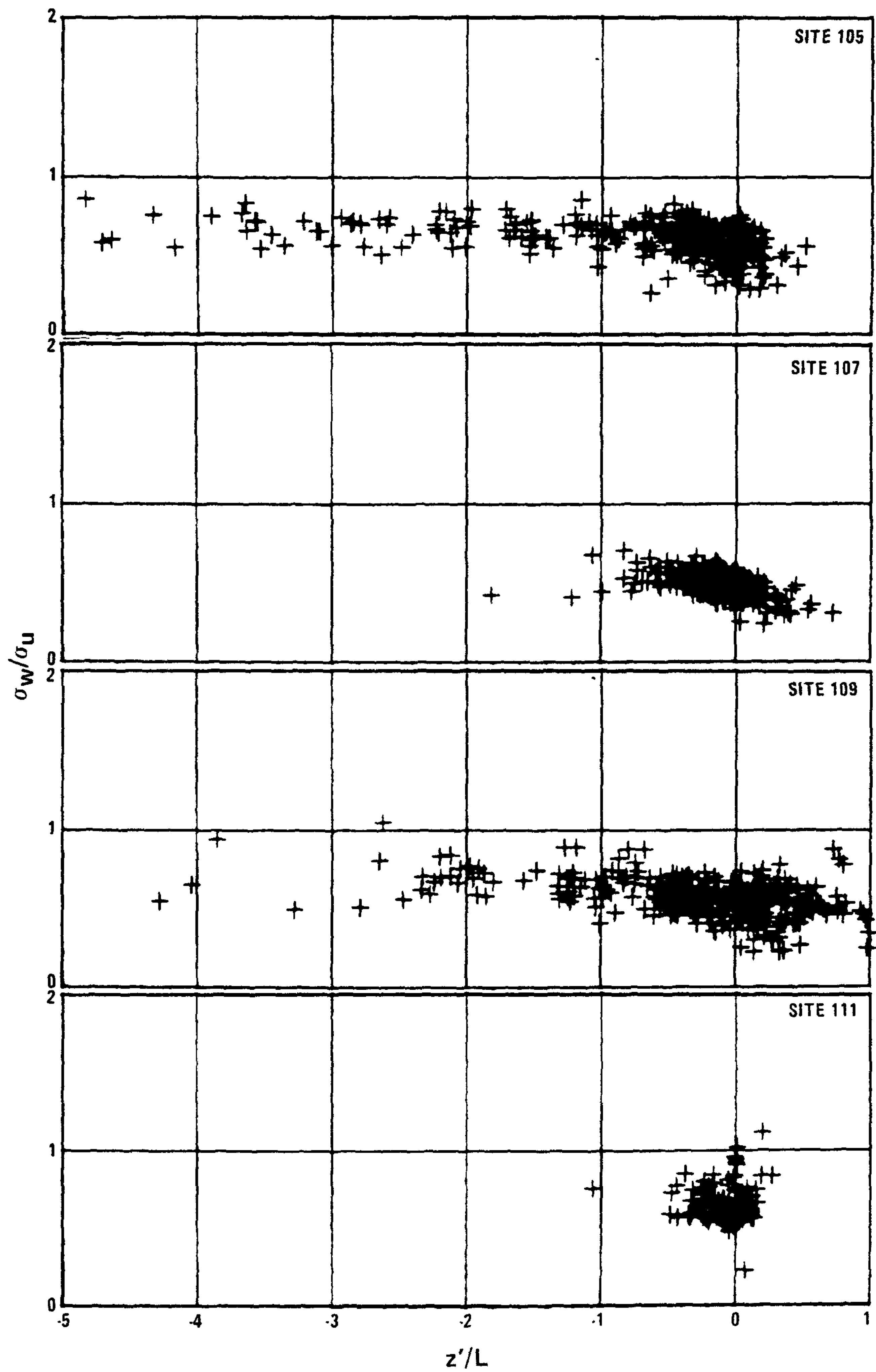


Figure 3.25 Plots of  $\sigma_w/\sigma_u$  vs.  $z'/L$  for the summer data set.

constant again at a value of about 0.5 for  $z/L < -1$ . The present data (Figure 3.25) indicate  $\sigma_w/\sigma_u$  to increase from the neutral value of 0.53 to about 0.67 at  $z'/L = -0.75$ , and remain essentially constant out to large negative values of  $z'/L$ . The influence of boundary layer depth was not apparent, although it may be represented by the scatter of the data points.

e. Intensity of Turbulence --

The vertical and horizontal components of turbulence intensity can be expressed through the similarity wind profile equation in the form:

$$\sigma_w/U = k\sigma_w/u^*/[\ln(z'/Z_0)-\psi(z'/L)] \quad (3.14)$$

and

$$\sigma_{u,v}/U = k\sigma_{u,v}/u^*/[\ln(z'/Z_0)-\psi(z'/L)] \quad (3.15)$$

where  $\psi(z'/L)$  is the correction to the logarithmic wind profile for diabatic conditions. The turbulence intensity components depend on the height of observation and surface roughness. They are nevertheless useful and frequently measured turbulence parameters and often recommended for parameterizations of dispersion in the surface boundary layer.

The diurnal variations of  $\sigma_v/U$  and  $\sigma_w/U$  for sites 105, 107, and 109, given in Figure 3.26 for the summer experimental period, indicate these quantities are a function of atmospheric stability, whereas the differences in the relative magnitude at the three sites reflect a land-use dependence. Results for the fall experimental period were similar; however, the turbulence components were noticeably smaller during the midday period, reflecting the decrease in convective activity

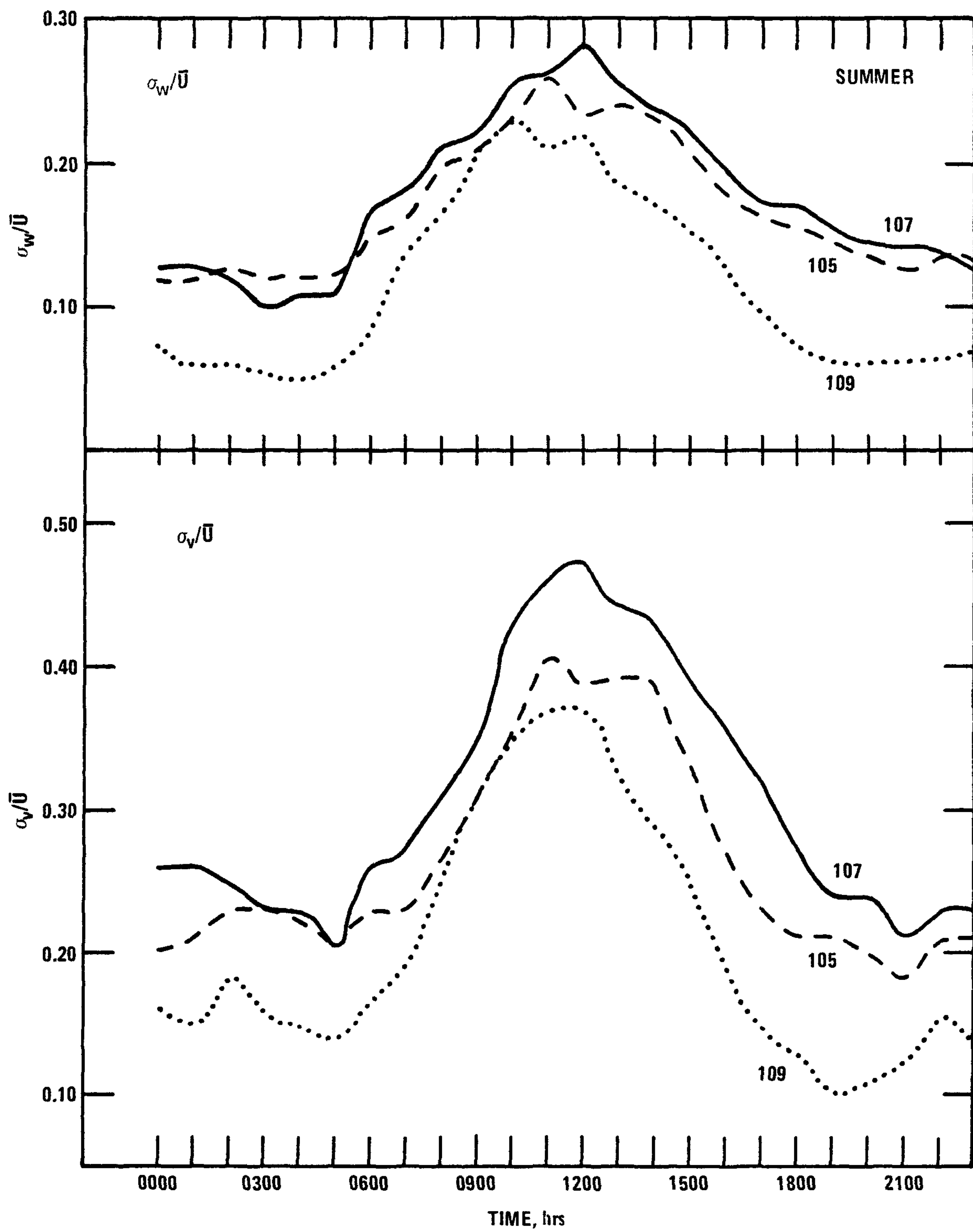


Figure 3.26. Diurnal variation of vertical (upper) and lateral (lower) intensities of turbulence for the summer data set.

during the fall season. Urban-rural turbulence intensity differences (sites 105 and 107 contrasted with site 109) are small during the morning transition period (0700-1000 h) and relatively large during the afternoon transition period (1300-1700 h). The similarity of turbulence intensities at all of the sites during the morning transition period is possibly the result of more rapid conversion of solar radiation to turbulent energy in the rural environment (relative to the urban environment), owing to the lower heat capacity and conductivity of the rural substrates. The larger values of turbulence intensity at the urban site during the afternoon period represent a true urban anomaly arising from the larger heat capacity and conductivity of the urban substrate.

Effects of atmospheric stratification on  $\sigma_w/U$  and  $\sigma_v/U$  are shown on Figure 3.27, where these quantities are plotted against  $z'/L$ . Each data point represents the average of at least five values for the given site over a discrete interval of  $z'/L$  (the scatter of the individual data points was large due to the influence of surface roughness which varied markedly as a function of wind direction as described in Section 3.1). The plots for sites 105, 107, and 109 each represent a total of about 400 data values with 80, 94, and 60 percent, respectively, occurring for  $0.5 > z'/L > -0.5$ . The plots for site 111, which was in operation less than two weeks, represent only 131 hourly data values - most of which were in the above range of  $z'/L$ . Both  $\sigma_w/U$  and  $\sigma_v/U$  appear to be functions of  $z'/L$  for small absolute values of  $z'/L$ . For unstable stratification, the scatter of the class-interval-averaged data points is too large to have confidence in the shape of the

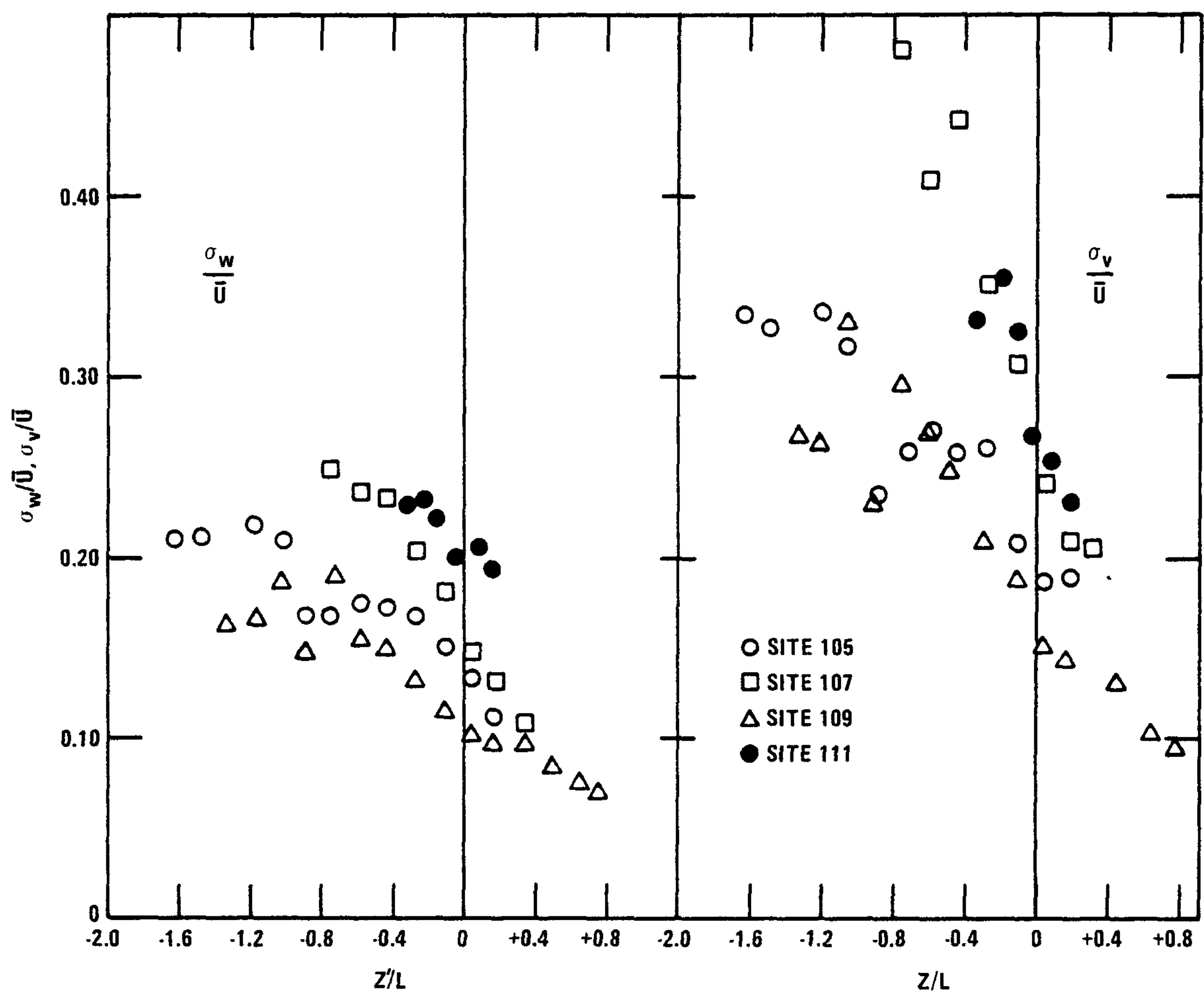


Figure 3.27. Vertical and lateral intensities of turbulence vs.  $Z'/L$  for summer data set.



curves; however, they do not continue at the near neutral ( $z'/L = 0$ ) value of the slopes. Near neutral stratification, the slope for  $\sigma_v/U$  is greater than for  $\sigma_w/U$ ;  $\sigma_v/U$  responds more directly to increasing buoyancy-generated turbulence, whereas  $\sigma_w/U$  is somewhat constrained by the proximity of the surface. A striking feature of Figure 3.27 is the apparent dependence of intensities on the specific site and thus  $Z_0$ ; turbulence intensities for the four sites are ordered roughly as expected from the computed surface roughness lengths.

Turbulence intensity statistics for neutral and slightly unstable stratifications are given in Table 3.6. Also given are average  $Z_0$  values and the number of observations making up the statistics. Note that some of the average turbulent intensities in the unstable data groups for the fall are less than for the corresponding neutral group; the former group is made up of relatively few observations and average  $Z_0$  values are smaller. Plots of the average site/season values of  $\sigma_w/U$  against the corresponding average  $z'/Z_0$  are shown in Figure 3.28a. The solid line represents the evaluation of Eq. 3.14 for neutral stratification ( $\sigma_w/u^*(0) = 1.3$ ,  $\psi(z/L) = 0.0$ ) and agrees well with the observed data points (plain symbols). This correspondence extends to the individual values of  $\sigma_w/U$  and  $Z_0$ , shown for the summer data set in Figure 3.29. The dashed line represents the evaluation of Eq. 3.14 for neutral stratification. The departure of the plots for site 107 from the expected form is due to  $\sigma_w/u^*$  being significantly less (1.20) than the value of 1.3 assumed in Eq. 3.14. Overall the plots demonstrate a dependence of  $\sigma_v/U$  on  $z'/Z_0$  inherent in Eq. 3.14.

The dashed line on Figure 3.28a represents the evaluation of Eq. 3.14 for slightly unstable stratification ( $z'/L = -0.5$ , for which according to Panofsky et al. (1977),  $\sigma_w/u^*(-0.5) = 1.76$ ). The site

Table 3.6. Averages and Standard Deviations (s.d.) of Intensity of Turbulence Components for Neutral and Slightly Unstable Conditions, Number of Observations, and Average Roughness Lengths for Summer (S) and Fall (F) Data Sets.

SITE	NO.	$Z_o$	$\sigma_u/U$	s.d.	$\sigma_v/U$	s.d.	$\sigma_w/U$	s.d.
NEUTRAL ( $.05 > z/L > -.05$ )								
105S	97	0.7	.239	.06	.187	.06	.136	.03
107S	107	1.3	.316	.05	.237	.04	.156	.02
109S	29	0.2	.197	.04	.154	.04	.102	.02
111S	36	1.6	.323	.04	.250	.04	.190	.02
105F	125	0.8	.260	.05	.193	.04	.139	.03
107F	111	1.1	.298	.04	.217	.03	.150	.02
109F	28	0.4	.203	.05	.149	.03	.116	.03
SLIGHTLY UNSTABLE ( $-.6 < z/L < -.4$ )								
105S	42	.70	.273	.07	.266	.08	.175	.04
107S	18	1.50	.421	.10	.440	.10	.240	.04
109S	30	.30	.254	.08	.250	.09	.150	.04
105F	16	.40	.235	.03	.219	.08	.147	.03
107F	12	1.00	.336	.05	.300	.06	.188	.03
109F	11	.03	.177	.02	.180	.04	.100	.03

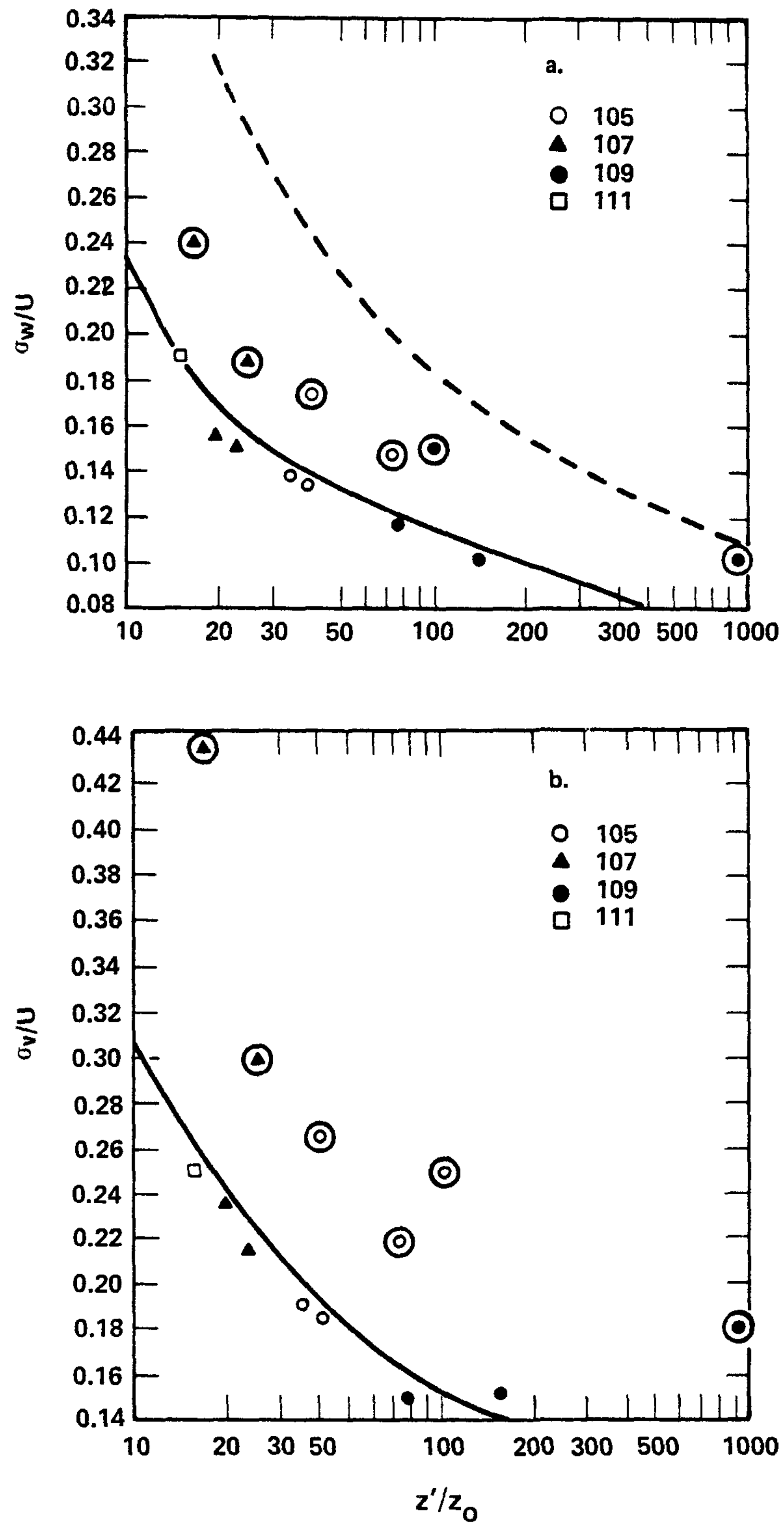


Figure 3.28. Plots of the site averaged values of  $\sigma_w/U$  (a) and  $\sigma_v/U$  (b) vs.  $z'/z_0$  for neutral (plain symbols) and slightly unstable (circled symbols) stratifications. The curves represent expected form from Eqs. 3.14 and 3.15.

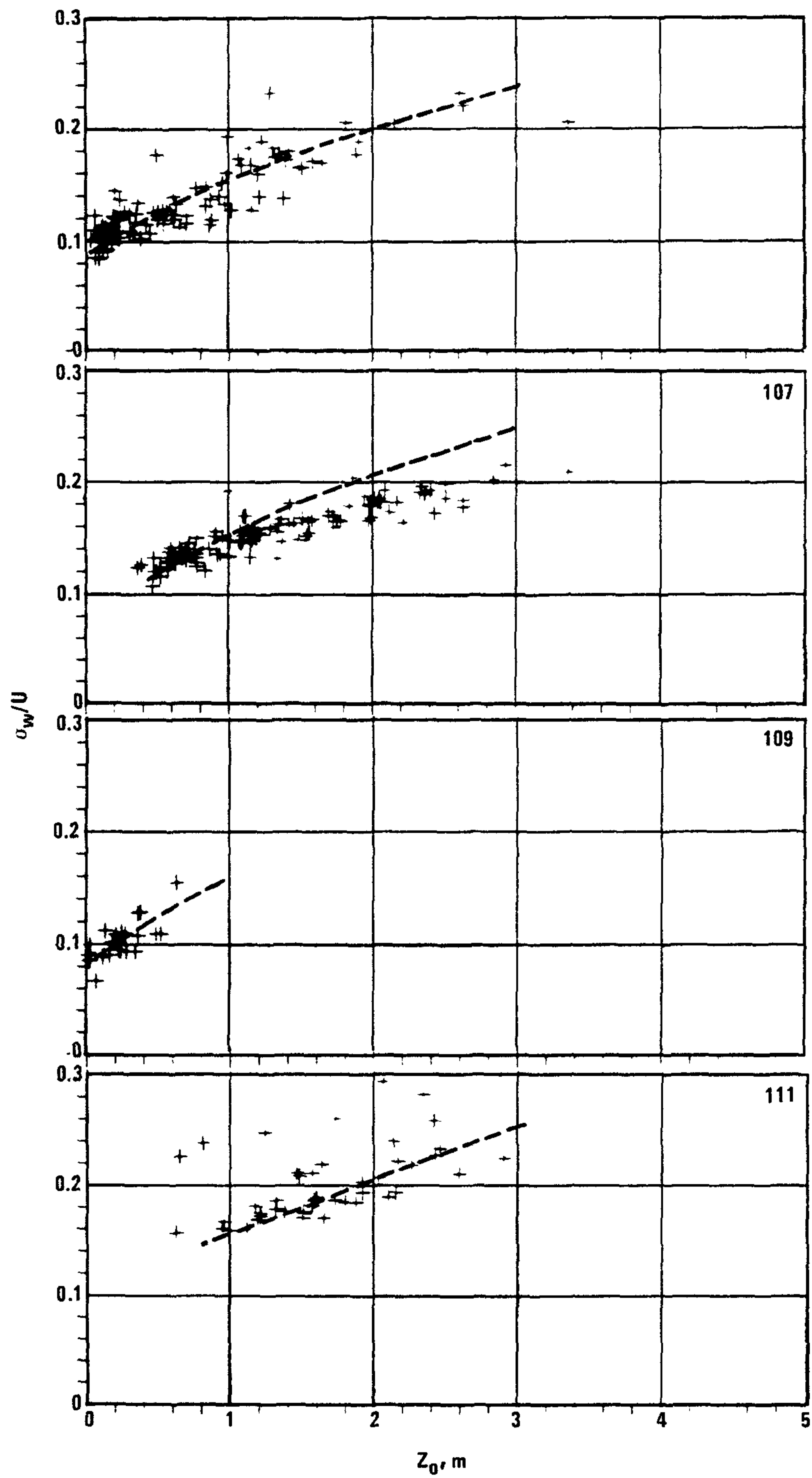


Figure 3.29. Individual plots of  $\sigma_w/U$  vs.  $Z_0$  for neutral stratification (summer data set). The dashed lines represent expected form from Eq. 3.14.

averaged data for  $-0.6 < z'/L < -0.4$ , indicated by the circled symbols, are well below their expected values, but still suggest a strong dependence on  $Z_0$ .

Site averaged values of  $\sigma_v/U$  are plotted against corresponding values of  $z'/Z_0$  in Figure 3.28b. The solid line is the evaluation of Eq. 3.15 for neutral stratification ( $\sigma_v/u^*(0) = 1.8$ ) and again is a good fit to the data. Since Monin-Obukhov similarity theory may not hold for  $\sigma_v/u^*$  in unstable stratification, no attempt was made to evaluate Eq. 3.12 for  $z'/L = -0.5$ . The data points for  $-0.6 < z'/L < -0.4$  are, however, given on Figure 3.28b. As for neutral stratification,  $\sigma_v/U$  appears to have a strong dependence on surface features for  $z'/Z_0 < 100$ .

### 3.2.2 Temperature Variance

The similarity prediction for  $\overline{T'^2}$  (see Table 1.1) is discussed here in terms of the standard deviation  $\sigma_T$  normalized by a scaling temperature  $T^* = -\overline{w'T'}/u^*$ . Dimensional considerations show that in the limit of free convection, the ratio  $\sigma_T/T^*$  should be proportional to  $(-z/L)^{-1/3}$ . For neutral stratification,  $z/L \rightarrow 0$ , both  $\sigma_T$  and  $\overline{w'T'}$   $\rightarrow 0$ , and the ratio is constant. In the limit as  $z/L \rightarrow +\infty$ , similarity theory predicts the ratio to be a constant.

The ratio  $\sigma_T/T^*$  for the summer data set is shown in Figure 3.30. For  $z'/L < 0$ , the data plots are similar at all four sites and are in good agreement with the ratio for the Kansas data. The solid line on the plots for site 105 represents the Wyngaard et al. (1971) fit to the Kansas data and is given by  $\sigma_T/T^* = 0.95(-z/L)^{-1/3}$ . In the limit  $z'/L \rightarrow 0$ ,  $\sigma_T/T^*$  for the St. Louis data is significantly larger than

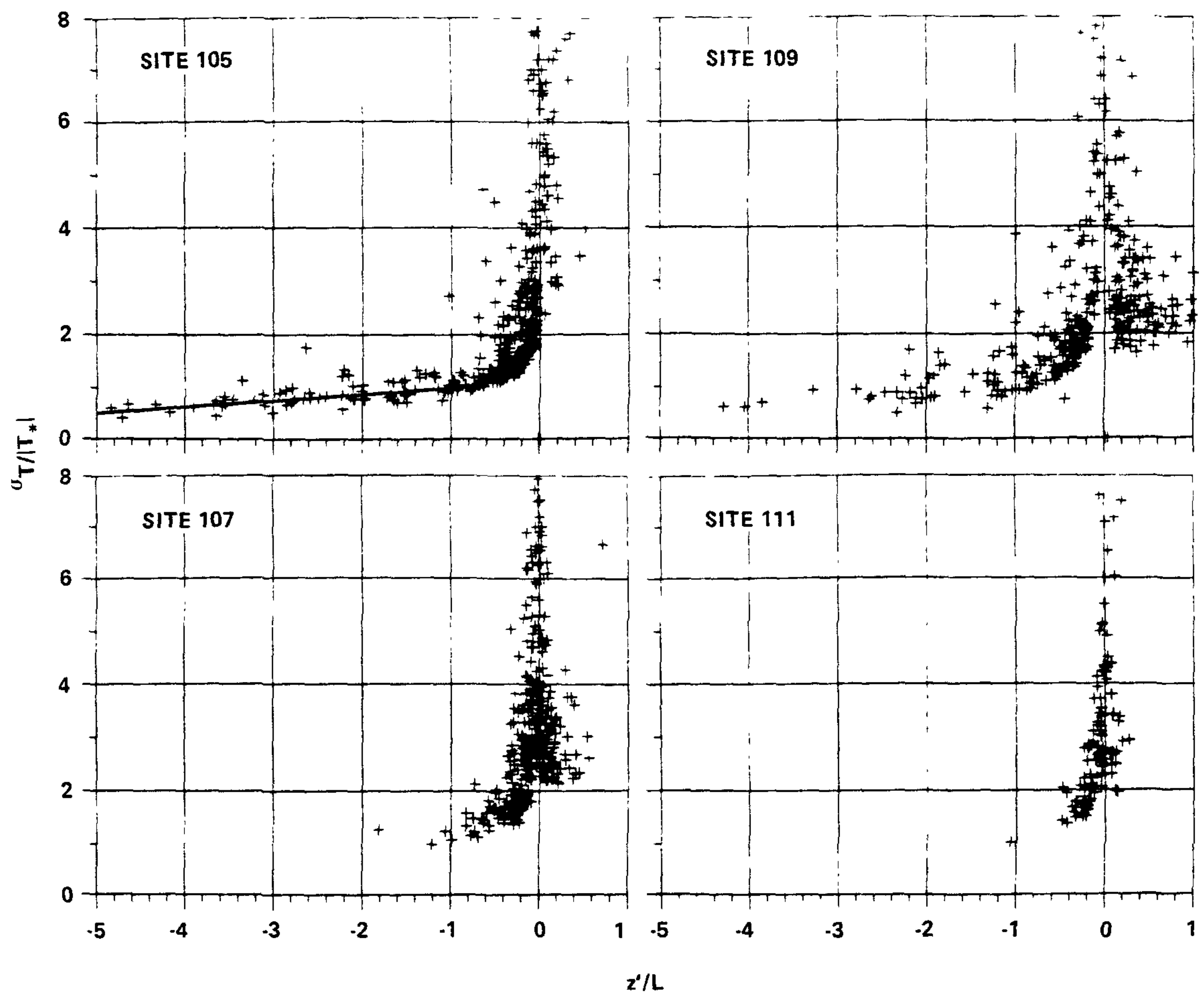


Figure 3.30. The ratio  $\sigma_T/T^*$  for the summer data set. The solid line on site 105 represents the Wyngaard et al. (1971) fit to the Kansas data ( $\sigma_T/T^* = 0.95(Z'/-L)^{-1/3}$ ).



for the Kansas or Minnesota data (these latter data sets give maximum ratios of about 3.0). We believe this is due to the 1-hour averaging time of the data often being over an unstationary period. For example, near the time of transition from stable to unstable conditions, the hourly average value of heat flux may be near zero, where in reality neutral conditions existed for a relatively short period of time. The temperature standard deviation on the other hand is based on periods of both the positive and negative heat flux and thus  $\sigma_T/T^*$  may obtain a large value.

For small positive values of  $z'/L$ , the Kansas and Minnesota data show  $\sigma_T/T^*$  to be between 1.5 and 2.0. Although insufficient to establish a definite trend,  $\sigma_T/T^*$  for the present data set appears to approach a value greater than 2.0 for stable stratification.

### 3.2.3 Covariance

The important covariances describing the nature of the momentum and heat transport are  $\overline{u'w'}$  and  $\overline{w'T'}$ , respectively. These when appropriately normalized are unity in the surface boundary layer. However, along with the buoyancy parameter  $g/T$ , they completely describe (through Monin-Obukhov similarity theory) the structure of the surface boundary layer. It is thus of interest to briefly describe their behavior for the four sites. Two other covariances are also discussed; the cross wind component of the stress  $\overline{v'w'}$ , which will be shown to be approximately zero, and the horizontal heat flux  $\overline{u'T'}$ . The final two covariances  $\overline{u'v'}$  and  $\overline{v'T'}$  were not calculated, but by definition are identically zero for horizontally homogeneous flow.

a. Momentum Flux--

The along and cross wind components of hourly-averaged vertical momentum flux are given in Table 3.7 for even hours of the summer data set. The values are given as  $-\overline{u'w'} \times 100$ . A value of 23, for example, indicates a downward momentum flux of magnitude  $0.23 \text{ m}^2/\text{sec}^2$ . The values of  $\overline{u'w'}$  appear to reflect the expected diurnal variation of wind speed and stability, and surface roughness (as expected from the similarity wind profile).

The  $\overline{v'w'}$  component of momentum flux is significant only during the afternoon hours (in a deep convective boundary layer). The maximum contribution to the average friction velocity,  $u^* = (\overline{u'w'^2} + \overline{v'w'^2})^{1/4}$ , from  $\overline{v'w'}$  is less than 1%; this lateral component was ignored in determination of  $u^*$ . Plots of  $u^*$  versus  $U$  for neutral stratification are given in Figure 3.31 for site 107. The slope of the estimated linear fit (solid line) is the square root of the drag coefficient and represents the effect of surface roughness. Estimated linear fits to the data for the other sites are also given in Figure 3.31. The slopes are about 0.11, 0.13, 0.07, and 0.15 for sites 105, 107, 109, and 111, respectively. Plots of  $U/u^*$  versus  $z'/L$  for sites 105, 107, and 109 are given in Figure 3.32 for the summer data set. The value of  $U/u^*$  decreases abruptly from stable stratification to a different constant value for each site at  $z'/L = -0.5$ . The scatter of the data points is in part due to the variation of  $Z_0$ .

b. Heat Flux--

The diurnal march of average heat fluxes ( $H = \rho C_p \overline{w'T'}$ ) for sites 105, 107, and 109 (summer data set) are depicted in Figure 3.33 along

Table 3.7. Average Hourly Values of  $-u'w'$  and  $-v'w'$  x100 (m<sup>2</sup>/sec<sup>2</sup>) for Summer Data Set.

		HOUR, CST											
	SITE	0000	0200	0400	0600	0800	1000	1200	1400	1600	1800	2000	2200
$-u'w'$	105	9	8	5	9	13	18	17	18	23	19	12	9
	107	10	8	5	9	17	24	23	23	26	22	13	12
	109	2	1	1	4	6	9	10	12	11	5	3	3
	111	11	9	9	13	27	33	36	44	49	32	19	17
$-v'w'$	105	0	0	0	1	0	0	1	2	3	2	1	0
	107	1	0	0	-1	-1	1	2	3	2	0	0	0
	109	0	0	0	0	-1	-1	0	2	0	0	0	0
	111	0	0	0	-1	-1	1	0	3	1	0	0	1

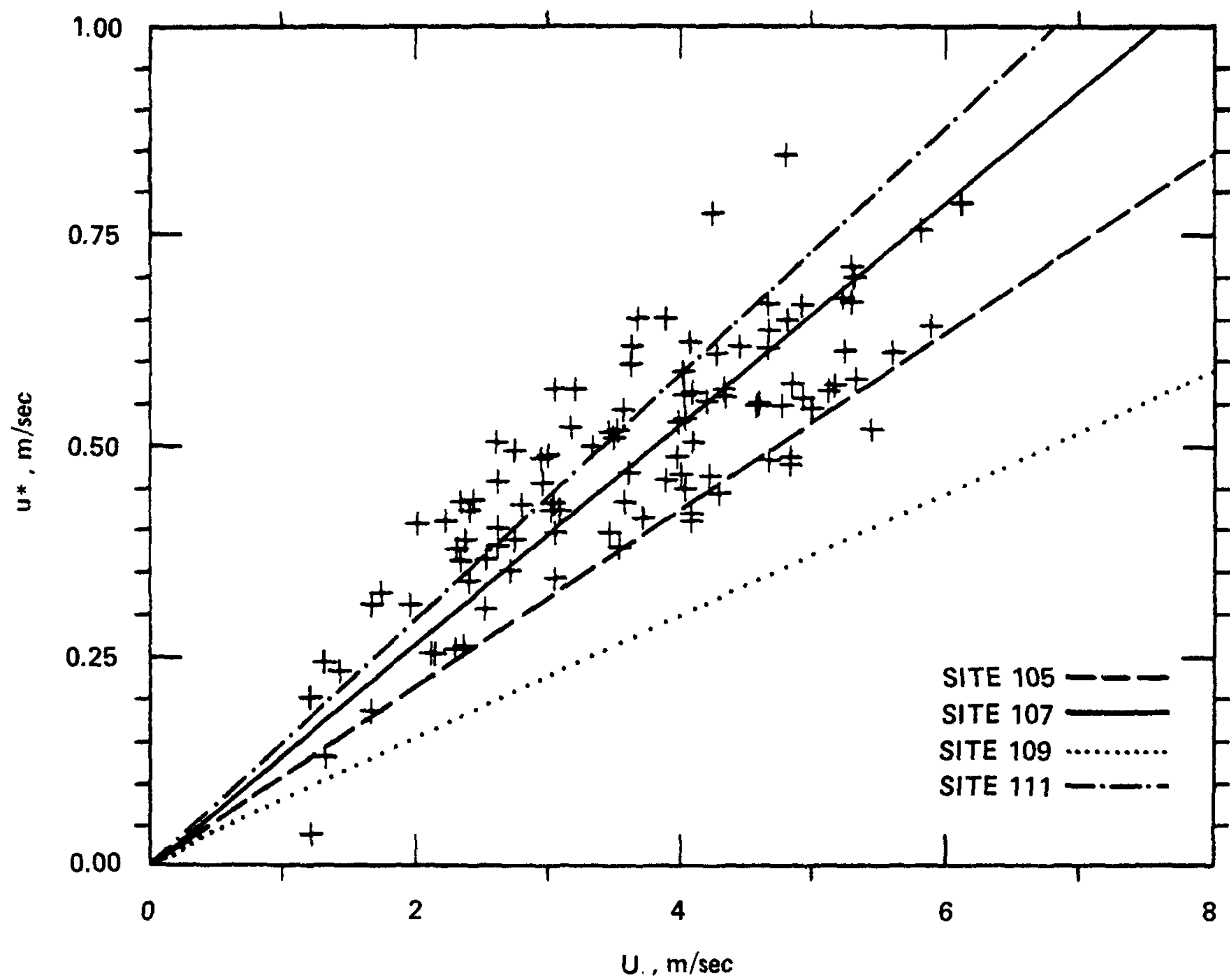


Figure 3.31. Plots of  $u^*$  vs.  $U$  for site 107 (summer data set, neutral stratification) and estimated linear fit to plots for all four sites.

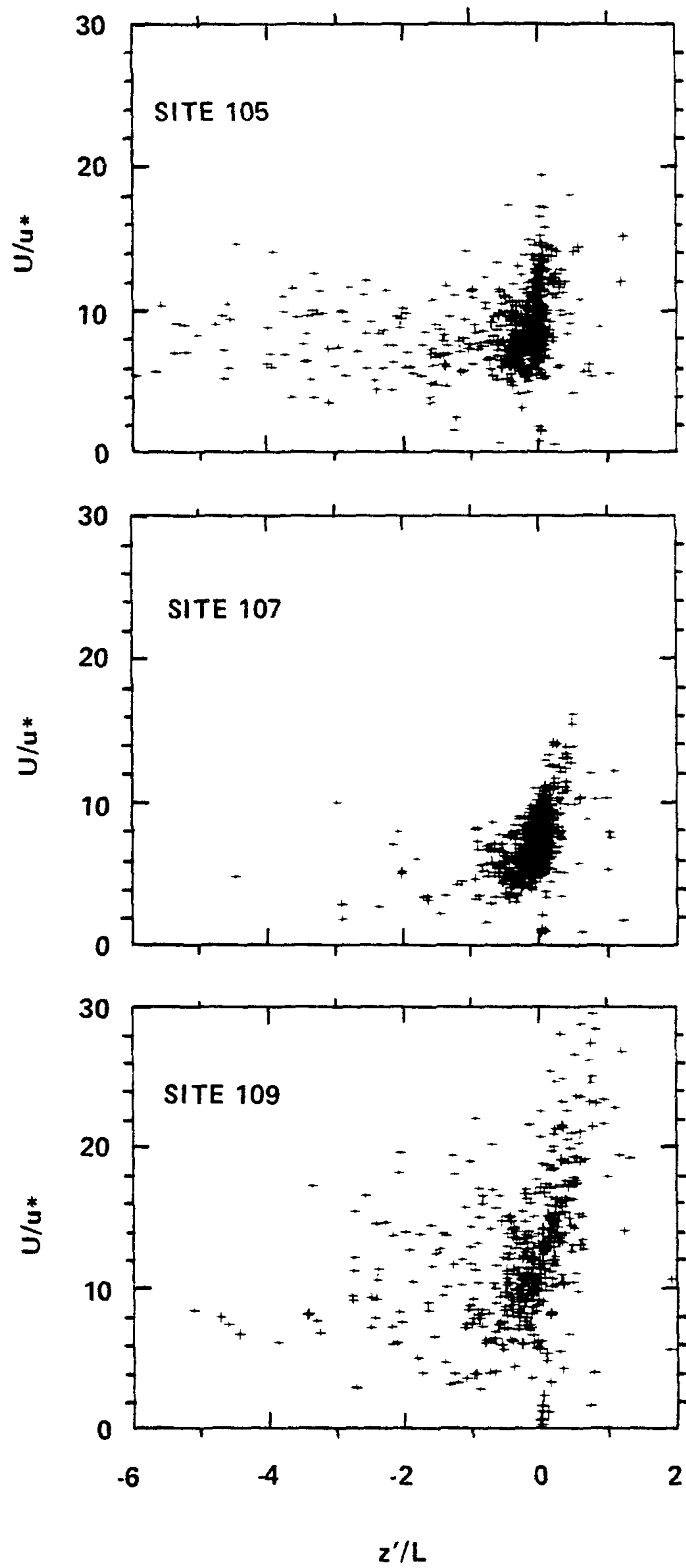


Figure 3.32. Plots of  $U/u^*$  vs.  $z'/L$ .

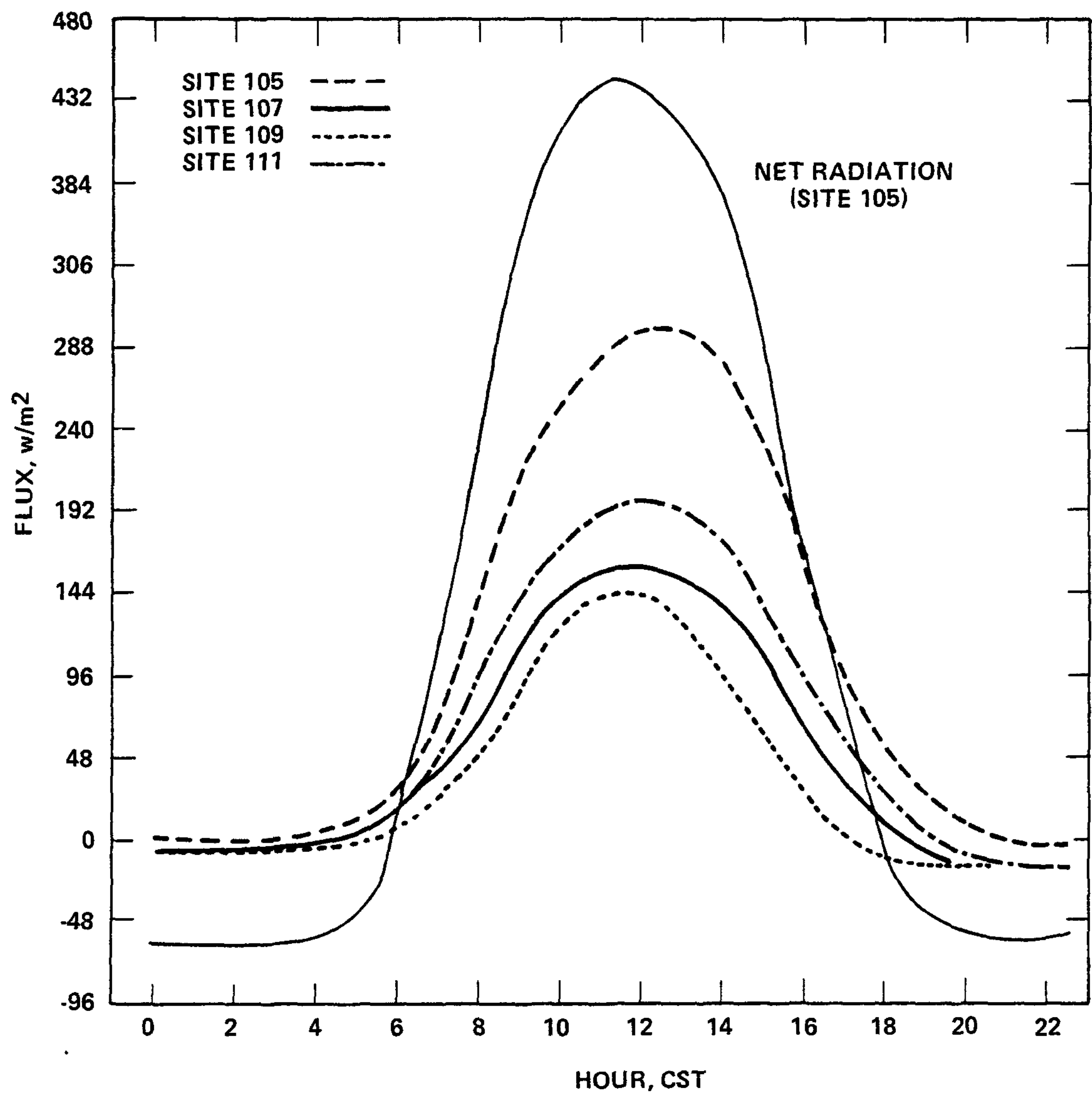


Figure 3.33. Diurnal variation of average heat flux for sites 105, 107, 109, and 111, and net radiation for site 105 (summer data set).



with the net radiation  $F_n$  for site 105 ( $F_n$  for site 109 was very similar). The peak afternoon heat flux for site 105, about  $300 \text{ w/m}^2$ , is significantly larger than for sites 107 and 109. The 105 heat flux remains positive throughout the night whereas at 107 and 109 it goes slightly negative. The contrast between the heat flux at site 105 and the heat flux at sites 107 and 109 is believed due to the characteristics of the surface and the resulting energy budgets. The few moisture flux measurements at sites 105 and 109, using the Lyman-alpha humidimeter, are helpful in this respect. Afternoon Bowen ratios,  $BR = H/LE$ , ( $LE$  is the latent flux) were on the order of 2.0 at site 105 and 0.5 at site 109. Ching et al. (1978) constructed a surface energy budget from this information in which the ground heat flux and anthropogenic heat sources constituted the residual term. These calculations suggest that the high afternoon heat flux at site 105 is not unreasonable considering the relatively small vegetated area available for evapotranspiration (See Table 3.1). Similarly, the differences between sites 105 and 107 are not unreasonable.

The horizontal heat flux, which is specified as a result of Monin-Obukhov similarity theory (see Table 1.1), appears as a horizontal gradient term in the thermal energy equation, and also appears in the buoyancy production term of the shear stress budget. While these terms are generally assumed small, they have not been measured in an urban area where advective processes may dominate boundary layer heating, especially during transition periods in the diurnal cycle (Ching et al., 1978).

The horizontal heat flux, normalized by  $u^*T^*$ , can be expressed as

$-\overline{u'T'}/\overline{w'T'}$ . This ratio is plotted as function of  $z'/L$  in Figure 3.34, wherein the solid line (site 105) represents the theoretical form postulated by Wyngaard et al. (1971) for  $z/L < 0$ , and is an excellent fit to the Kansas data. The ratio for the present data set is significantly larger than for the Kansas data. For large negative  $z'/L$ ,  $-\overline{u'T'}$  is on the order of  $\overline{w'T'}$  in the present data set; for Kansas data, it is about  $0.25\overline{w'T'}$ . The larger values may result from horizontal temperature gradients associated with the urban area. The ratio in Figure 3.34 is similar to that found by Zubkovskii and Tsvang (1966) for a site near an urban area. The rural site (Figure 3.34) has similarly large values of the ratio, suggesting possible nonhomogeneous conditions may also exist there.

### 3.3 SPECTRAL REPRESENTATION

#### 3.3.1 Introduction

While the total variance is a useful turbulence parameter, the distribution of variance as a function of frequency, i.e., the energy spectrum, provides a better description of the turbulent structure. The energy spectrum is obtained through the Fourier transform of the auto-correlation coefficient  $R(t)$  by:

$$F(n) = 4 \int_0^{\infty} R(t) \cos(2\pi n t) dt. \quad (3.16)$$

$F(n)$  represents the fractional contribution of the variance at frequency  $n$  to the total variance such that the integral of  $F(n)$  over all frequencies is equal to unity. It is customary in dealing with geophysical time series to work with the absolute spectrum,  $S(n) = \sigma^2 F(n)$ , multiplied by frequency  $n$  and plotted against  $\log n$ . Such a representation

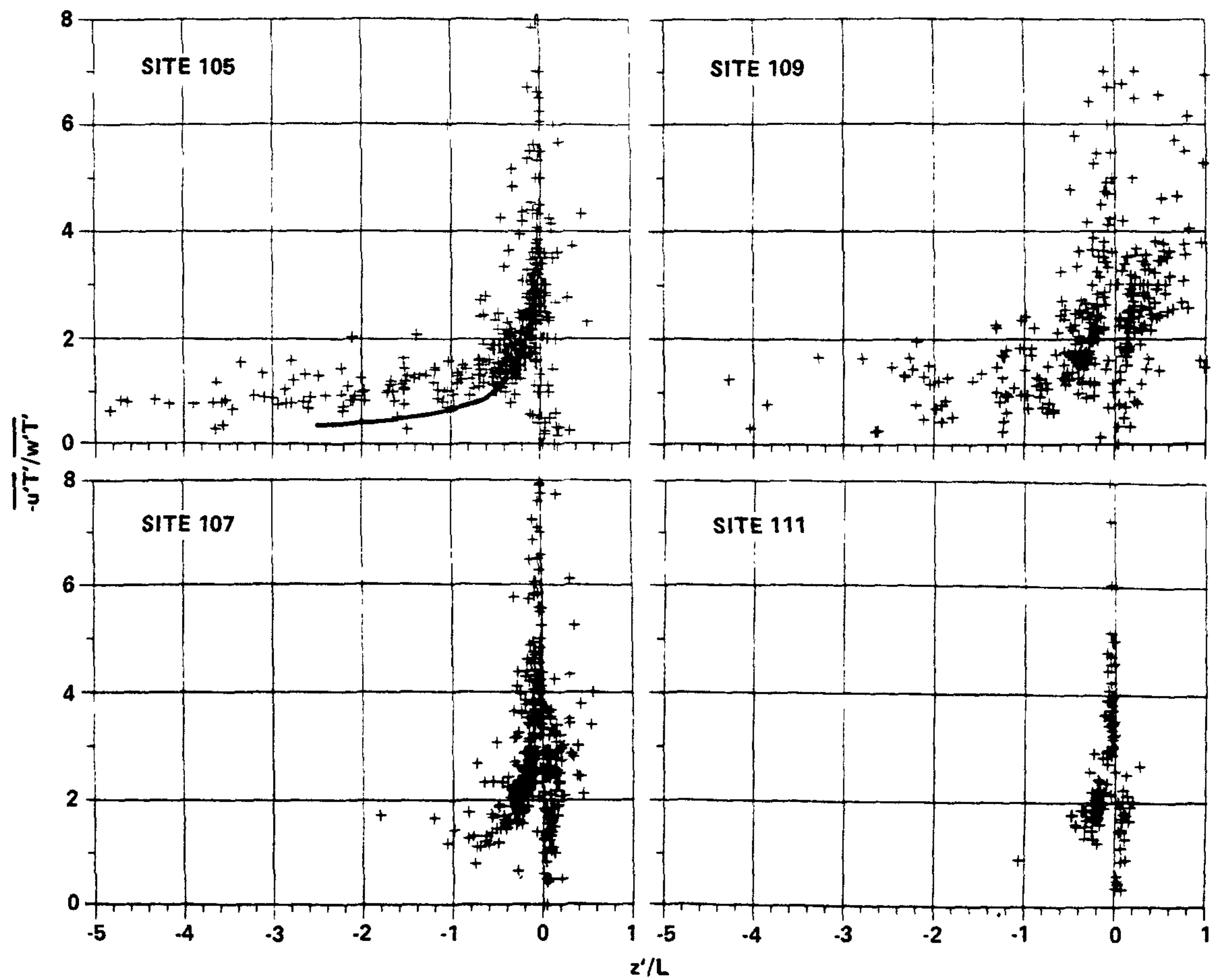


Figure 3.34. Ratio  $\overline{-u'T'}/\overline{w'T'}$  vs.  $z'/L$  (summer data set). The solid line (site 105) represents the theoretical form of Wyngaard et al.(1971).

usually results in a distinct peak in the spectrum that is apparently a function of stratification (see Kaimal et al., 1972), and usually considered to be the length scale of the predominate eddies contributing to the total variance. This length scale and other spectral features determined for the St. Louis summer data set are discussed here relative to the underlying surface roughness features and to similar determinations for the Kansas and Minnesota data sets.

### 3.3.2 Background

Monin-Obukhov similarity theory predicts:

$$F(n) = \frac{nS(n)}{\sigma^2} = G(z/L, f) \quad (3.17)$$

where  $f = nz/U$  is reduced frequency. Thus, spectral representations of the velocity components have generally been normalized by  $\sigma^2$  (or alternately by  $u_*^2$  since the two are related as a function of  $z/L$ ). The procedure used here follows that of Kaimal et al. (1972) where the spectra are normalized by  $u_*^2 \phi_\epsilon^{2/3}$ . The dimensionless dissipation rate for turbulent energy  $\phi_\epsilon$  is defined as:

$$\phi_\epsilon = kz_\epsilon/u_*^3. \quad (3.18)$$

The dissipation rate of turbulent energy per unit volume  $\epsilon$  is obtained through the Kolmogorov hypothesis for the inertial subrange of the one-dimensional wave number spectrum:

$$F(\kappa) = \alpha \epsilon^{2/3} \kappa^{-5/3}. \quad (3.19)$$

Here  $\kappa$  is the one-dimensional wave number and  $\alpha$  is an universal constant equal to approximately 0.5 (Kaimal et al., 1972; Wyngaard and Coté, 1971; Kaimal, 1973). Wave number spectra are converted to frequency

spectra through the Taylor (1938) frozen turbulence hypothesis, which implies that the statistics of a homogeneous stationary turbulent field at a fixed point are essentially the same as if the spatial pattern is frozen and moved past the fixed point with the mean wind speed  $U$ . With  $\kappa = 2\pi n/U$  and  $\kappa F(\kappa) = nS(n)$ , Eq. 3.19 yields:

$$nS(n) = \alpha \epsilon^{2/3} (2\pi n/U)^{-2/3} \quad (3.20)$$

where  $\epsilon$  can be obtained by:

$$\epsilon = (2\pi n/U)(nS(n)/\alpha)^{3/2} \quad (3.21)$$

when  $nS(n)$  is evaluated at a frequency  $n$  within the inertial subrange.

Combining Eqs. 3.18 and 3.21, we obtain a normalization which brings all spectra into coincidence in the inertial subrange; spectra for the longitudinal velocity component can then be expressed as:

$$\frac{nS_u(n)}{u_*^2 \phi_\epsilon^{2/3}} = 0.27 f^{-2/3}. \quad (3.22)$$

The spectral forms for the lateral and vertical velocity components, which differ by a factor of 4/3 (as a consequence of local isotropy), are given by:

$$\frac{nS_v(n)}{u_*^2 \phi_\epsilon^{2/3}} = \frac{nS_w(n)}{u_*^2 \phi_\epsilon^{2/3}} = 0.36 f^{-2/3}. \quad (3.23)$$

### 3.3.3 Dimensionless Dissipation Rate

The dissipation rate of turbulent kinetic energy, calculated from the vertical velocity spectra through Eq. 3.21, is given in Figure 3.35 for sites 105, 107, and 109. . Each data point represents a one-hour data sample with  $u^* > 0.15$  m/sec,  $U > 2.0$  m/sec, and an apparent

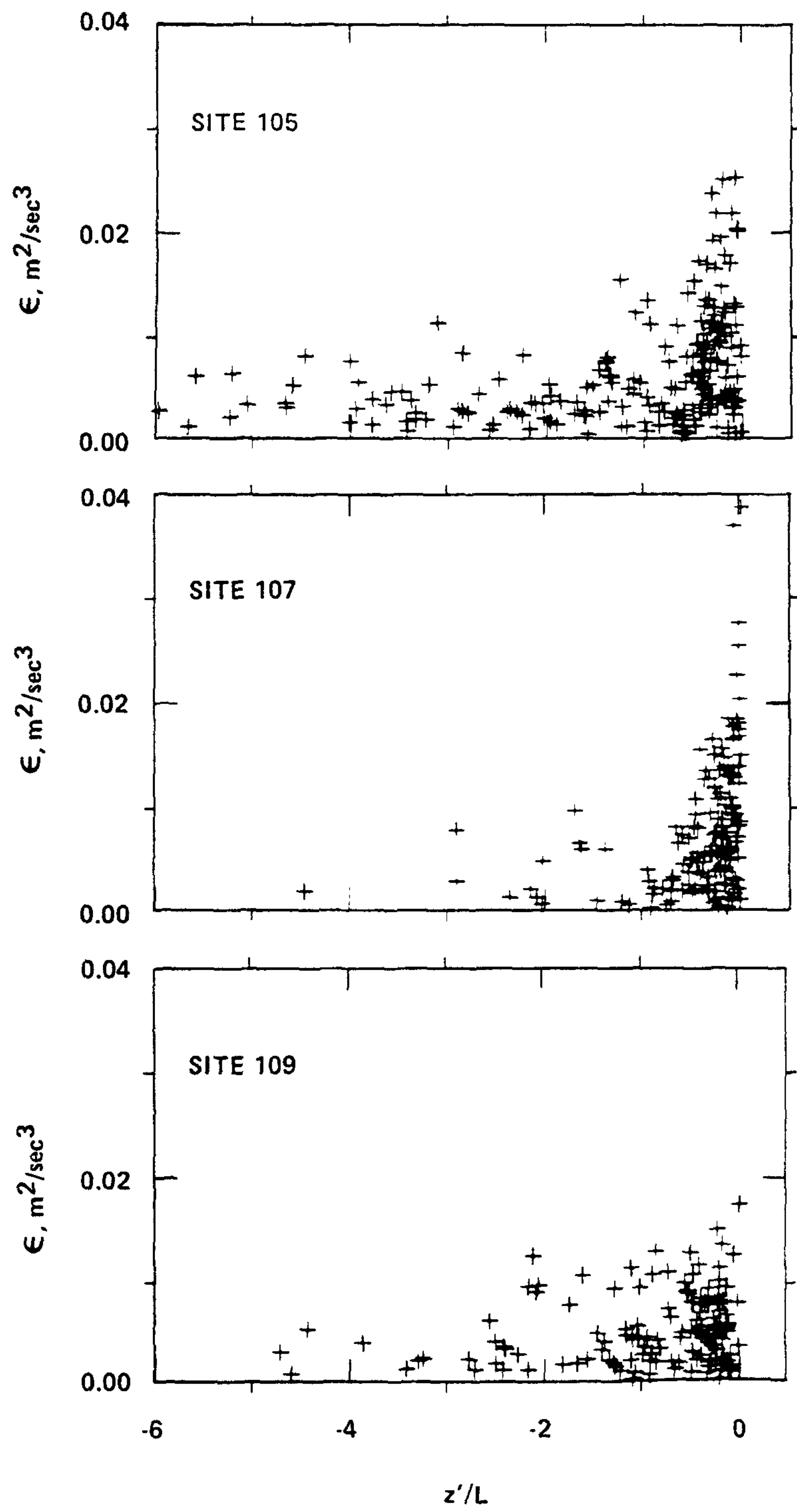


Figure 3.35. Turbulent energy dissipation rate  $\epsilon$  vs.  $z'/L$ .

-2/3 spectral slope in the inertial subrange (subjectively determined). The dissipation rate for unstable stratification appears independent of  $z'/L$  and lower in magnitude at the urban sites. The ratio  $\epsilon/\overline{g w' T'}/T$ , given in Figure 3.36, decreases with  $-z'/L$ . For site 105, the ratio is less than unity for  $z'/L < -0.5$  and decreases to about 0.5 at  $z'/L = -6$ . Since the shear production term is positive but small as compared to  $\overline{g w' T'}/T$ , the transport terms apparently remove energy from the surface layer at a rate greater than the dissipation rate at large  $z'/-L$ . Wyngaard and Coté (1971) suggested an upward transport of turbulent energy during convective conditions at about the same rate as the buoyancy production.

It is convenient to nondimensionalize all terms in energy equation by  $kz/u_*^3$  ( $k$  is the Karman constant), to obtain:

$$\phi_\epsilon = \phi_m - z'/L + R' \quad (3.24)$$

where  $\phi_m$  is the nondimensionalized mechanical production rate, and  $R'$  represents the residual due to the vertical transport terms and also includes any inhomogeneity effects.

Plots of  $\phi_\epsilon$  versus  $z'/L$  for site 105 are shown on Figure 3.37a. The solid curve is the estimated fit to the data points. The dashed line represents the dimensionless dissipation rate for the Kansas data (Wyngaard and Coté, 1971) expressed as  $\phi_\epsilon^{2/3} = 1 + 0.5(z/-L)^{2/3}$ . Except for neutral stratification ( $z'/L = 0$ ), the two curves differ markedly. The estimated fit to the plots for sites 105, 107, and 109



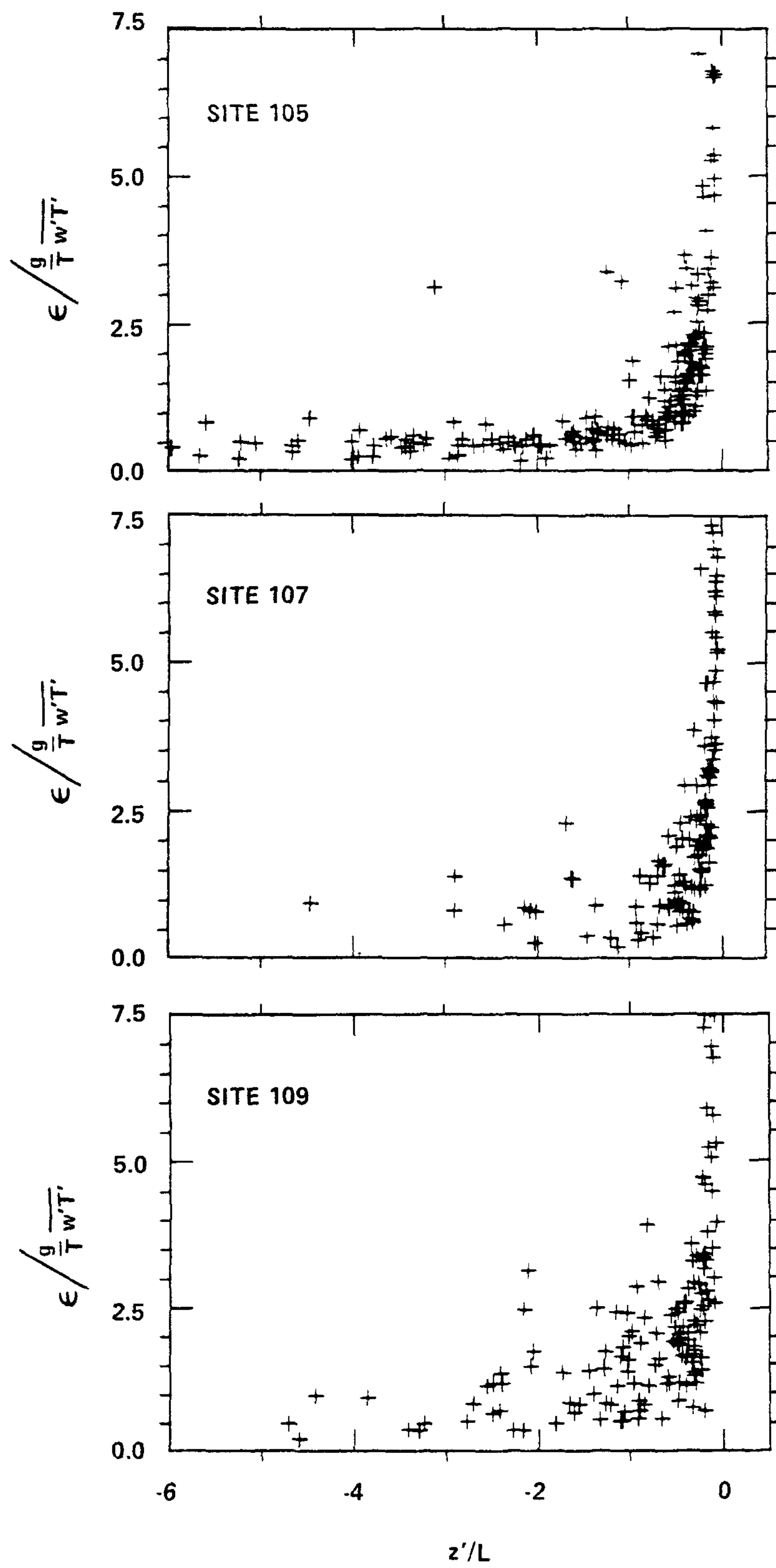


Figure 3.36. The ratio  $\epsilon / \overline{gw'T'}/T$  vs.  $z'/L$ .

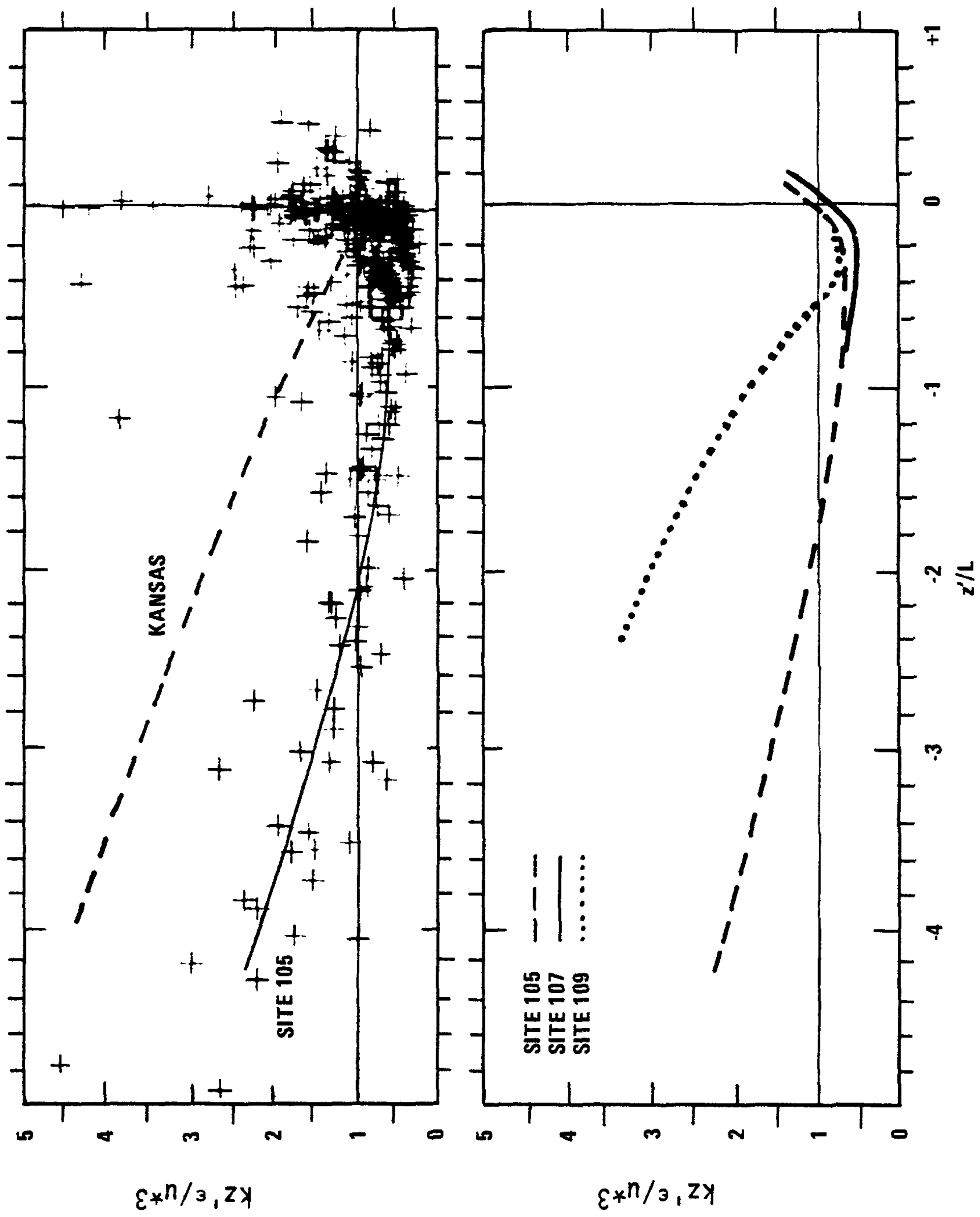


Figure 3.37. Estimated fit to plots of the nondimensionalized energy dissipation rate vs.  $z'/L$  for a) site 105 and Kansas data (plots are for site 105) and b) for sites 105, 107 and 109.

are given on Figure 3.37b. For neutral stratification,  $\phi_\epsilon$  is about 1.0, 0.7, and 1.0 for sites 105, 107, and 109, respectively. For unstable stratification, the curve for site 109 has the same basic magnitude and trend as the Kansas data. Note that for small negative values of  $z'/L$ ,  $\phi_\epsilon$  is less than unity at all three sites.

### 3.3.4 Vertical Velocity Spectra

The  $nS(n)$  spectra for the velocity components and temperature were computed for hourly data samples from which a linear trend was removed. The procedure for obtaining the spectrum from a time series is outlined in Appendix B. The result was eleven spectral estimates each averaged over  $2^x$  ( $x=0,10$ ) raw spectral points over equally spaced log-frequency intervals. Thus, the first spectral estimate consists of the first raw spectral point, whereas the eleventh estimate represents an average over 1024 points.

Vertical velocity spectra, normalized by  $u_*^2 \phi_\epsilon^{2/3}$  and plotted against reduced frequency  $f = nz/u_*$ , are given in Figure 3.38 for three stratification classes for sites 105, 107, and 109. The data screening procedure for the spectral plots was the same as given above for the dissipation plots except the criteria for stable spectra were relaxed to  $u_* > 0.10$  m/sec and  $U > 1.0$  m/sec to obtain a larger sample. All spectra are in coincidence in the inertia subrange (because of the normalization procedure) and the scatter increases toward the low frequency end. The scatter, however, is not larger than expected from the uncertainty of the individual spectral estimates. The dashed lines on the plots represent a composite Kansas spectrum for neutral stratification (Kaimal et al., 1972). The solid lines above or below represent the

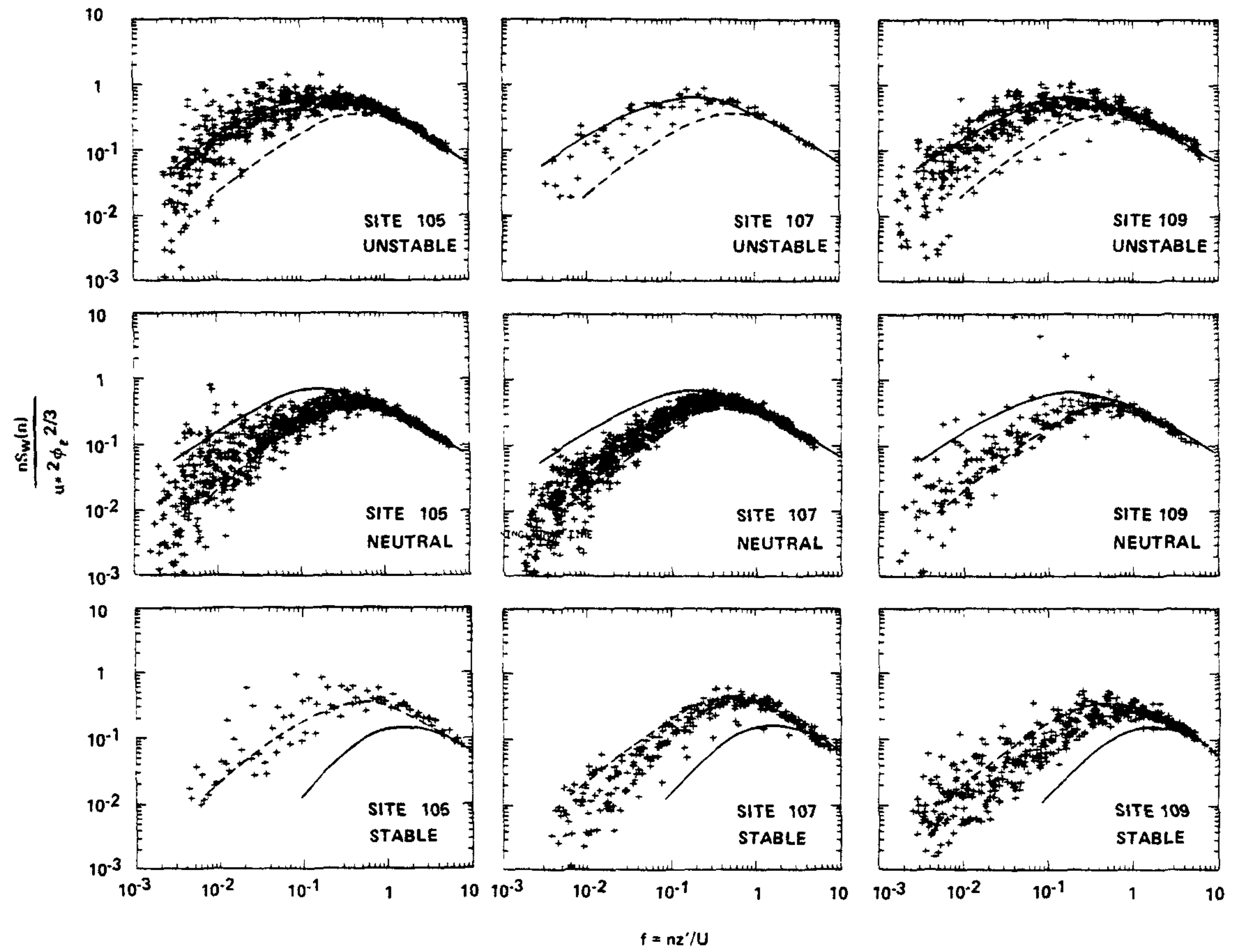


Figure 3.38. Vertical velocity spectra for sites and stability classes indicated. Dashed lines are Kaimal et al. (1974) composite spectrum for  $z'/L=0$ . Solid lines above and below are the Kaimal spectra for  $z'/L=-2$  and  $1$  respectively.

Kaimal spectra for  $z'/L = -2$  or  $+1$ , respectively. The peak of the St. Louis spectra are shifted towards lower frequencies compared to the Kansas spectra, especially for neutral and stable stratifications. For a given stratification class, no obvious differences occur among the spectra for the St. Louis sites. In general, these spectra are in agreement with the Monin-Obukhov similarity prediction (i.e., the spectral form appears to be a function of  $z'/L$  and  $f$ ).

The spectral representations shown in Figure 3.38 are inadequate for comparison of the spectra for different sites. Turbulence length scales derived from the spectral form provide a quantitative means of comparison of the spectra for different sites and atmospheric influences. Three commonly referenced length scales are the wavelength corresponding to the peak in the logarithmic power spectra  $L_m = U/n_m$  ( $m$  refers to the value associated with the peak in the spectrum), the Eulerian integral length scale  $L_i = U \int_0^\infty \bar{R}(t) dt$ , and the dissipation length scale  $L_\epsilon = \sigma_w^3/\epsilon$ . For homogeneous, fully-developed turbulence these length scales are not independent of each other. For the  $w$  spectra and neutral-to-stable horizontal velocity spectra, which are expressible in the form:

$$S(n) = \frac{A}{1 + Bn^{5/3}}, \quad (3.25)$$

Kaimal (1973) has shown that:

$$L_m = 2\pi L_i = \pi L_\epsilon. \quad (3.26)$$

Kaimal (1973), Hanna (1968), and Wamser and Müller (1977) have shown empirically the relationship between  $L_m$  and  $L_\epsilon$  to be valid for  $w$  spectra. The procedure for this study was to fit Eq. 3.25 to the raw

spectra estimates to determine A and B and subsequently the length scale and dissipation rate (see Appendix B). However, Eq. 3.25 was fitted over different ranges of the spectrum such that independent estimates of  $L_m$ ,  $L_j$ , and  $L_e$  could be obtained (e.g.,  $L_j$  was determined by giving greater weight to the low frequency end of the spectrum and  $L_e$  by giving more weight to the high frequency end). The relationships between these several length scales were approximately as given by Eq. 3.26 and thus only  $L_m$  is discussed here.

Information on the maximum wavelength of the spectrum is conveniently and historically presented in terms of the associated normalized frequency  $f_m = n_m z' / U = z' / L_m$ . This inverse normalized length scale is plotted against  $z' / L$  in Figure 3.39 for site 105, 107, and 109. The ratio is essentially constant for very unstable stratification at a value of about 0.18 for site 109 and 0.15 for site 105. For neutral stratification the ratio is 0.31, 0.29, and 0.36 for sites 105, 107, and 109, respectively. The data scatter for stable stratification is large; however, it is obvious that the ratio increases with increasing stability and the slope is greater for site 109 than 107. The solid line shown on the plots for site 109 is the empirical fit to the Kansas data (Kaimal et al., 1972), which has a value of 0.5 at  $z' / L = 0$  and 0.17 for unstable stratification. Eversole (1979) found  $z' / L_m(w)$  to be about 0.13 for unstable stratification at the Boulder tower.

The diurnal variation of  $L_m(w)$ , visually estimated from plots, is given in Figure 3.40. A land-use influence is apparent;  $L_m$  is generally larger at the urban sites during the nocturnal hours, reflecting the less stable conditions associated with the urban heat island and larger

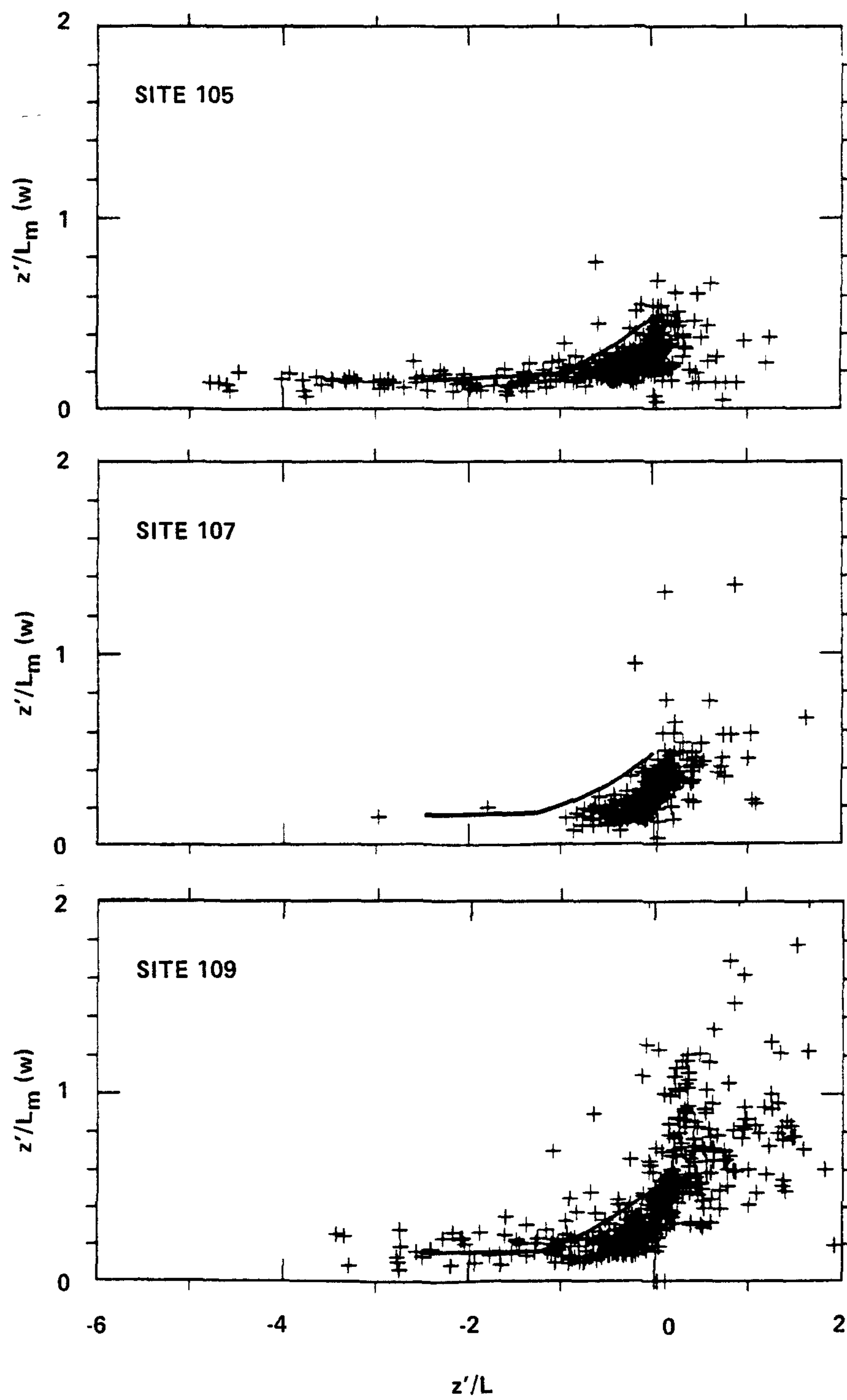


Figure 3.39. Plots of  $z'/L_m(w)$  vs.  $z'/L$  for summer data set. The solid lines represent results for Kansas data set (Kaimal et al, 1972).



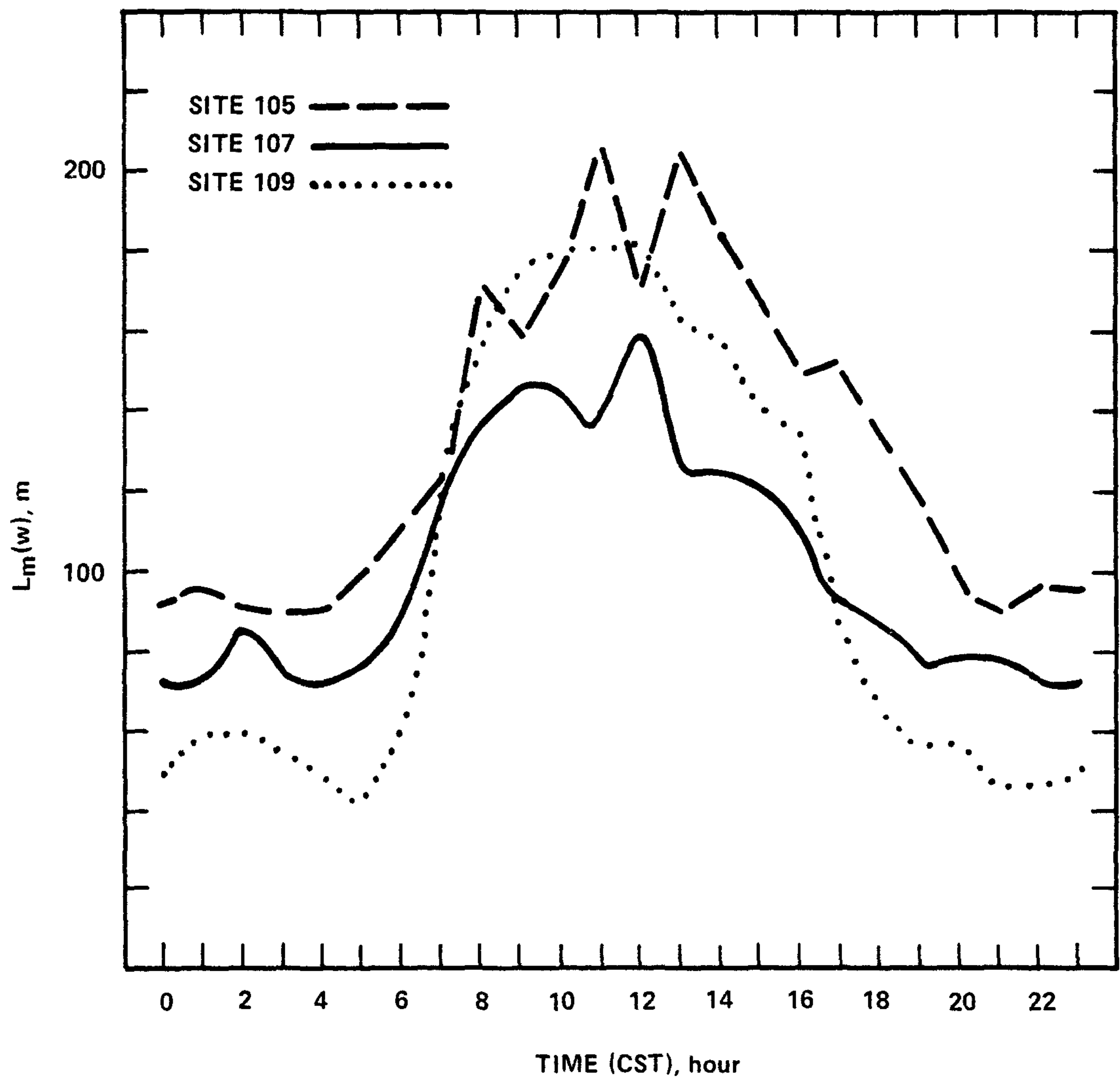


Figure 3.40 Estimated fit to plots of diurnal variation of  $L_m(w)$  for sites 105, 107, and 109.

surface roughness. During the convective period,  $L_m$  for site 107 is significantly lower than for sites 105 and 109. This, we believe, reflects the difference in stratification at the sites which are strongly influenced by surface features. In other words, the midday values of  $L_m$  at site 107 are driven by  $z'/L$  values in the range of 0 to -1, while those for sites 105 and 109 are driven by  $z'/L$  values extending to -6. Surface features strongly influence boundary layer structure at the height of measurement; however, the differences in  $L_m(w)$  between sites 107 and 105 would be expected to decrease at greater distances above the surface. The more rapid decrease of  $L_m(w)$  at site 109 during the late afternoon hours suggests a boundary layer gradually decreasing in height in the urban area, but collapsing rather quickly in the rural environs.

Wamser and Müller (1977), using data at 50 m from a tower in suburban Hamburg, Germany, found  $L_m(w)$  to be inversely proportional to the surface roughness length during neutral and convective conditions. This is in contrast to the St. Louis data set, where  $L_m(w)$  is larger for the urban area. The data, however, do not appear to be strongly influenced by surface roughness as suggested in Figure 3.41, where  $L_m(w)$  is plotted as a function of wind direction for site 107. In contrast to Figure 3.3 ( $z_0$  versus wind direction) essentially no variation of  $L_m(w)$  with wind direction exists.

### 3.3.5 Horizontal Velocity Components

The spectral plots for the lateral and longitudinal velocity components are given in Figures 3.42 and 3.43, respectively. The dashed lines again represent the generalized spectra of Kaimal et al. (1972)

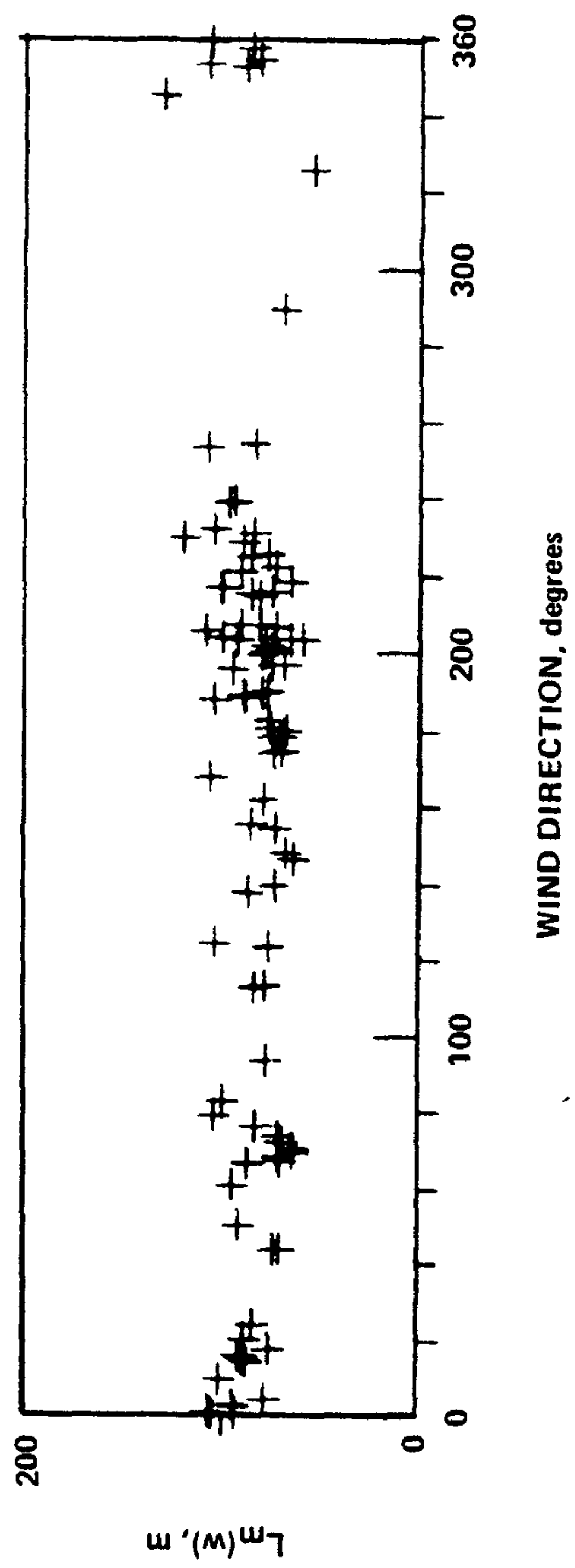


Figure 3.41.  $L_m(w)$  vs. wind direction for site 107 for neutral stratification.

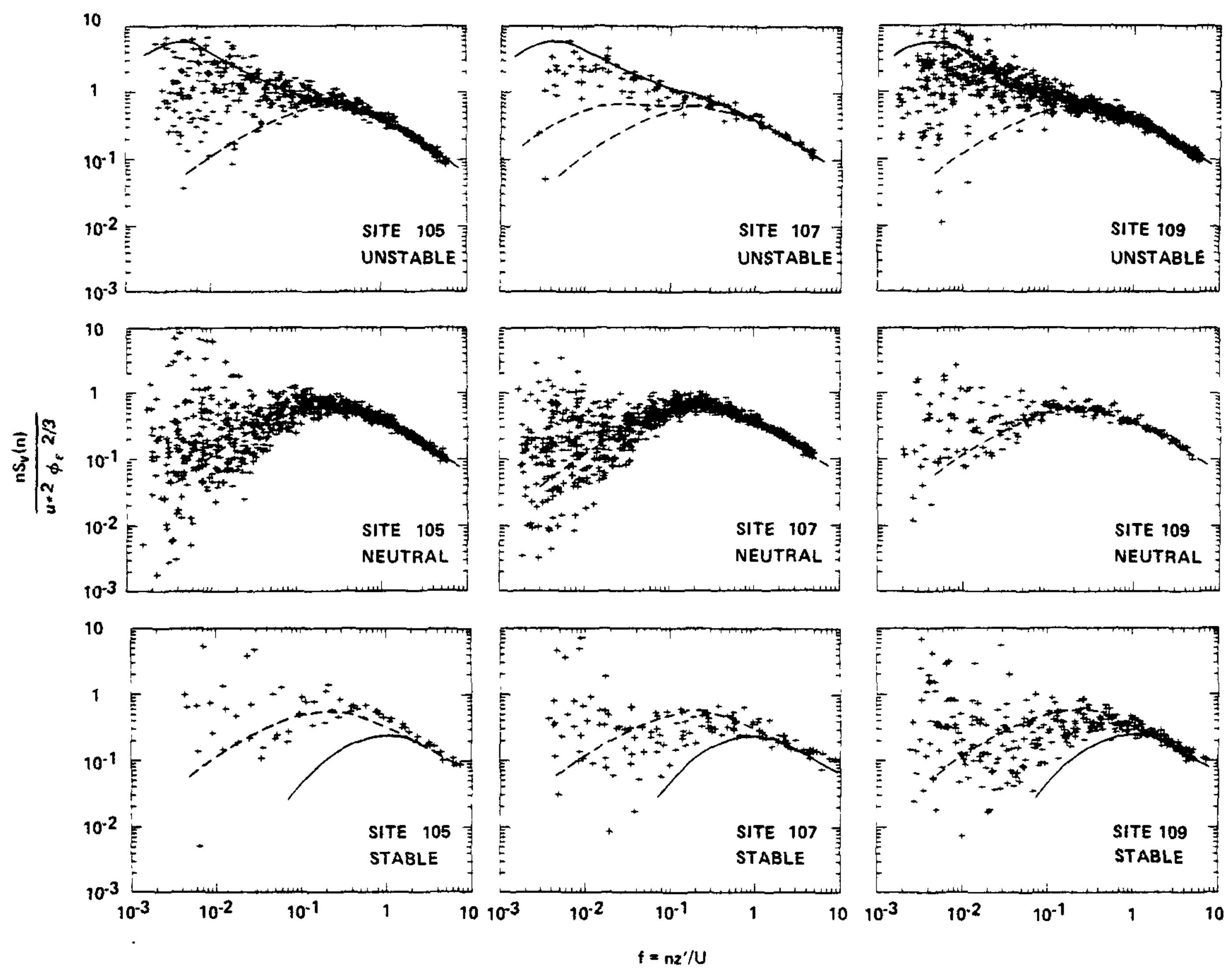


Figure 3.42. Lateral velocity spectra for sites and stability classes indicated. Dashed and solid lines are as indicated for Figure 3.38. The upper dashed line for site 107 is an exclusive zone (see text).

# SPECTRA FOR LONGITUDINAL VELOCITY COMPONENT

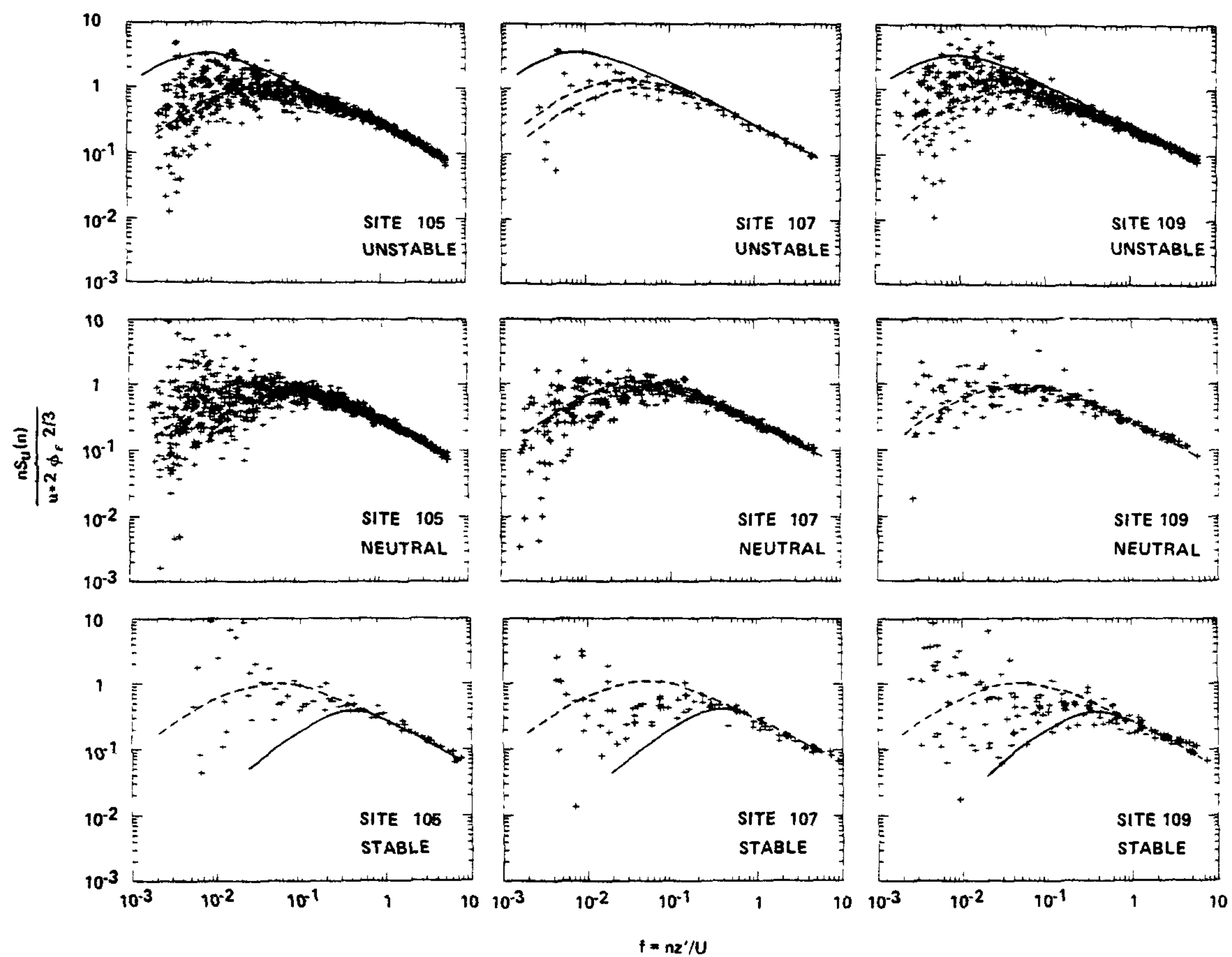


Figure 3.43. Same as for Figure 3.42 for longitudinal velocity component.

for neutral stratification, and the solid lines for  $z'/L = -2$  or  $+1$ . The upper dashed line for site 107 (unstable stratification) on both figures is what Kaimal et al. describe as the upper limit of an exclusion zone given by  $z'/L = -0.0$ . They suggest a step shift in energy as the atmosphere passes from neutral to unstable stratification; consequently no spectra should fall within this region.

The St. Louis spectra, while qualitatively compatible with the Kaimal form, exhibit some obvious anomalies. For example, the peak in the stable spectra appears to be shifted to lower frequencies, and a low frequency mesoscale component occurs for both stable and neutral stratifications. The mesoscale component, which is more pronounced for the lateral velocity, corresponds to wavelengths on the order 3 to 10 km. These longer wavelengths may be due to both land use and urban scale induced perturbations on the flow. However, the mesoscale component is also present in the data for the rural site.

The existence of the mesoscale spectral components makes identifying a representative peak in the spectral plots difficult for unstable stratification. Kaimal (1978) discussed the unstable horizontal velocity spectra as consisting of three regions: an inertial subrange region that falls off as  $f^{-2/3}$  (this region follows Monin-Obukhov similarity, i.e.,  $nS(n)=f(z'/L,f)$ ); a low frequency energy generation region governed by the height of the mixed layer  $z_i$ ; and a transition or matching region between the above two. The inertial subrange and the matching region described by Kaimal are generally apparent in the St. Louis unstable spectra. The low frequency region is masked by the mesoscale energy, and the lack of a mixed layer scaling length in the analysis.

The diurnal variation of the peak wavelength in the lateral and longitudinal velocity components are shown on Figures 3.44 and 3.45. These visually smoothed and averaged plots are based on Eq. 3.25, which may not be completely appropriate for the horizontal velocity components (especially the lateral component), and may also be contaminated by energy at mesoscale frequencies. Thus they should be interpreted with caution and only in a relative sense, and may be considered an underestimate.

Urban influences appear in the data. Spectral peaks for the nocturnal hours are highest at site 105 and during the convective hours lowest at site 107. The former feature is likely associated with the urban heat island and the latter with the relatively less unstable conditions existing at site 107 during the afternoon period.

The afternoon transition of  $L_m(u,v)$  at all sites is in contrast to that indicated by Caughey and Kaimal (1977). They suggest a rapid collapse of convection near sunset. Our data (which are supported by aircraft measurements of turbulence over St. Louis during the same period) suggest the layer of vigorous mixing decreases more gradually over a 3 to 4 hour period. Urban lidar mixing heights from Figure 3.19 are superimposed on Figures 3.44 and 3.45. The lidar mixing heights are approximately equal to  $L_m$  during the morning transition period and considerably larger than  $L_m$  during the evening transition. The peak wavelength is believed to more accurately reflect the actual height of mixing in the atmosphere than the lidar mixing heights. The decrease in the lidar mixing heights later than the spectral peak is believed due



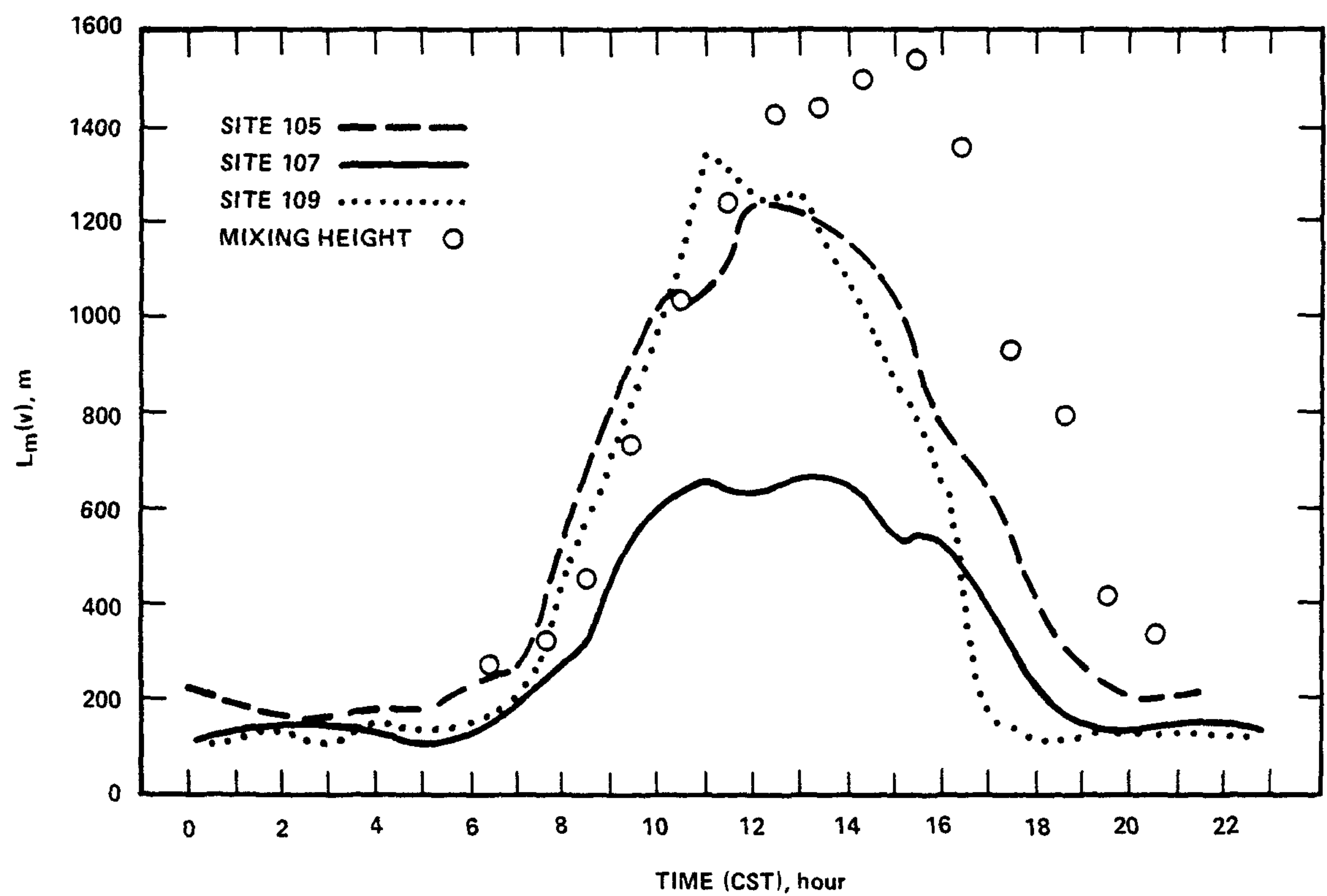


Figure 3.44. Estimated fit to plots of diurnal variation of  $L_m(v)$  for sites 105, 107, and 109. Open circles represent urban mixing heights.

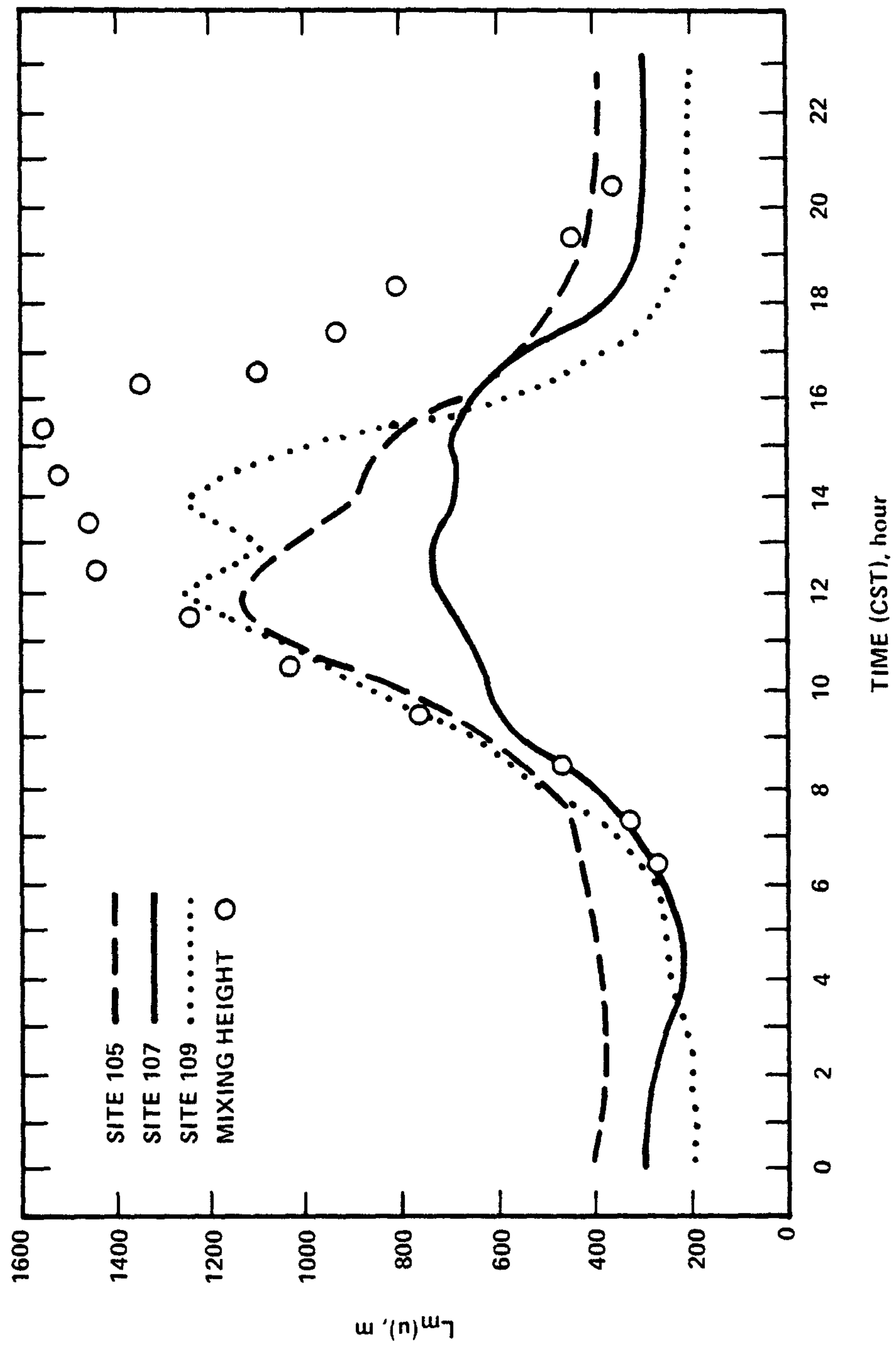


Figure 3.45 Same as for Figure 3.44 for  $L_m(u)$ .

to residual aerosol, which may take several hours to be advected out of the city.

Urban mixing heights and heat flux from Figure 3.19,  $L_m(v)$  for site 105, and  $\sigma_v$  for both sites 105 and 109 are given in Figure 3.46 for the heating period of the day. The peak wavelength appears to be a better indicator of  $\sigma_v$  than  $z_j$ . Also note the similarities between the diurnal anomalies of  $\sigma_v$  for sites 105 and 109 on Figure 3.46 and the diurnal anomalies of  $L_m(v)$  on Figure 3.44. These features suggest that mixed layer turbulence responds more directly to  $L_m$  than to  $z_j$ .

Kaimal et al. (1976) and Kaimal (1978) determined  $L_m(u,v)$  to be about 1.3 to 1.5 $z_j$ . While Figures 3.45 and 3.46 do not indicate these values, the form assumed for the spectral shape from which the peak was determined (Eq. 3.25) would generally underestimate the peak. Visual inspection of the unstable spectral plots on Figures 3.42 and 3.43 suggest that spectral peaks on the order of 1500 to 3000 m would not be unreasonable. However, the observations were made at a height of about 0.02 $z_j$  and could be responding to a mixture of surface layer and mixed layer scaling.

### 3.3.6 Temperature Spectra

Within the inertial subrange, Corrsin (1951) proposed the temperature spectrum as given by:

$$F(\kappa) = \beta \epsilon^{-1/3} N^* \kappa^{-5/3} \quad (3.27)$$

where  $\beta$  is a constant with a value of approximately 0.8 (Wyngaard and Coté, 1971) and  $N^*$  is the dissipation rate of  $\overline{T^2}/2$ . Kaimal et al. (1972) developed the following normalization based on this form, which

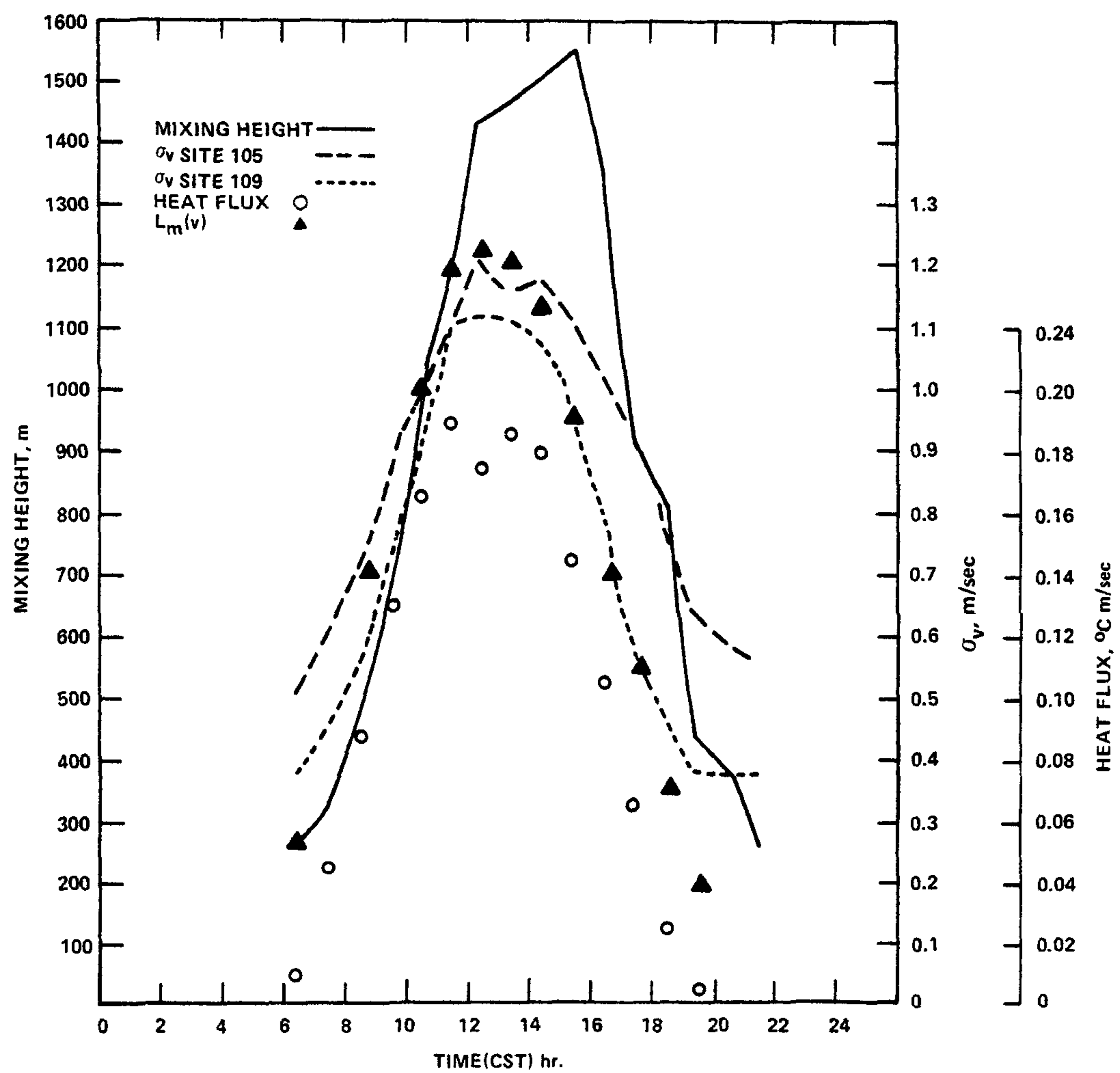


Figure 3.46. Comparison of  $z_j$ ,  $L_m$ ,  $\overline{w'T'}$ , and  $\sigma_v$  for urban sites and  $\sigma_v$  for rural site for heating period of the day.

collapses all spectra to a common form within the inertial subrange:

$$\frac{nS_T(n)}{T_*^2 \phi_N N_* \phi_\epsilon^{-1/3}} = 0.43 f^{-2/3}. \quad (3.28)$$

Here  $\phi_N = kzN^*/u_*T_*^2$  is the normalized dissipation rate of temperature and all other symbols have been defined previously.

The normalized temperature spectra for three stratification classes and three sites are shown in Figure 3.47. Again the Kaimal et al. (1972) composite spectra are given for comparison. Similar to the velocity spectra, the peaks in St. Louis stable temperature spectra appear shifted to lower frequency, but to a larger extent, for site 107 as compared to site 109. The neutral spectra are generally ill-defined and, along with the stable spectra, have a significant mesoscale component. The spectra for the unstable stratification consist of a broad peak and generally lack a mesoscale component. Again, differences between the urban sites and site 109 are not obvious if they exist at all.

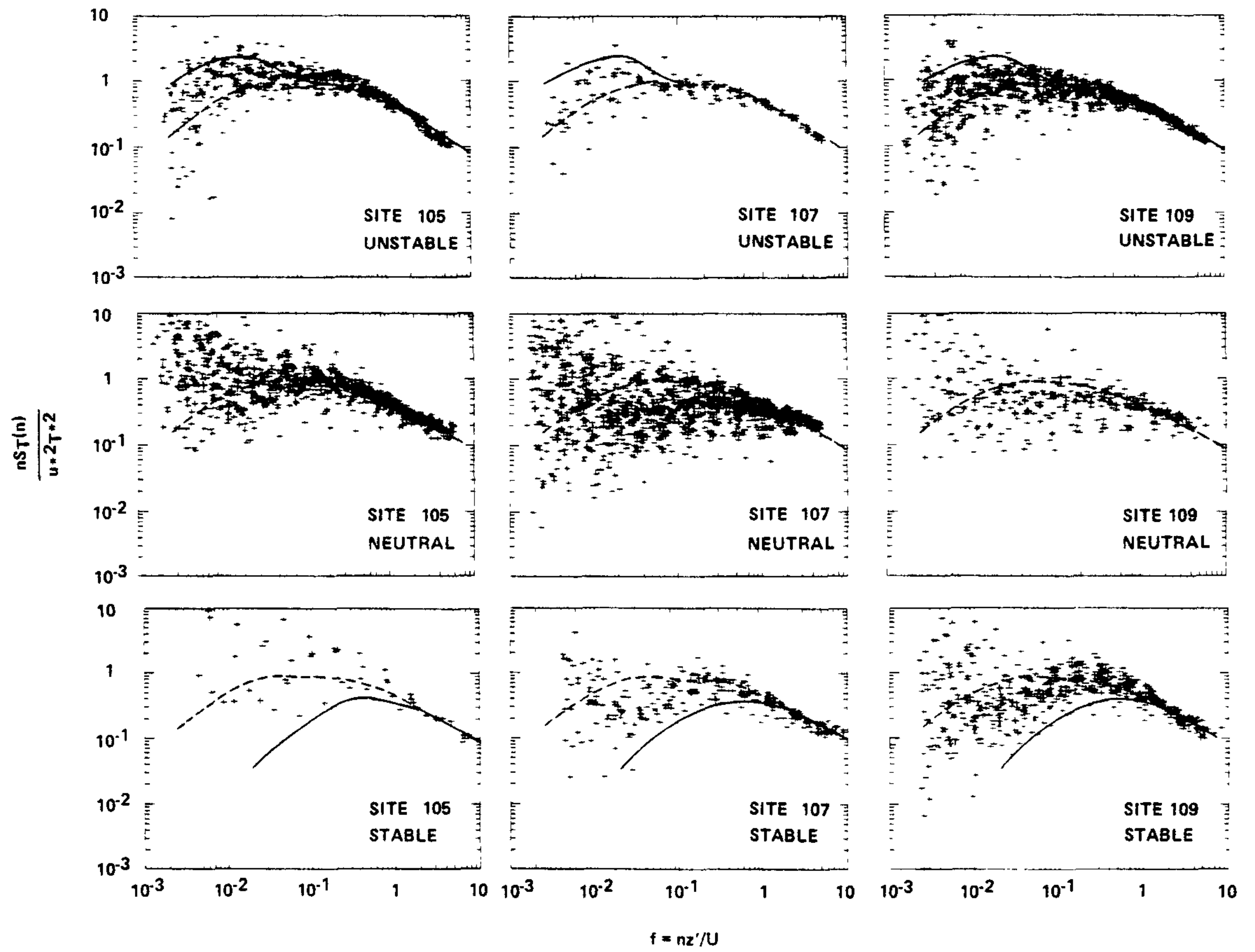


Figure 3.47. Temperature spectra for sites and stability classes indicated. Dashed and solid lines are as indicated for figure 3.38.

## 4.0 SYNTHESIS OF RESULTS

### 4.1 INTRODUCTION

The basic purpose of this study was the evaluation of Monin-Obukhov similarity theory for description of turbulence above the complex and rough urban surface. Discussions relative to this topic are contained in Section 4.3. However, the analyses presented in Section 3 also encourage discussion with respect to general boundary layer phenomena and urban anomalies not directly addressed by similarity theory. These latter topics are briefly addressed below.

### 4.2 BOUNDARY LAYER PHENOMENA

Land-use features varied significantly among the four sites. Thus at the outset each site was characterized numerically by an estimated displacement length and a site-averaged roughness length calculated through the similarity wind profile formulation. Estimated displacement lengths ranged from 2 to 6 m at the urban sites and site-averaged roughness lengths from 0.7 to 1.7 m (Table 3.1). Surface roughness length varied significantly with wind direction at both urban and rural sites, suggesting the surface features were not homogeneous in space. The surface wind stress was proportional to  $Z_0$  (as expected from the method of calculation of  $Z_0$ ). Relatively large values of stress occurred at the urban sites throughout the diurnal cycle. The value of  $u^*$  for the convective period of the day was 0.2 or larger at all sites.

The surface energy budget also varied with the composition of land-use features. Afternoon values of heat flux at the urban commercial site (105), which had a high percentage of paved areas and few trees,



were about twice those at the rural site (109). During the nocturnal hours, the heat flux was generally negative at site 109, but was seldom negative at site 105. Latent heat flux was significantly greater at site 109 than at site 105; afternoon Bowen ratios of 0.5 and 2.0 were characteristic of sites 109 and 105, respectively. The heat flux at urban site 107, which had numerous tall trees, was similar to that at site 109 during daylight hours. At night, site 107 had a zero or very small negative heat flux characteristic of an urban site.

The boundary layer stratification reflected the land-use features responding to the ambient air flow and solar radiation. Based on computations of  $z'/L$ , which includes the effects of both heat flux and surface stress, site 109 was strongly stable at night and strongly unstable during the afternoon. Site 105 was neutral and strongly unstable for the two periods, respectively. Site 107 was essentially neutral at night but only slightly to moderately unstable during the convective period of the day (due to the large surface stress and relatively small heat flux).

Partly in response to the temporal and spatial variation of stratification, the diurnal variation of most turbulence parameters differed significantly between the urban and rural environs. The turbulent wind standard deviations, turbulence intensities, and the spectral peak wavelengths were without exception higher at the urban sites during nocturnal hours due to the urban heat island and associated deeper momentum boundary layer. The turbulence parameters tended to converge during the morning transition period (i.e., the normalized turbulence structure was similar in both the urban and rural environs between 0800 and 1000 h)

and diverged during the afternoon transition of the boundary layer to stable stratification.

The afternoon transition of the boundary layer from unstable to stable stratification in both urban and rural environs occurred over a relatively long period of time. Both horizontal and vertical turbulent intensity components peaked out about noon and declined steadily to near their nocturnal equilibrium value by 1800 h. The velocity variances while peaking about noon declined only slightly to 1400 and then steadily to 1900 h. The peak wavelength in all of the velocity components exhibited behavior similar to the velocity variances, i.e., they decline steadily after 1400 h and well in advance of decline in lidar-determined mixing heights. These observations suggest that free convection turbulence should be scaled with the peak wavelength of the horizontal velocity components rather than the height of the mixed layer. During the late afternoon period these two scale lengths may differ significantly. Turbulent mixing to the top of the "mixed layer", as specified by lidar or temperature-dewpoint profiles, probably does not cease abruptly after the heat flux peaks. We suggest, however, that the probability of any thermal reaching the top of the "mixed layer" decreases significantly past 1300 to 1400 h and continues to decrease to a near zero value prior to sunset, such that the peak in the energy spectrum is continually shifting to higher frequencies. The probability of a thermal reaching  $z_i$  or any height within the mixed layer after 1400 h likely depends on the height and strength of the mixed layer capping inversion and on the surface energy budget, which may have significant spatial variability in urban environs.

### 4.3 SIMILARITY THEORY

Results of the validation tests of current similarity parameterizations using this data set were mixed. The nondimensionalized turbulence parameters (i.e., the velocity and temperature variances, turbulence intensities, and spectra) for site 109 generally behaved as expected from similarity theory; the average magnitude of the data plots as a function of  $z'/L$  was consistent with corresponding plots for ideal sites. However, the scatter of the data points was large; probably due to the nonhomogeneous distribution of land-use features and the abrupt change in roughness features near the tower in the easterly quadrants. A fully developed turbulent boundary layer may not have existed with easterly winds. The observational scatter for site 109 is representative of other nonideal sites (e.g., see Weber et al. 1975) and is indicative of the uncertainty inherent in the application of the similarity approach to practical diffusion problems.

The nondimensionalized turbulence parameters for the urban sites were generally an orderly function of  $z'/L$ ; the data plots exhibited less scatter than the corresponding ratio for site 109. The plots of some urban parameterizations (e.g., see  $\sigma_T/T^*$  in Figure 3.30) were in very good agreement with the empirical expressions derived by others for flat homogeneous sites (e.g., Kansas). Other nondimensionalized ratios for the urban sites, for example  $\sigma_w/u^*$ , depart noticeably from Monin-Obukhov similarity theory as empirically verified for homogeneous sites of small roughness (Figure 3.10). The departure is most apparent in the region of forced convection where the slope of  $\sigma_w/u^*$  with  $-z'/L$  is smaller than expected. For large  $-z'/L$  (approaching free convection),

the ratio was lower than expected; however, the slope is approximately proportional to  $(-z'/L)^{1/3}$  as predicted by similarity theory. Even under neutral stratification the data suggest site specific differences; the normalized vertical velocity variance decreases with increasing  $Z_0$ . Similar anomalies occurred with  $\sigma_v/u^*$  and  $\sigma_u/u^*$ ; a decrease in the ratios with increasing roughness under neutral conditions Figure 3.7, and lower than predicted values for slightly unstable stratification (Figure 3.10). The lateral and vertical turbulence intensities were essentially as expected from the similarity wind profile equation for neutral stratification, but much lower in magnitude than expected for  $z'/L = -0.5$  (Figure 3.28). The nondimensionalized dissipation rate of turbulent kinetic energy behaved much like the ratio  $\sigma_w/u^*$ . At urban site 107,  $\phi_\epsilon$  was significantly less than the expected value of unity for neutral stratification, and at site 105 it was lower than expected throughout the range of unstable stratification (Figure 3.37). The data plots for site 109 were in general agreement with similarity theory; however, the scatter of the plots was large.

The differences between the derived empirical similarity forms for the urban sites and those for the rural site are about 10 to 15% for neutral and stable stratifications and about a factor of two for unstable stratification. For many applications (e.g., atmospheric diffusion estimates) these differences are within the reliability of the application form such that Monin-Obukhov similarity theory, or a simple modification thereof, can be applied to urban areas (such as the forms given in Tables 3.3 to 3.5 for the urban sites).

The general consistency of the departure of the urban data from

similarity theory suggests that it may be possible to describe a physical basis for the departure. The normalized eddy energy budget (Eq. 3.24), along with the expression for  $\epsilon$  given by Eq. 3.7 and  $L_\epsilon$  given by Eq. B-8 relates the velocity and dissipation parameterizations to other relevant parameters through:

$$\sigma_w/u^* = ((\phi_m - z'/L + R')/1.2f_m)^{1/3} \quad (4.1)$$

Thus the anomalies in  $\sigma_w/u^*$  and  $\phi_\epsilon$  may reflect corresponding anomalies in  $\phi_m$ ,  $f_m$ ,  $z'/L$ , and in the residual term  $R'$  representing primarily vertical transport and advection of turbulent energy. The possibility that errors in calculating these terms contribute to the anomalies in the similarity parameterizations is examined below.

The reduced frequencies  $f_m = z'/L_m(w)$  averaged for neutral stratification were 0.31, 0.29, and 0.36 for sites 105, 107, and 109, respectively. Average peak wavelengths for the three sites were 93, 89, and 86 m, respectively. For unstable stratification,  $f_m$  was again smaller and  $L_m$  larger for the urban sites. This trend is opposite to that required to give the observed variation of average  $\sigma_w/u^*$  for the three sites (Figure 3.7). The existence of a larger spectral length scale above the rough urban surface, however, raises the possibility that  $\phi_m$  may be less than unity for neutral stratification and may account in part for the lower values of  $\sigma_w/u^*$  and  $\phi_\epsilon$  at the urban sites. Assuming  $R' = 0$  for neutral stratification ( $z'/L = 0$ ), values of  $\phi_\epsilon = 0.65$  and 1.03 are required for sites 107 and 109, respectively, to satisfy Eq. 4.1 for the observed values of  $\sigma_w/u^*$  and  $f_m$ . These values of  $\phi_m$  are consistent with the values of  $\phi_\epsilon$  for neutral stratification shown in Figure 3.37.



Mixing length may be defined as (Sutton, 1960):

$$l \equiv u^*/dU/dz \quad (4.2)$$

where  $l$  is conventionally equated to  $kz'$  to obtain the differential equation of the logarithmic wind profile for neutral stratification (Eq. 1.2). This formulation of the wind profile does not contain a scaling parameter characteristic of the roughness elements and thus is valid only at heights significantly above the roughness elements. Tennekes (1973) suggested this minimum height to be on the order of  $100z_0$ . The urban data reported herein were obtained at heights of 20 to  $50z_0$ .

A schematic comparison of the normalized neutral velocity profile and that suggested by Garratt (1978a) for flow in the immediate vicinity of the roughness elements is shown in Figure 4.1. The velocity does not increase as rapidly with height above the rough surface as predicted by the logarithmic law. Consequently  $\phi_m$  determined using  $kz'$  as the mixing length may be less than unity. Garratt (1978a, 1978b) has shown this to be the case above a rough surface of trees and shrubs ( $z_0 = 0.4$  m). He found  $\phi_m$  for neutral stratification increasing from 0.58 to unity over a range of  $z/z_0$  from 20 to 85. Garratt's results are in agreement with wind tunnel measurements by Raupach et al. (1980), and are indirectly supported by the present data base (by the behavior of  $\sigma_w/u^*$  and  $\phi_\epsilon$  for neutral stratification). However, Mulhearn (1979), in a review of wind tunnel studies, found  $\phi_m$  to be generally greater than unity above rough surfaces.

For unstable stratification the departure of the urban data from empirically accepted forms is more obvious and also more difficult to

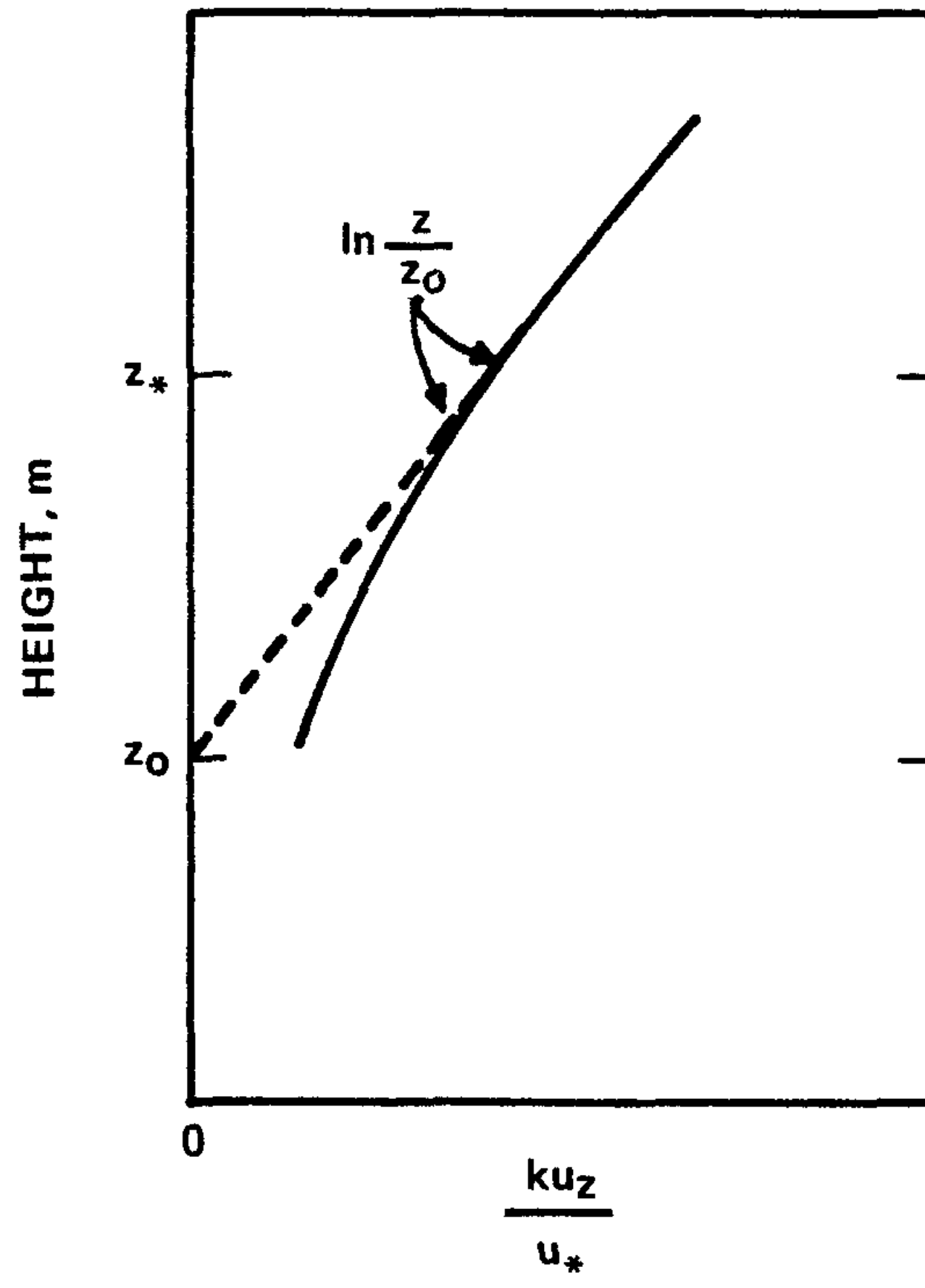


Figure 4.1. Normalized velocity profile in vicinity of roughness elements (neutral stratification).



explain. Comparison of the plots of  $\sigma_w$  and  $\sigma_v$  versus  $u_f$ , for sites 105 and 109, given in Figures 3.11 and 3.18, suggests either the heat flux is less effective in the production of turbulent energy above a rough surface, or the heat flux at site 105, which is larger than at site 109 by a factor of two, is in error. This is further confirmed in Figures 3.14 and 3.23. If the heat flux at site 105 were halved a universal similarity form could be specified without regards to surface features. We have examined and rejected the possibility of significant error in the heat flux at site 105 (and consequently in  $z'/L$ , Eq. 4.1). This conclusion is supported by the fall data set, where the average midday heat flux at site 105 was smaller than the heat flux at sites 107 and 109. Yet the derived empirical similarity relationships are consistent with the summer data set (Figures 3.13 and 3.14). However, the buoyancy parameter for sites 109 and 107 could be underestimated by as much as 20% during the afternoon hours due to neglecting the effects of water vapor fluctuations (Brook, 1978).

Eq. 4.1 was evaluated for  $R'$  for unstable stratification using observed values of  $\sigma_w/u^*$  and  $f_m$ , and the Businger et al. (1971) expression for  $\phi_m$ . For site 109 the residual term was essentially constant at a value of -0.15, for  $z'/L$  between -1 and -5. For site 105, the residual term was -0.8, -1.4, and -3.2 for  $z'/L = -1, -2, \text{ and } -5$ , respectively. Thus there appears to be a significant net removal of turbulent energy from the surface layer at site 105 of about 60 to 80% of the buoyancy production.

The residual term (Eq. 4.1) includes both vertical flux of turbulent energy and advective effects. The data plots for sites 105 have

relatively little scatter, suggesting that advection and nonhomogeneity of the turbulent field are not significant features contributing to the anomaly in the urban turbulence structure. It is unlikely that the advective component would have the same magnitude and sign regardless of wind direction. Thus the anomalies in the similarity parameters for site 105 may be associated with vertical transport of eddy energy away from the surface layer (possibly associated with urban-scale circulation features) or other undetermined effects.

#### 4.4 CONCLUSIONS

The major thrust of this study was to describe the structure of turbulence in the surface boundary layer of an urban area. The approach was through evaluation of the present data base in light of recent empirical verifications of Monin-Obukhov and free convection similarity theories (i.e., the results of the Kansas and Minnesota boundary layer experiments). From the extensive analyses of the turbulence data obtained in the St. Louis environs, it is concluded that many nondimensionalized turbulence parameterizations (e.g.,  $\sigma_w/u^*$ ,  $\sigma_u/u^*$ ,  $\sigma_v/u^*$ ) for the urban sites differ significantly from those for the rural site; the parameterizations for the rural site were in general agreement with similarity theory. The following more specific findings amplify this general conclusion:

- \* The standard deviation of the vertical velocity at both urban and rural sites can be described as a function of  $u^*$  and  $u_f$ . The horizontal velocity components scale with  $u^*$  and  $w^*$ . In this respect the urban data can be described within the framework of similarity theory.

- \* The empirical similarity constants derived for the urban sites were smaller than those for the rural sites.
- \* For neutral stratification the normalized velocity standard deviations were inversely proportional to surface roughness. The nondimensionalized dissipation rate had a similar tendency: it was considerably less than unity at site 107. These anomalies from similarity theory are believed due to the roughness wake region extending to the height of the instrumentation at site 107.
- \* For unstable stratification the urban velocity standard deviations, turbulence intensities, and  $\phi_\epsilon$  were smaller than expected from similarity theory. Flux divergence of turbulent energy due to organized and possibly stationary vertical motions over portions of the city is the likely cause of the anomalies.
- \* For stable stratification the velocity variances were a linear function of  $u^*$  (i.e.,  $\sigma_w/u^* = \text{constant}$ ) at each of the sites. The individual slopes (for each site) appear to be a function of  $Z_0$ .
- \* Temperature spectra at all sites compared well with the Kansas empirical form of Monin-Obukhov similarity theory.
- \* Turbulence length scales were larger for the urban site suggesting that  $\phi_m$  may be correspondingly smaller above the rough urban surface.
- \* The peak wavelength of the longitudinal velocity spectrum appears more appropriate for free convection scaling than  $z_i$ . During the afternoon transition of the boundary layer to stable stratification, the two length scales may differ significantly.

## REFERENCES

- Ariel', N. Z., and Ye. D. Nadezhina, 1976: Dimensionless turbulence characteristics under various stratification conditions. *Izv., Atmos. and Ocean physics*, 12, 492-497 (English Edition).
- Arya, S. P. S., 1975: A drag partition theory for determining the large-scale roughness parameter and wind stress on the arctic pack ice. *J. Geophys. Res.*, 80, 3447-3454.
- Arya, S. P. S., and A. Sundararajan, 1976: An assessment of proposed similarity theories for the atmospheric boundary layer. *Boundary-Layer Meteor.*, 10, 149-166.
- Benoit, R., 1977: On the integral of the surface layer profile-gradient functions. *J. Appl. Meteor.*, 16, 859-860.
- Binkowski, F. S., 1974: On the empirical relationship between the Richardson number and the Monin-Obukhov stability parameter. *Atmos. Environ.*, 9, 453-454.
- Binkowski, F. S., 1979: A simple semi-empirical theory for turbulence in the atmospheric surface layer. *Atmos. Environ.*, 13, 247-253.
- Bowne, N. E., and J. T. Ball, 1970: Observational comparison of rural and urban boundary layer turbulence. *J. Appl. Meteor.*, 9, 862-873.
- Brook, R. R., 1972: The measurement of turbulence in a city environment. *J. Appl. Meteor.*, 11, 443-450.
- Brook, R. R., 1978: The influence of water vapor fluctuations on turbulent fluxes. *Boundary-Layer Meteor.*, 15, 481-487.
- Brutsaert, W., 1975: Comments on surface roughness parameters and the height of dense vegetation. *J. Meteor. Soc. Japan*, 53, 96-97.
- Buck, A. L., 1976: The variable path Lyman-alpha hydrometer and its operating characteristics. *Bull. Amer. Meteor. Soc.*, 57, 1113-1118.
- Builtjes, P. J. H., 1975: Determination of the Eulerian longitudinal integral length scale in a turbulent boundary layer. *Appl. Sci. Res.*, 31, 397-399.
- Busch, N. E., 1973: The surface boundary layer. *Boundary-Layer Meteor.*, 4, 213-240.
- Businger, J. A., 1959: A generalization of the mixing-length concept. *J. Meteor.*, 16, 516-523.

- Businger, J. A., 1974: Aerodynamics of vegetated surfaces. Presented at the Seminar on Heat and Mass Transfer in the Environment of Vegetation, Dubrovnik, Yugoslavia, August 26-30.
- Businger, J. A., J. C. Wyngarrd, Y. Isumi and E. F. Bradley, 1971: Flux-profile relationships in the atmospheric surface layer. *J. Atmos. Sci.*, 28, 181-189.
- Caughey, S. J., and J. C. Kaimal, 1977: Vertical heat flux in the convective boundary layer. *Quart. J. Roy. Meteor.*, 103, 811-815.
- Ching, J. K. S., J. F. Clarke and J. M. Godowitch, 1978: The variability of the heat flux and mixed layer depth over St. Louis, Missouri. *Proc., WMO Symposium on Boundary Layer Physics Applied to Special Problems of Air Pollution, Norrkoping, Sweden*, pp. 71-78.
- Corrsin, S., 1951: On the spectrum of isotropic temperature fluctuations in an isotropic turbulence. *J. Appl. Phys.*, 22, 469-473.
- Counihan, J., 1971: Wind tunnel determination of the roughness length as a function of the fetch and roughness density of three-dimensional roughness elements. *Atmos. Environ.*, 5, 637-642.
- Counihan, J., 1975: Adiabatic atmospheric boundary layers: a review and analysis of data from the period 1880-1972. *Atmos. Environ.* 9, 871-905.
- Deardorff, J. W., 1970: Convective velocity and temperature scales for the unstable planetary boundary layer and for Raleigh convection. *J. Atmos. Sci.*, 27, 1211-1213.
- Deardorff, J. W., and G. E. Willis, 1975: A parameterization of diffusion into the mixed layer. *J. Appl. Meteor.*, 14, 1451-1458.
- Donaldson, C. dup., 1973: Construction of dynamic model of the production of atmospheric turbulence and the dispersal of atmospheric pollutants. *Workshop on Micrometeorology (edited by D. A. Haugen)*, American Meteorology Society, Boston, pp. 313-390.
- Dyer, A. J., B. B. Hicks and K. M. King, 1967: The fluxatron - a revised approach to the measurement of eddy fluxes in the atmosphere. *J. Appl. Meteor.*, 6, 408-413.
- Dyer, A. J., B. B. Hicks and V. Sitaraman, 1970: Minimizing the leveling error in Reynolds stress measurement by filtering. *J. Appl. Meteor.*, 9, 532-534.
- Dyer, A. J., and B. B. Hicks, 1972: The spatial variability of eddy fluxes in the constant flux layer. *Quart. J. Roy. Meteor. Soc.*, 98, 206-212.



- Endlich, R. M., F. L. Ludwig and E. E. Uthe, 1978: Graphs of objectively determined mixing depth and integrated aerosol at St. Louis during the RAPS program. Technical Note 2, SRI International, California, 31 pp.
- Eversole, R. A., 1979: Spectral characteristics of boundary layer over irregular terrain. Atmospheric Science Paper No. 314, Colorado State University, Fort Collins, Colorado, 115 pp.
- Fichtl, G. H., and Prem Kumar, 1974: The response of a propeller anemometer to turbulent flow with the mean wind vector perpendicular to the axis of rotation. *Boundary-Layer Meteor.*, 6, 363-379.
- Garratt, J. R., 1977: Review of drag coefficients over oceans and continents. *Mon. Wea. Rev.*, 105, 915-929.
- Garratt, J. R., 1978a: Flux profile relations above tall vegetation. *Quart. J. Roy. Met. Soc.*, 104, 199-211.
- Garratt, J. R., 1978b: Transfer characteristics for a heterogeneous surface of large aerodynamic roughness. *Quart. J. Roy. Meteor. Soc.*, 104, 491-502.
- Gill, G. C., 1975: Development and use of the Gill UVW anemometer. *Boundary-Layer Meteor.*, 8, 475-495.
- Graham, I. R., 1968: An analysis of turbulence statistics at Fort Wayne, Indiana. *J. Appl. Meteor.*, 7, 90-93.
- Hanna, S. R., 1968: A method for estimating the vertical eddy transport in the planetary boundary layer using characteristics of the vertical velocity spectrum. *J. Atmos. Sci.*, 25, 1026-1033.
- Hanna, S. R., 1969: Urban micrometeorology. ATDL No. 25, Air Resources Atmospheric Turbulence and Diffusion Laboratory, Oak Ridge, Tennessee, 20 pp.
- Haugen, D. A., J. C. Kaimal and E. F. Bradley, 1971: An experimental study of the Reynold stress and heat flux in the atmospheric surface layer. *Quart. J. Roy. Meteor. Soc.*, 97, 168-180.
- Hicks, B. B., 1972: Propeller anemometers as sensors of atmospheric turbulence. *Boundary-Layer Meteor.*, 3, 214-228.
- Hicks, B. B., 1976; Reply to comments by J. H. Shreffler on "A procedure for the formulation of bulk transfer coefficients over water." *Boundary-Layer Meteor.*, 10, 237-240.
- Horst, T. W., 1972: A computer algorithm for correcting noncosine response in the Gill anemometer. Battelle Northwest Laboratories Annual Report for 1971, BNWL-1651 PTI, pp. 183-186.

- Horst, T. W., 1973: Correction for the response errors in a three-component propeller anemometer. *J. Appl. Meteor.*, 12, 716-725.
- Isumi, Y., and J. S. Caughey, 1976: Minnesota 1973 atmospheric boundary layer experiment data report. AFCRL-TR-76-0038, 27 pp.
- Jackson, P. S., 1978: Wind structure near a city center. *Boundary-Layer Meteor.*, 15, 323-340.
- Jones, P. M., M. A. B. de Larrinaga and C. B. Wilson, 1971: The urban wind velocity profile. *Atmos. Environ.*, 5, 89-102.
- Kaimal, J. C., and D. A. Haugen, 1969: Some errors in the measurement of Reynold stress. *J. Appl. Meteor.*, 8, 460-462.
- Kaimal, J. C., and D. A. Haugen, 1971: Comments on minimizing the leveling error in Reynold stress measurement by filtering. *J. Appl. Meteor.*, 10, 337-339.
- Kaimal, J. C., J. C. Wyngaard, Y. Izumi and O. R. Cote, 1972: Spectral characteristics of surface layer turbulence. *Quart. J. Roy. Meteor. Soc.*, 98, 563-589.
- Kaimal, J. C., 1973: Turbulence spectra, length scales and structure parameters in the stable surface layer. *Boundary-Layer Meteor.*, 4, 289-309.
- Kaimal, J. C., J. C. Wyngaard, D. A. Haugen, O. R. Cote and Y. Izumi, 1976: Turbulent structure in the convective boundary layer. *J. Atmos. Sci.*, 33, 2152-2169.
- Kaimal, J. C., 1978: Horizontal velocity spectra in an unstable surface layer. *J. Atmos. Sci.*, 35, 18-24.
- Kutzbach, J., 1961: Investigations of the modification of wind profiles by artificially controlled surface roughness. Univ. of Wisconsin, Dept. of Meteor., Annual Report, pp. 71-113.
- Lettau, H., 1969: Note on aerodynamic roughness-parameter estimation on the basis of roughness-element description. *J. of Appl. Meteor.*, 8, 828-832.
- Lumley, J. L., and H. A. Panofsky, 1964: *The Structure of Atmospheric Turbulence*. New York, Interscience, 239 pp.
- Merry, M., and H. A. Panofsky, 1976: Statistics of vertical motion over land and water. *Quart. J. Roy. Meteor. Soc.*, 102, 255-260.
- Monin, A. S., and A. M. Obukhov, 1954: Basic laws of turbulent mixing in the atmosphere near the ground. *Tr. Akad. Nauk. SSSR. Geofiz. Inst.*, 151, 163-187.



- Monin, A. S., and A. M. Yaglom, 1965: Statistical Fluid Mechanics: Mechanics of Turbulence, Volume 1. English edition edited by J. L. Lumley, 1971, Cambridge, Mass., MIT press, 769 pp.
- Mulhearn, P. J., 1979: A note on momentum transfer above very rough surfaces. Quart. J. Roy. Meteor. Soc., 721-723.
- Nickerson, E. C., and V. E. Smiley, 1975: Surface layer and energy budget parameterizations for mesoscale models. J. Appl. Meteor., 14, 297-300.
- Obukhov, A. M., 1946: Turbulence in an atmosphere with non-uniform temperature. Tr. Akad. Nauk. SSSR. Geofiz. Inst., No. 1 (English translation in Boundary-Layer Meteor., 2, 7-29, 1971).
- Oke, T. R., 1974: Review of Urban Climatology 1968-1973. World Meteor. Org., Tech. Note No. 134, WMO-NO. 383, 132 pp.
- Panofsky, H. A., H. Tennekes, D. H. Lenschow and J. C. Wyngaard, 1977: The characteristics of turbulence velocity components in the surface layer under convective conditions. Boundary-Layer Meteor., 11, 355-362.
- Pasquill, F., 1970: Wind structure in the atmospheric boundary layer. Phil. Trans. Roy. Soc., Ser. A, 269, 439-456.
- Paulson, C. A., 1970: The mathematical representation of wind speed and temperature in the unstable atmospheric surface layer. J. Appl. Meteor., 9, 857-861.
- Peschier, J. Jr., 1972: Wind and temperature profiles in an urban area. Master's Thesis, University of Texas, Austin, Texas, 33pp.
- Peterson, E. W., 1969: Modification of mean flow and turbulent energy by a change in surface roughness under conditions of neutral stability. Quart. J. Roy. Meteor. Soc., 95, 561-575.
- Plate, E., and A. A. Quraishi, 1965: Modeling of the velocity distribution inside and above tall crops. J. Appl. Meteor., 4, 400-408.
- Priestley, C. H. B., 1954: Convection from a large horizontal surface. Australian J. Phys., 6, 279-290.
- Ramsdell, J. V., 1975: Wind and turbulence information for vertical and short take-off and landing (V/STOL) operations in built-up urban areas - results of meteorological survey. Battelle, Pacific Northwest Laboratories, Richland, Washington, 216 pp.
- Raupach, R. M., A. S. Thom and I. Edwards, 1980: A wind-tunnel study of flows close to regularly arrayed rough surfaces. Boundary-Layer Meteor., 18, 373-397.

- R. M. Young Company, 1973: Instructions, Gill UVW Anemometer. Traverse City, Michigan, 20 pp.
- Schiermeier, F. A., 1978: Air monitoring milestone: RAPS field measurements are in. *Env. Sci., and Tech.*, 12, 644-651.
- Singleton, R. C., 1969: An algorithm for computing the mixed radix fast Fourier transform. *IEEE Trans. on Audio and Electroacoustics*, 17, 93-103.
- Sutton, O. G., 1960: Atmospheric Turbulence. John Wiley and Sons, Inc., New York, 111 pp.
- Taylor, G. I., 1938: The spectrum of turbulence. *Proc. Roy. Soc., A*, 164, 476-490.
- Tennekes, H., 1973: The logarithmic wind profile. *J. Atmos. Sci.*, 30, 234-238.
- Tennekes, H., and J. L. Lumley, 1972: A First Course in Turbulence. The MIT Press, Cambridge, Mass., 300 pp.
- Webb, E. K., 1955: Autocorrelations and energy spectra of atmospheric turbulence. Tech. Paper No. 5, Div. of Meteor. Phys., C.S.I.R.O., Melbourne, 28 pp.
- Wamser, C., and H. Müller, 1977: On the spectral scale of wind fluctuations within and above the surface layer. *Quart. J. Roy. Meteor. Soc.*, 103, 721-730.
- Weber, A. H., J. S. Irwin, J. P. Kahler and W. B. Peterson, 1975: Atmospheric turbulence properties in the lowest 300 meters. EPA-600/4-75-004, Environmental Protection Agency, Research Triangle Park, N. C., 152 pp.
- Wesely, M. L., and B. B. Hicks, 1975: Comments on "Limitations of the eddy-correlation technique for the determination of turbulent fluxes near the surface". *Boundary-Layer Meteor.*, 9, 363-367.
- Wynngaard, J. C. and O. R. Coté, 1971: The budgets of turbulent kinetic energy and temperature variance in the atmospheric surface layer. *J. Atmos. Sci.*, 28, 190-201.
- Wynngaard, J. C., and O. R. Coté, 1974: The evolution of a convective planetary boundary layer - a higher-order-closure model study. *Boundary-Layer Meteor.*, 7, 289-308.
- Wynngaard, J. C., O. R. Coté and Y. Izumi, 1971: Local free convection, similarity, and the budgets of shear stress and heat flux. *J. Atmos. Sci.*, 28, 1171-1182.

- Yokoyama, O., 1971: An experimental study on the structure of turbulence in the lowest 500 meters of the atmosphere and diffusion in it. Report No. 2, National Institute for Pollution and Resources, Japan, 115 pp.
- Zubkovskii, S. L., and L. R. Tsvang, 1966: Horizontal turbulent heat flow. *Izv., Atmos. and Ocean Physics*, 2, 1307-1310 (English Edition).

## APPENDIX A

### Gill UVW ANEMOMETER

Computed values of stress, heat flux, and vertical velocity variance are extremely sensitive to the condition, exposure, and leveling precision of the Gill anemometer. Thus a special leveling device was attached to the Gill instruments used in this study and extensive pre- and post-field wind tunnel calibration tests conducted. The leveling method, calibration, and response characteristics of the Gill instrument are discussed below.

#### A-1 Leveling

A number of investigators have discussed errors in the stress and heat flux resulting from tilt of the w sensor (Kaimal and Haugen, 1971; Dyer, et al., 1970; Dyer and Hicks, 1972; Wesely and Hicks, 1975). Errors on the order of 14% per degree of tilt for the stress and 4% for the heat flux are typical under ideal conditions. Kaimal and Haugen (1969) concluded that tilt should be less than  $0.1^\circ$  for sensors used in the measurement of stress. The instruments used in this study were aligned on the towers using a high-precision plumb bob level attached to the shaft of the anemometer, as shown in Figure A-1. The leveling system, aligned with the w-arm, had a precision of  $0.1^\circ$ . The alignment of the w-arm on the towers was further checked with a transit from the ground. In all cases, the w-arm was vertical within the accuracy of the transit.

The plumb bob leveling device interfered with the flow over the back of the u and v arms. Consideration was given for this interference



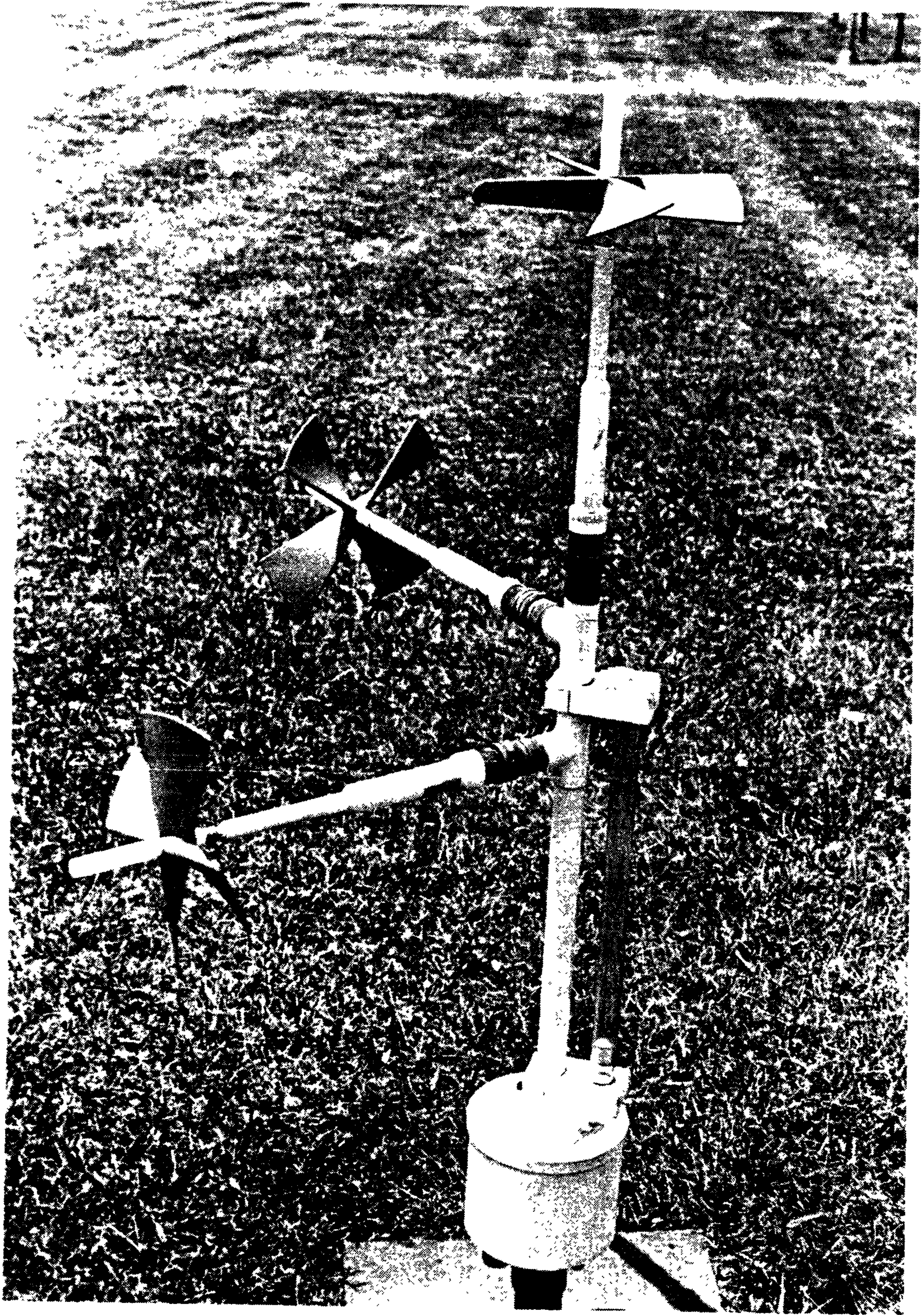


Figure A-1. Photograph of Gill anemometer showing attached plumb bob leveling device.



in the calibration of the instrument and in the orientation of the instruments on the towers with respect to the prevailing wind. For the summer experimental period the u and v arms were oriented to  $135^{\circ}$  and  $225^{\circ}$ , respectively; the orientation for the fall period was  $190^{\circ}$  and  $280^{\circ}$ , respectively.

## A-2 Calibration

The Gill UVW anemometer was designed to respond only to the component of the wind parallel to the propeller shaft, i.e., a true cosine response. However, the manufacturer's calibration (R. M. Young Company, 1973) indicates a deviation from the cosine response which increases as the wind becomes more normal to the shaft. A computer algorithm for correcting for noncosine response in the Gill anemometer based on the manufacturer's calibration is given by Horst (1972, 1973). Hicks (1972) showed that the cosine correction for the horizontal components was a function of wind speed. The vertical correction was essentially linear over a range of elevation angles of  $\pm 30^{\circ}$  and equal to approximately 1.25 times the indicated velocity. Hicks also found that the response of the Gill instrument deteriorates significantly when employed in the field for an extended period. Because of such characteristics of the instrument and the addition of the leveling device to the shaft, the Gill instruments used in this study were extensively calibrated in the EPA wind tunnel. Conclusions and operational procedures resulting from the calibration program are:

1. The correction function for noncosine response was relatively constant for wind speeds greater than 2.0 m/sec. Those hours with

- wind speeds less than 2 m/sec were normally not used in the analyses, and a single cosine correction function was applied to all the data.
2. The anemometer had a much better response at small angles ( $\pm 10^\circ$ ) to the normal when the flow was from the shaft side of the propeller. This was especially evident at higher tunnel speeds and is due to turbulence created by the flow over the shaft. To eliminate this source of error, shaft extenders were used on all anemometers as suggested by Hicks (1972). A shaft extender is a small cylindrical piece of plastic about 8 cm long and the same diameter as the shaft. It is affixed to the propeller such that the physical configuration is symmetrical on both sides of the propeller. Dyer et al. (1967) found that use of the shaft extender provided a more symmetrical response and reduced the stall angle from  $40^\circ$  to  $20^\circ$ .
  3. The leveling system attached to anemometer affected the response when the wind was from the back side. This was accounted for in the cosine correction for the instrument.
  4. Pre- and post-field speed calibrations were not significantly different. However, the bearing friction of the instrument increased appreciably. The average starting speeds were about 41 cm/sec and 72 cm/sec for the pre- and post-field tests, respectively. Average stalling speeds were considerably lower, about 28 and 41 cm/sec, respectively.
  5. The distant constant of the Gill instrument is about 1 m for the wind parallel to the shaft, and 2.5 m for the wind normal to the shaft (Gill, 1975; Hicks, 1972). The EPA wind tunnel tests gave similar results. These are expressed as time constants as a function of tunnel speed and angle of attack to the propeller in Figure A-2.



### A-3 Response Characteristics

The Gill anemometer is usually treated as a simple linear system having a time constant  $\tau$  responding to a sine function input. For two in-phase systems, the fractional response as a function of frequency  $\omega$  is given by:

$$f_{1,2}(\omega) = (1 + \omega^2 \tau_1 \tau_2) / ((1 + \omega^2 \tau_1^2)(1 + \omega^2 \tau_2^2)) \quad (\text{A-1})$$

Eq. A-1 is evaluated in Table A-1 for selected variances and covariances for three cyclic frequencies ( $n = \omega/2\pi$ ), and for the time constants appropriate to 2 and 5 m/sec (Figure A-2). The Gill anemometer has an obvious high-frequency loss in response, which is larger for low wind speeds and for the w component. This problem is not considered serious in the present study since, at the height of instrument exposure (31 m), little turbulent energy is contained at reduced frequencies ( $f = nz/U$ ) greater than 3 ( $n \sim 0.3$ ). Horst (1973) has shown that data corrected only for cosine response give estimates of the second moments comparable to that of a sonic anemometer, up to frequencies of 0.3.

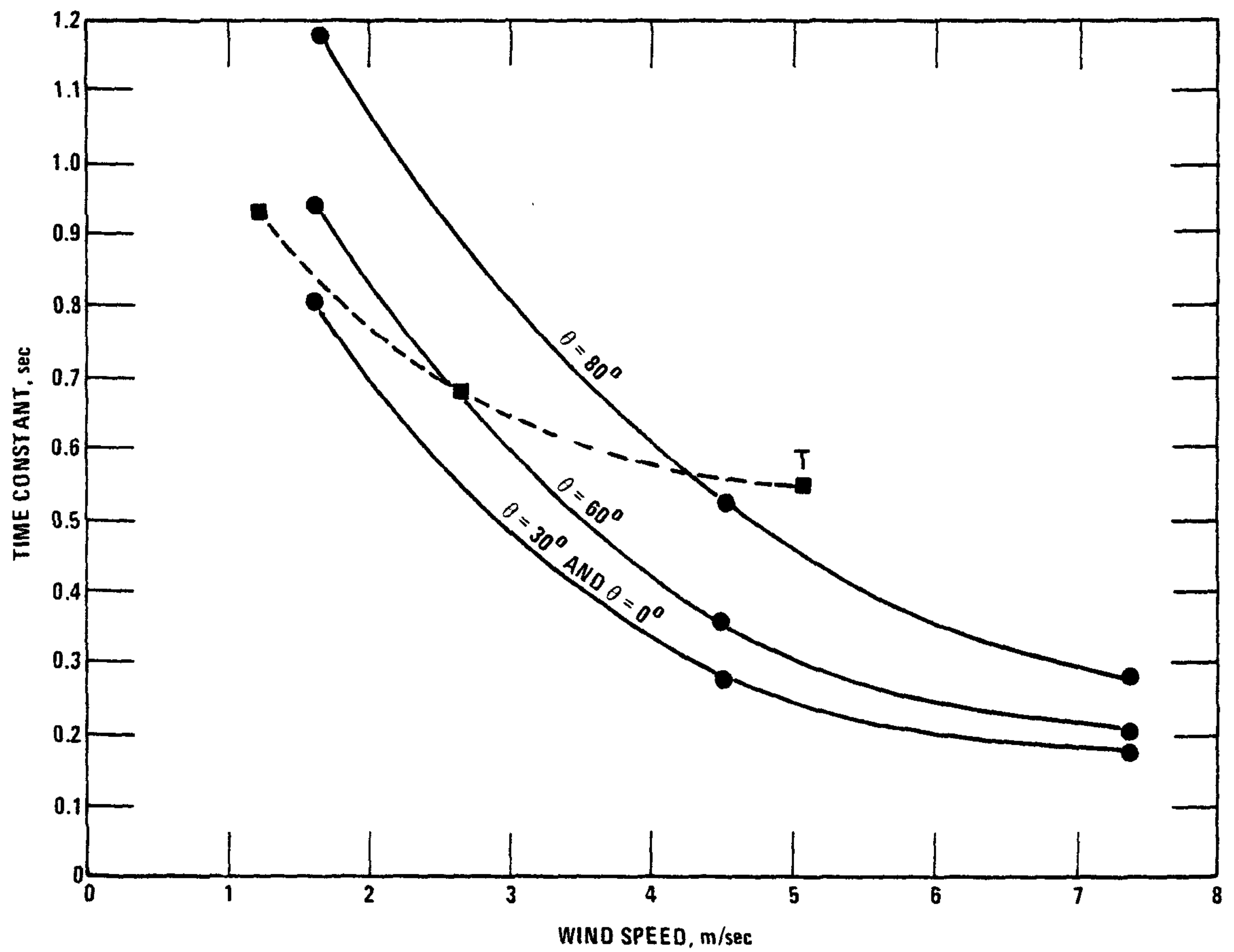


Figure A-2. Time constant as a function of wind speed for the temperature system (dashed line) and Gill anemometer for four wind angles to the propeller.

Table A-1. Effect of Instrument Response on Second Moments.

		$\overline{u'^2}$	$\overline{w'^2}$	$\overline{u'w'}$	$\overline{w'T'}$
f	n	$u = 2 \text{ m sec}^{-1}$			
.15	.01	1.0	.99	1.0	1.0
1.5	.1	.85	.64	.71	.70
15	1.0	.05	.02	.03	.03
f	n	$u = 5 \text{ m sec}^{-1}$			
.06	.01	1.0	.99	1.0	1.0
.6	.1	.98	.93	.95	.91
6	1.0	.23	.12	.18	.10

## APPENDIX B

### DATA PROCESSING

#### B-1 Initial Processing

A simplified flow diagram of data processing is shown in Figure B-1. The RAMS tapes contained both 1-min average RAMS data and 1/2-sec turbulence data in PDP 8 computer language. The turbulence data were subsequently extracted through TRANSLATOR, converted to UNIVAC language and packed on the TURB tapes. Both RAMS and TURB tapes have been archived.

TURBCALC is the basic data processing program. One-hour data blocks (7200, 1/2-sec values) from each of the five sensors (temperature, humidity, and three components of the wind) were read by TURBCALC in integer form, along with initialization and calibration factors. The following operations and computations were then carried out within TURBCALC or by subroutines called by TURBCALC in the listed order:

1. The integer format of the data was converted back to voltage values as originally input to the data acquisition system (with a loss of resolution of 2.4 mv). All subsequent processing was in voltages and the calibration factors were applied just prior to the output stage to convert the results to engineering units.
2. The anemometer data were corrected for noncosine response through subroutine COSCO.
3. Hourly average values of the voltages were computed for each of the sensors along with quantities representing the mean wind speed and standard deviation of elevation angle. Mean wind direction and

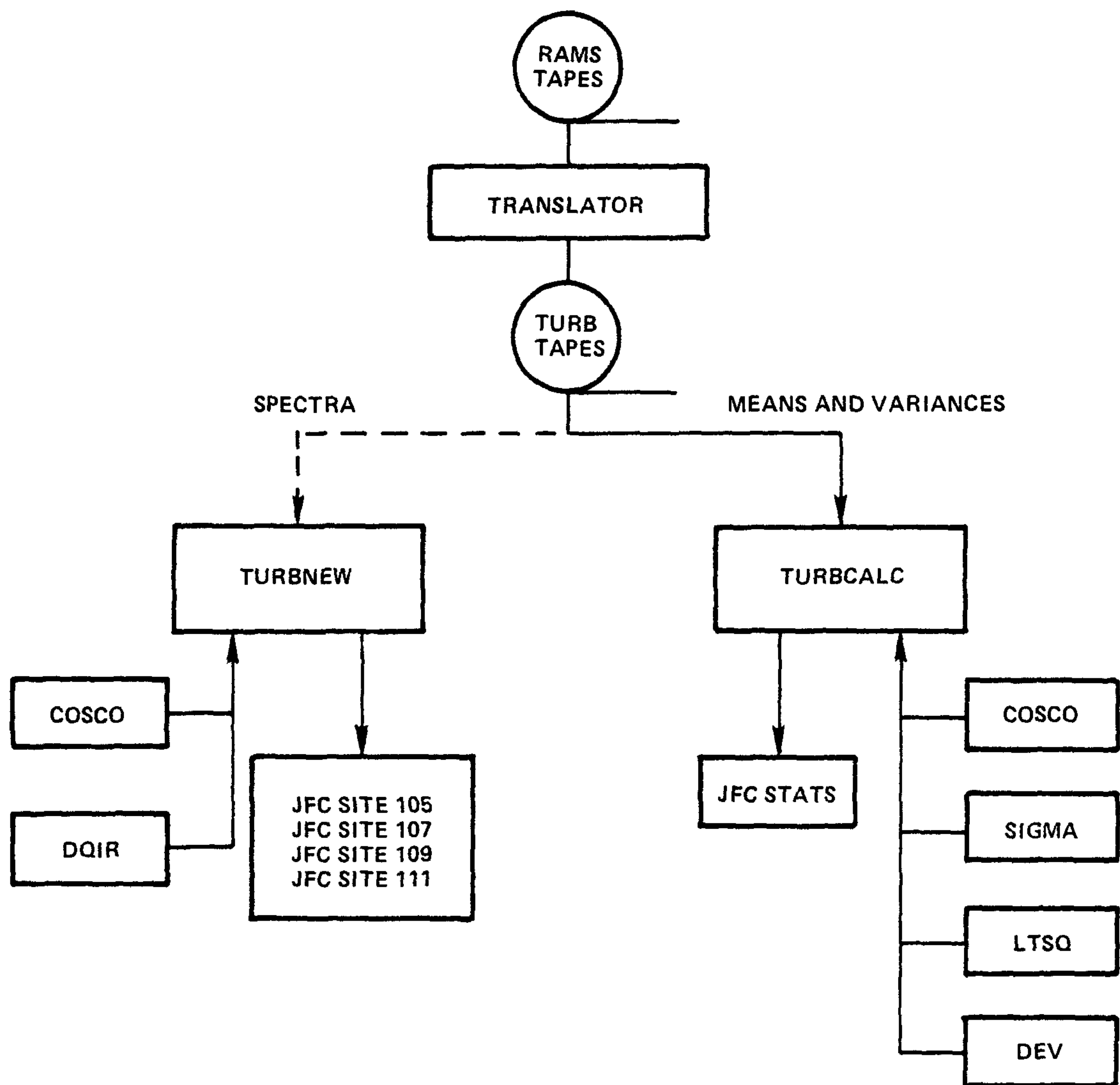


Figure B-1. Simplified flow diagram of data processing.

standard deviation of azimuth angle were obtained through subroutine SIGMA.

4. The basic data were then subjected to trend removal through subroutine LTSQ, which applies a 2<sup>nd</sup>-order least-squares fit to the hourly time series.
5. Subroutine DEV takes the results of LTSQ and calculates the departure of the points in the time series from the trend vector. New time series of the turbulent components of  $u'$ ,  $v'$ ,  $w'$ ,  $T'$ ,  $q'$  were obtained in which  $u'$  is in the direction of the mean wind and  $v'$  is in the cross wind direction.
6. Hourly variances and covariances were computed from the turbulence time series and surface boundary layer parameters calculated (e.g., heat flux, stress, Monin-Obukhov length, etc.).
7. Calibration factors were applied and the computed parameters printed out and written to a disk file, JFCSTATS.

## B-2 Spectral Computations

Processing of the data for the spectral computations was accomplished through the left-hand branch of the flow diagram in Figure B-1. TURBNEW is the driving program which calculates the mean wind speed and covariances for normalizing the spectra; it then calls DQIR. DQIR in turn calls several subroutines which detrend the data, compute the spectrum by a FFT routine, fit a preassumed spectral shape to spectral estimates, and write the output for each site to an individual file. The time series were linearly, rather than quadratically, detrended as was done for TURBCALC. The rationale for this approach was that a more

severe filter could be applied to the spectral estimates if necessary. The detrended time series were applied to a mixed-radix fast Fourier transform (FFT) algorithm (Singleton, 1969). The 7200, 1/2 second hourly data samples applied to the FFT resulted in 3600 spectral estimates for each component (u, v, w, and T). A subsequent processing routine provided 14 values of  $S(v)$  and  $v^{5/3}S(v)$  averaged over 256 raw spectral values, and 11 values of  $vS(v)$  averaged on a logarithmic scale (i.e., over consecutive  $2^x$  points for  $x = 0$  to 10). This averaging procedure was the only smoothing applied to the spectral estimates. The latter output was used for visual representation of the data (see Figures 3.38, 3.42, 3.43, and 3.47).

The large volume of data mandated some form of objective analysis. It was assumed at the outset that the form of the w spectra and the neutral-to-stable horizontal velocity spectra could be expressed as:

$$vS(v) = \frac{A_v}{1 + B_v^{5/3}} \quad (B-1)$$

(Kaimal, 1972, 1978; Kaimal et al., 1972).  $vS(v)$  represents the spectral estimate at count  $v$ . Eq. B-1 was fitted to the raw spectral estimates by a least-squares technique over 1 to 1800 points and 4 to 1800 points. The latter range, which represents an extreme filtering of the low frequency component, was used for the w spectra; the former range was used for horizontal component spectra. Thus two sets of values for A and B were generated for each hourly time series.

The procedure for fitting Eq. B-1 to the spectrum assumed a -2/3 slope in the inertial subrange. Spectra which by a subjective analysis



obviously did not have a  $-2/3$  slope in the inertial subrange were not included in the analyses of section 3.3. The number of spectra for each site and component used in the analyses are given in Table B-1. Site 105 had the highest percentage of spectra with an apparent  $-2/3$  slope. Site 111 had a very low percentage of spectra with a  $-2/3$  slope and thus was not included in the analyses of Section 3.3.

Given the spectral form of Eq. B-1, all statistics and length scales associated with the spectrum can be specified from the values of A and B. At the low frequency end of the spectrum, i.e., as  $\nu \rightarrow 0$ ,  $S(\nu) = A$ ; at the high frequency end (in the inertial subrange),  $\nu S(\nu) = (A/B)\nu^{-2/3}$ . The peak in the spectrum, obtained through differentiation of Eq. B-1, is at  $\nu_{\max} = 1.275b$ , where  $b = 1/B^{3/5}$ .

Count  $\nu$  is converted to frequency through  $\nu = Nn/R$ ; N is the number of data points in the time series (7200) and R is the sampling rate (2 per sec). The wavelength of the spectral peak  $L_m$  is given by:

$$L_m = \frac{U}{n_m} = \frac{UN}{1.275bR} \quad (B-2)$$

where  $n_m$  is the frequency corresponding to the peak in the  $nS(n)$  spectrum.

The variance of the time series is given by  $\sigma^2 = \int_0^\infty S(n)dn$ . Applying this to Eq. B-1 gives:

$$\sigma^2 = 1.98Ab - A/2. \quad (B-3)$$

For large b, the last term may be dropped with very minor effect on the total variance.

Table B-1. Number of spectra for each site, spectral component, and stability class used in the analyses.

SPECTRAL COMPONENT	$z'/L$	TOTAL AND PERCENT SPECTRA USED IN ANALYSES					
		SITE 105		SITE 107		SITE 109	
		TOTAL	%	TOTAL	%	TOTAL	%
u'	-.5 to -2	70	90	16	38	74	55
	+.05 to -.05	83	92	115	28	33	41
	+.5 to +1	7	86	24	33	51	25
v'	-.5 to -2	70	55	16	63	74	24
	+.05 to -.05	83	77	115	62	33	48
	+.5 to +1	7	86	24	50	51	51
w'	-.5 to -2	70	80	16	38	74	55
	+.05 to -.05	83	86	115	77	33	64
	+.5 to +1	7	100	24	96	51	75
T'	-.5 to -2	70	63	16	81	74	99
	+.05 to -.05	83	93	115	94	33	91
	+.5 to +1	7	71	24	92	51	94

The integral length scale can be obtained through:

$$L_i = \frac{S(n)U}{4\sigma^2} \quad (B-4)$$

(Builthjes, 1975). From Eqs. B-2, B-3, and B-4 it can be shown that:

$$L_i = \frac{UN}{7.92bR} = \frac{L_m}{6.21}. \quad (B-5)$$

This result is very close to the theoretical form derived by Webb (1955).

Tennekes and Lumley (1972) derived a length scale from consideration of the rate of dissipation of kinetic energy as:

$$L_\epsilon = \sigma_w^3 / \epsilon. \quad (B-6)$$

Using the expression for  $\sigma_w$  given by Eq. 3.19, which can be expressed as:

$$\epsilon = (A/B\alpha)^{3/2} 2\pi R / UN \quad (B-7)$$

and using Eqs. B-2 and B-3, we obtain for the w and v components ( $\alpha = 0.667$ ):

$$L_\epsilon = \frac{0.2414UN}{bR} = L_m / 3.25. \quad (B-8)$$

Because of the redundancy of the three length scales by the above calculation techniques, only  $L_m$  and  $\epsilon$  are discussed in Section 3.3.

<b>TECHNICAL REPORT DATA</b> <i>(Please read Instructions on the reverse before completing)</i>		
1. REPORT NO.	2.	3. RECIPIENT'S ACCESSION NO.
4. TITLE AND SUBTITLE		5. REPORT DATE
AN EXPERIMENTAL STUDY OF TURBULENCE IN AN URBAN ENVIRONMENT		6. PERFORMING ORGANIZATION CODE
7. AUTHOR(S)		8. PERFORMING ORGANIZATION REPORT NO.
J.F. Clarke, J.K.S. Ching and J.M. Godowitch		
9. PERFORMING ORGANIZATION NAME AND ADDRESS		10. PROGRAM ELEMENT NO.
same as 12		CDWA1A/02-1324 (FY-82)
		11. CONTRACT/GRANT NO.
12. SPONSORING AGENCY NAME AND ADDRESS		13. TYPE OF REPORT AND PERIOD COVERED
Environmental Sciences Research Laboratory - RTP, NC Office of Research and Development U.S. Environmental Protection Agency Research Triangle Park, NC 27711		In-house
		14. SPONSORING AGENCY CODE
		EPA/600/09
15. SUPPLEMENTARY NOTES		
16. ABSTRACT		
<p>The structure of turbulence in the urban surface boundary layer is discussed. Wind and temperature fluctuations were measured with fast-response sensors at a height of 31 m at a rural and three urban sites in the St. Louis environs. The second moments of the fluctuations were computed for one-hour time series and analyzed within the framework of Monin-Obukhov similarity theory. The results are discussed relative to observed land-use features and calculated surface roughness lengths for each of the sites.</p> <p>Average surface roughness lengths ranged from 0.7 to 1.7 m for the urban sites. The normalized velocity and temperature variances for the rural site were consistent with similarity theory. For the urban sites, the normalized velocity variances showed an orderly departure from similarity theory for both neutral and unstable stratifications.</p> <p>The urban anomalies are discussed relative to the terms in the turbulent kinetic energy budget equation. For neutral stratification, the normalized velocity variances are up to 15% lower at the urban sites compared to the rural site. They appear to be inversely proportional to surface roughness length. For unstable stratification, the normalized velocity variances for the urban sites are about 50% lower than for the rural site.</p>		
17. KEY WORDS AND DOCUMENT ANALYSIS		
a. DESCRIPTORS	b. IDENTIFIERS/OPEN ENDED TERMS	c. COSATI Field/Group
18. DISTRIBUTION STATEMENT	19. SECURITY CLASS (This Report)	21. NO. OF PAGES
RELEASE TO PUBLIC	UNCLASSIFIED	167
	20. SECURITY CLASS (This page)	22. PRICE
	UNCLASSIFIED	

